Yuji Hasegawa

TECHNISCHE UNIVERSITÄT WIEN
Vienna University of Technology

Diplomarbeit

Spin and Path Weak Values in Neutron Optical Experiments

ausgeführt am
Atominstitut
der Technischen Universität Wien

unter der Anleitung von

Assistant Prof. Dipl.-Ing. Dr. Yuji Hasegawa

durch

Tobias Denkmayr
Vormarkt Nonsbach 60
4982 Obernberg am Inn

June 20, 2013

Tobias Denkmayr

Abstract

Quantum mechanical measurements inevitably induce a disturbance on the system. If the interaction strength is weak enough, so called weak measurements are performed. Together with pre and post selected states they allow to extract the weak value of an observable. Here we want to determine the weak value using neutron matter waves with polarimeter and interferometer setups. In particular, three different kinds of experiments are proposed: (i) the first allows to measure the weak value of the spin operator using either an interferometer or a polarimeter, (ii) the second experiment is designed to extract the path weak value in a neutron interferometer and (iii) the combination of both experiments forms the third one, which allows to measure a so called 'Cheshire Cat'. Furthermore, the polarimeter experiment designed to extract the spin operator's weak value was carried out at the TRIGA Mark II research reactor of the Institute of Atomic and Subatomic Physics of the Vienna University of Technology. The results agree very well with the theory and favor further investigation of weak values with neutrons.

Kurzfassung

Wird eine Messung an einem quantenmechanischen System durchgeführt, so bewirkt dies unweigerlich eine Störung dieses Systems. Ist die Stärke der Wechselwirkung dieser Messung klein genug, so werden sogenannte 'weak measurements', zu Deutsch 'schwache Messungen', vorgenommen. Gemeinsam mit pre und post selektierten Ensembles erlauben diese den schwachen Messwert ('weak value') einer Observable zu messen. Mit Hilfe der Materiewellen von Neutronen wollen wir den schwachen Messwert in Polarimeter und Interferometer Experimenten bestimmen. Dazu werden drei verschiedene Arten von Experimenten vorgeschlagen: (i) das erste erlaubt es den schwache Messwert des Spin Operators entweder mittels eines Polarimeters oder eines Interferometers zu messen, (ii) das zweite ermöglicht es in einem Interferometer Experiment den schwachen Messwert des Pfad Operators zu bestimmen und (iii) die Kombination dieser beiden bildet das dritte, welches dazu ausgelegt ist, das sogenannte 'Cheshire Cat' Paradoxon nachzuweisen. Außerdem wurde das Polarimeter Experiment, welches so ausgelegt wurde, dass man den schwachen Messwert des Spin Operators bestimmen kann, am TRIGA Mark II Forschungsreaktor des Atominstituts der technischen Universität Wien durchgeführt. Die Resultate dieser Messung stimmen sehr gut mit der Theorie überein und befürworten eine weitere Untersuchung von schwachen Messwerten mit Neutronen.

Contents

1. Introduction **5**

2. Theoretical background **6**
2.1. Measurements in quantum mechanics 6
2.2. Weak measurements 8
2.2.1. Spin-(1/2) particles and weak measurements 11
2.3. Associated experiments 13
2.3.1. First realization of a weak measurement 13
2.3.2. Beam deflection measurement via interferometric weak value amplification 17
2.3.3. Average trajectories of single photons 19
2.4. Technique of neutron polarimeter optics 23
2.4.1. Neutron spin 23
2.4.2. Polarizing supermirrors 24
2.4.3. DC-coils 25
2.4.4. A polarimeter beamline 26

3. Weak value measurements using neutrons **28**
3.1. Weak values of the spin operator 28
3.1.1. Determining the absolute of the spin operator's weak value 28
3.1.2. Polarimeter experiment for the determination of the absolute of the spin operator's weak value 33
3.1.3. Determining the spin operator's complete weak value 38
3.1.4. Experimental value range 40
3.2. Weak values of the path operator 41
3.2.1. Estimates of the measurement strength's influence 48
3.2.2. Influences of imperfect experimental circumstances 55
3.2.3. Other path operators 62
3.2.4. Expected results for the individual weak values of $\hat{\Pi}_I$ and $\hat{\Pi}_{II}$ 67
3.2.5. Evaluation of $\hat{\sigma}_y^s$ and $\hat{\sigma}_z^s$ 70
3.3. The 'Cheshire Cat' - a quantum paradox 77

4. Spin weak values in a neutron polarimeter **85**
4.1. The experimental setup 85
4.1.1. DC1 adjustment 85
4.1.2. DC2 adjustment 87
4.1.3. Pre and post selection of the spin state 88
4.2. Raw data 89
4.3. Measurement results 92
4.4. Discussion of the measurement results and concluding remarks 96

5. Conclusion **98**

A. Acknowledgement **99**

Bibliography **100**

1. Introduction

Quantum mechanics is one of the most successful physical theories of the last century [1]. However, it is not at all intuitively conceivable. The theoretical physicist Michio Kaku put this the following way:
'*It is often stated that of all the theories proposed in this century, the silliest is quantum theory. In fact, some say that the only thing that quantum theory has going for it is that it is unquestionably correct.*' [2]
One of the most problematic aspects of quantum mechanics is the measurement process [3]. It is well known that any system that gets measured, is disturbed in some way through the measurement [4]. It is interesting to ask what happens if the disturbance on the system gets smaller and smaller, i.e. if the interaction strength is reduced. To describe the evolution of a system under the influence of a measurement with very little interaction strength, the theory of weak measurements was developed [5]. In a so called weak measurement the disturbance of the system is reduced to a minimal amount. A weak measurement is a slight change in the particle's impulse or a very small rotation of the particle's spin. The theory predicts that, if weak measurements are combined with well prepared und analyzed ensembles, surprising effects occur. This preparation is generally called pre selection of the ensemble, the analysis post selection. One example for those strange effects are eigenvalues that lie outside the eigenvalue range of an operator. Imagine for example to measure the value 100 for the spin of a spin-(1/2) particle [5]. Such a large eigenvalue is called a weak value. Moreover, the weak value can be interpreted as the ensemble's eigenvalue between pre and post selection. This means that for anything that interacts with the system in the weak regime it really looks like the ensemble has the impossible large spin value. Strange as this may seem, it has already been experimentally confirmed in an experiment using photons [6]. While performing experiments with weak values it has also been found that they can be used as a mean of amplification.
All experiments involving weak measurements and weak values, that were performed so far, used photons [6–8]. There are no experiments using matter waves. The use of massive particles like electrons [9], neutrons [10], atoms or molecules [11] in experiments is of prime importance to further develop the theory of weak measurements, since experiments involving photons only, do not actually need quantum mechanics, but can be explained classically as well in many cases. Since the neutron spin can be considered as a two level quantum system, it is possible to come up with neutron polarimeter experiments to extract the weak value of the spin operator. If an interferometer is used the spin can be combined with another two level quantum system: the path. This allows to test how weak measurements come into play with the topic of complementarity and wave particle duality. The path degree of freedom can be used to extract the spin weak value and vice versa. Additionally it can be shown that the weak value itself is accessible without a weak measurement using neutrons. This raises the question about the meaning of the weak value outside the weak regime. While some say, that the weak value is only defined through weak measurements, others claim, that it is simply a transition probability amplitude [12]. To answer those questions novel experiments have to be carried out. How such experiments could be designed is shown in the following chapters.

2. Theoretical background

The first chapter of this thesis gives a short overview of the concept of measurements in quantum mechanics. After that the idea and the theoretical treatment of so called weak measurements are presented. To elucidate this unfamiliar concept several experiments dealing with it are discussed.

2.1. Measurements in quantum mechanics

Let $|a'\rangle$ be the eigenket of a Hermitian operator $\hat{A}$ that represents some observable, so that

$$\hat{A}|a'\rangle = a'|a'\rangle, \tag{2.1}$$

where a' is called the eigenvalue of $\hat{A}$.[a]
An arbitrary ket $|\alpha\rangle$ can now be expressed as a linear superposition of those eigenkets

$$|\alpha\rangle = \sum_{a'} c_{a'}|a'\rangle = \sum_{a'} |a'\rangle\langle a'|\alpha\rangle. \tag{2.2}$$

Similarly the operator itself can be expanded in the same basis

$$A = \sum_{a'} a'|a'\rangle\langle a'|. \tag{2.3}$$

Therefore before a measurement of the observable $\hat{A}$ is made, the system is assumed to be in a superposition of many states [13].
Take for example a spin $\frac{1}{2}$ particle, e.g. a neutron. The spin-wave function of such a particle can be constructed by a superposition of the two states $|S_z;+\rangle$ and $|S_z;-\rangle$, where $|S_z;+\rangle$ describes the spin state aligned parallel to the z-axis and $|S_z;-\rangle$ that anti parallel. These two states are orthogonal and form a basis, which can be used to express arbitrary states in the spin space. In this basis the $\hat{S}_z$ operator can be written as

$$\hat{S}_z = \frac{\hbar\hat{\sigma}_z^s}{2} = \frac{\hbar}{2}\left(|S_z;+\rangle\langle S_z;+| - |S_z;-\rangle\langle S_z;-|\right), \tag{2.4}$$

where $\hat{\sigma}_z^s$ is the Pauli spin matrix. The most general spin wave function is given by

$$|\psi_s\rangle = |\hat{S}\cdot\hat{n};+\rangle = \cos\left(\frac{\theta}{2}\right)\mathrm{e}^{-i\phi/2}|S_z;+\rangle + \sin\left(\frac{\theta}{2}\right)\mathrm{e}^{i\phi/2}|S_z;-\rangle, \tag{2.5}$$

[a] If there are two (or more) linearly independent eigenkets of $\hat{A}$ having the same eigenvalue, then the eigenvalues of the two eigenkets are said to be degenerate. For the following considerations we assume that we are dealing with nondegenerate systems.

where θ and ϕ describe the polar and the azimuth angle, with respect to the z-axis, respectively. For $\phi = 0$ and $\theta = 0$ the spin state is aligned parallel to the z-axis.
Now the following question arises: What happens if a measurement takes place? A measurement disturbs the quantum system in a way that the wave function collapses into a single state [14]. More precisely, if the measurement yields the eigenvalue a' then the system collapses into the eigenstate $|a'\rangle$. Quantum mechanics does not allow us to predict the outcome of the measurement in advance, i.e. we do not know in which state the wave function is going to collapse. However, it is possible to calculate the probability P that a certain experimental outcome will occur. The relation

$$P(a') \equiv \langle a'|\alpha\rangle\langle\alpha|a'\rangle = |\langle a'|\alpha\rangle|^2 \tag{2.6}$$

states the probability that the outcome a' is detected when the observable $\hat{A}$ is measured. One can further define the expectation value $\langle\hat{A}\rangle$ of the observable $\hat{A}$ as

$$\langle\hat{A}\rangle \equiv \frac{\langle\alpha|\hat{A}|\alpha\rangle}{\langle\alpha|\alpha\rangle}, \tag{2.7}$$

which can be regarded as the average value of the measurement, if many measurements of the same observable $\hat{A}$ are repeated. Often it is simply given by $\langle\hat{A}\rangle = \langle\alpha|\hat{A}|\alpha\rangle$, but it is important to bear in mind that this form is only valid as long as the state $|\alpha\rangle$ is normalized.
Since this concept is very important let us consider an experimental example, that can be realized easily using the techniques of neutron optics. Suppose some device prepares a quantum state in a way that its wave function is given by

$$|\psi\rangle = |S_x;+\rangle = \sqrt{\frac{1}{2}}\left(|S_z;+\rangle + |S_z;-\rangle\right). \tag{2.8}$$

Now imagine that we perform a measurement of the spin's z-component. The probability of detecting neutrons with a $(S_z;+)$-spin component is

$$P(S_z;+) = \langle S_z;+|\left(\sqrt{\frac{1}{2}}|S_z;+\rangle + \sqrt{\frac{1}{2}}|S_z;-\rangle\right)\left(\sqrt{\frac{1}{2}}\langle S_z;+| + \sqrt{\frac{1}{2}}\langle S_z;-|\right)|S_z;+\rangle = \frac{1}{2}, \tag{2.9}$$

which means that we have a 50% chance of detection. Since the system is described only by a superposition of two eigenstates, this also means, that we have an equal probability to detect a neutron with $(S_z;-)$-spin component. The expectation value of $\hat{\sigma}_z^s$ is given by

$$\begin{aligned}\langle\hat{\sigma}_z^s\rangle &= \left(\sqrt{\frac{1}{2}}\langle S_z;+| + \sqrt{\frac{1}{2}}\langle S_z;-|\right)\left(|S_z;+\rangle\langle S_z;+| - |S_z;-\rangle\langle S_z;-|\right)\times \\ &\quad\times\left(\sqrt{\frac{1}{2}}|S_z;+\rangle + \sqrt{\frac{1}{2}}|S_z;-\rangle\right) \\ &= \left(\sqrt{\frac{1}{2}}\langle S_z;+| + \sqrt{\frac{1}{2}}\langle S_z;-|\right)\left(\sqrt{\frac{1}{2}}|S_z;+\rangle - \sqrt{\frac{1}{2}}|S_z;-\rangle\right) \\ &= \left(\frac{1}{2} - \frac{1}{2}\right) = 0,\end{aligned} \tag{2.10}$$

which makes perfect sense. The z-component of the state $|S_x;+\rangle$ is zero. For each measurement we have an equal chance of detecting the positive eigenvalue $+\frac{1}{2}$ and the negative one $-\frac{1}{2}$. If we perform many measurements our measurements will yield an average of zero.
To summarize, a quantum system can be described as a superposition of eigenstates. A measurement yielding an eigenvalue disturbs it in a way, that its wave function collapses into the corresponding eigenfunction. Such a measurement is called a 'strong' measurement. Quantum mechanics forbids us to predict the outcome of each measurement with certainty, however Eq. (2.6) allows us to calculate the probability of a certain outcome and Eq. (2.7) yields the average value when many measurements are performed.

2.2. Weak measurements

Quantum-mechanically a measurement of the observable $\hat{A}$ can be described by an interaction Hamiltonian $\hat{H}_i$, between the quantum system and the measurement apparatus. This leads to an evolution of the system according to

$$|\psi(t)\rangle = U(t,t')|\psi(t')\rangle, \tag{2.11}$$

with the time evolution operator $U(t,t')$, which is defined as

$$U(t,t'=0) \equiv U(t) = \mathrm{e}^{-i\hat{H}_i t}, \tag{2.12}$$

with $\hbar = 1$ for simplicities sake. The standard form of an interaction Hamiltonian is given by

$$\hat{H}_i = -g(t)\hat{q}\hat{A}, \tag{2.13}$$

where $\hat{q}$ is a canonical variable of the measuring device. $\hat{p}$ is the conjugate momentum to $\hat{q}$ and $g(t)$ is a normalized function such that its time integral is unity. The difference $p_f - p_i$ between the device's final and initial value is called its pointer reading and registers the value of $\hat{A}$ [3]. A real measuring device's initial wave function $|\Phi_i\rangle$ is a Gaussian with spread Δp centered around $p = 0$, i.e

$$|\Phi_i\rangle = \int \mathrm{d}p\ \mathrm{e}^{-\Delta^2 p^2}, \tag{2.14}$$

where $\Delta q \equiv \Delta$ and $\Delta p = \frac{1}{(2\Delta)}$ are the spread in q and p space respectively. Again $\hbar$ was set equal to one. According to Eq. (2.2), the quantum system's initial state $|\Psi_i\rangle$ can be expanded in a linear superposition of eigenstates of $\hat{A}$. Let the whole system's wave function be $|\psi\rangle$. It consists of the measuring device's and the prepared systems's initial wave function coupled by the interaction Hamiltonian. It can be shown that it evolves into

$$\begin{aligned}
|\psi'\rangle &= \mathrm{e}^{-i\int \mathrm{d}t\ \hat{H}_i}|\psi\rangle = \mathrm{e}^{-i\int \mathrm{d}t\ \hat{H}_i}|\Psi_i\rangle|\Phi_i\rangle = \mathrm{e}^{i\int \mathrm{d}t\ g(t)\hat{q}\hat{A}}|\Psi_i\rangle|\Phi_i\rangle \\
&= e^{i\hat{q}\hat{A}}\sum_{a'} c_{a'}|a'\rangle \int \mathrm{d}q\ \exp\left(\frac{-q^2}{4\Delta^2}\right)|q\rangle = \sum_{a'} c_{a'} \int \mathrm{d}p \int \mathrm{d}q\ \mathrm{e}^{iq(a'-p)} \exp\left(\frac{-q^2}{4\Delta^2}\right)|a'\rangle|p\rangle \\
&= \sum_{a'} c_{a'} \int \mathrm{d}p\ \mathrm{e}^{-\Delta^2(p-a')}|a'\rangle|p\rangle
\end{aligned} \tag{2.15}$$

under the action of $\hat{H}_i$ [15]. Looking at Eq. (2.14) one has to distinguish between two cases: For small Δp the sum represents many single sharply peaked Gaussians, each centered around one of the eigenvalues a'. A sketch of how the wave function would look like can be seen in Fig. 2.1. The limit of $\Delta p \to 0$ represents the case for an ideal measurement. The measurement

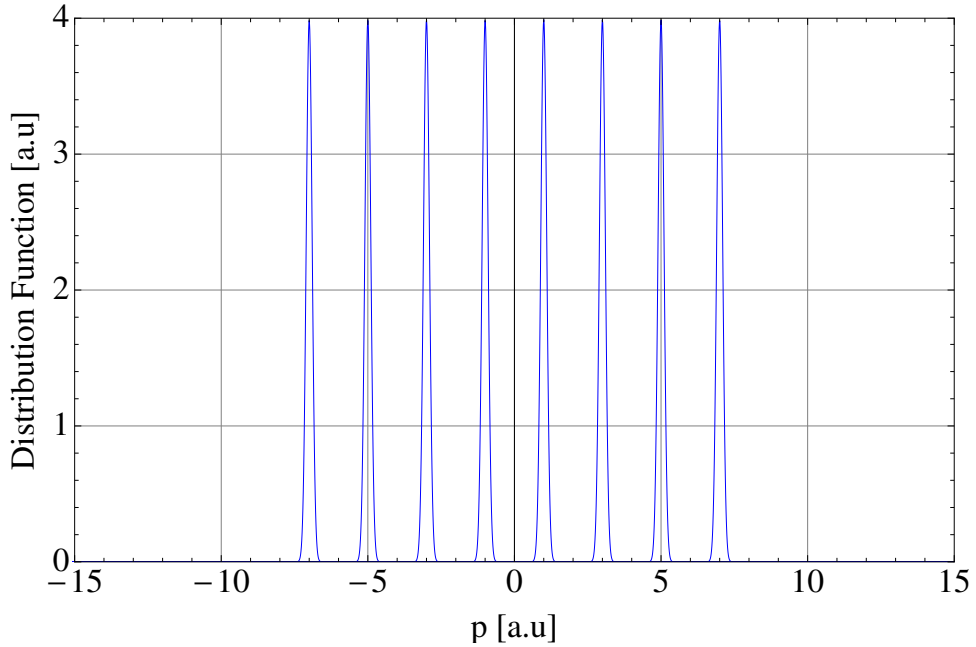

Figure 2.1.: Sketch of Eq. (2.14) for small Δp: Many single sharply peaked Gaussians around the eigenvalues a'.

will always yield an eigenvalue a' with the probability $P(a') = |c_{a'}|^2$ and the quantum state collapses into $|a'\rangle$ if a' is measured.
For large Δp, i.e. for the case of a weak measurement, the single spikes become a sum of strongly overlapping broad Gaussians, as can be seen in Fig. 2.2. The probability distribution for such a system will approximate a single, broad Gaussian peaked at the mean value of $\hat{A}$. It has to be stressed that a single measurement of this kind does not give any information about the quantum system, since the measuring device's initial spread in momentum space is much bigger than $\langle \hat{A} \rangle$, and one cannot distinguish the results of the measurements. Nevertheless it is possible, to obtain the whole probability distribution and find the mean value of $\hat{A}$, by repeating the same experiment over and over again.
Before developing the theory of weak measurements further one should bear in mind the most important point presented so far: One of the key characteristics of an ideal or 'strong' measurement is a small initial pointer spread in momentum space, i.e. the pointers are distinguishable. In contrast to that, a weak measurement has a large, indistinguishable pointer spread. The most important point is, that a strong measurement will yield an eigenvalue, while a single weak measurement does not give any significant information about the system.
Very interesting effects arise, if a quantum system is post selected, i.e. if a strong measurement is performed right after the weak one. This leads to a collapse of the wave function into a certain eigenstate

$$|\Psi_f\rangle = |b'\rangle = \sum_{a'} c'_{a'} |a'\rangle, \tag{2.16}$$

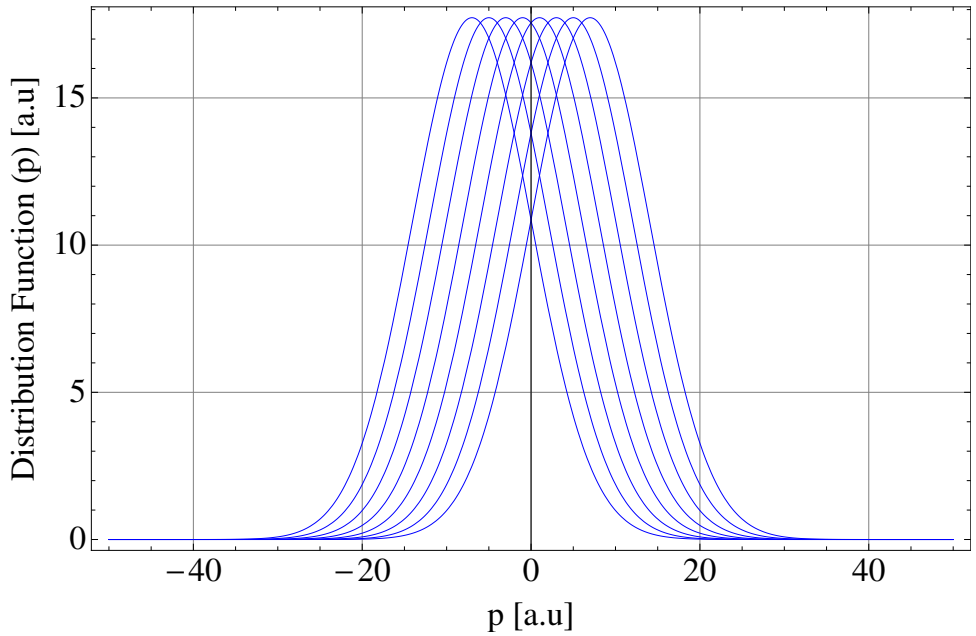

Figure 2.2.: Sketch of Eq. (2.14) for big Δp: The Gaussians are now very broad and overlap strongly.

and therefore

$$|\Phi_f\rangle = \langle\Psi_f|\Phi_i\rangle = \sum_{a'} c_{a'} c'^{*}_{a'} \int \mathrm{d}p \; \mathrm{e}^{-\Delta^2(p-a')}|p\rangle. \tag{2.17}$$

With the wave function in Eq. (2.17), it is possible to calculate a probability distribution, which is given by a sum of Gaussians with complex coefficients. This can lead to complicated cancellation effects capable of producing a distribution, whose peak is shifted far to one side. This shift makes it possible to measure eigenvalues far outside their range, in some cases.
This effect was first studied by Yakir Aharanov, David Albert and Lev Vaidman (AAV) in 1988 [5]. They showed that the effects of weak measurements can be understood by simply Taylor expanding the quantum system's evolution caused by the measuring process, which leads to the definition of the weak value.

$$\begin{aligned}
|\Phi_f\rangle = \langle\Psi_f|\Phi_i\rangle &= \langle\Psi_f|\mathrm{e}^{i\hat{q}\hat{A}}|\Psi_i\rangle|\Phi_i\rangle \approx \left(\langle\Psi_f|\Psi_i\rangle + i\hat{q}\langle\Psi_f|\hat{A}|\Psi_i\rangle + \cdots\right)|\Phi_i\rangle \\
&\equiv \langle\Psi_f|\Psi_i\rangle\left(1 + i\hat{q}\langle\hat{A}\rangle_w + \cdots\right)|\Phi_i\rangle \approx \langle\Psi_f|\Psi_i\rangle \int \mathrm{d}q \; \mathrm{e}^{i\hat{q}\langle\hat{A}\rangle_w} \exp\left(\frac{-q^2}{4\Delta^2}\right)|q\rangle \\
&= \langle\Psi_f|\Psi_i\rangle \int \mathrm{d}q \; \mathrm{e}^{-i\Delta^2\left(p-\langle\hat{A}\rangle_w\right)^2}|p\rangle
\end{aligned} \tag{2.18}$$

Eq. (2.18) describes a single broad Gaussian centered on $\langle\hat{A}\rangle_w$. It is defined as

$$\langle\hat{A}\rangle_w \equiv \frac{\langle\Psi_f|\hat{A}|\Psi_i\rangle}{\langle\Psi_f|\Psi_i\rangle} \tag{2.19}$$

and it can be interpreted as the ensemble's eigenvalue between pre and post selection. If $|\Psi_i\rangle$ or $|\Psi_i\rangle$ are eigenstates of $\hat{A}$, the weak value is equal to the strong one. $\langle\hat{A}\rangle_w$ is not bound by the eigenvalues and may yield very large outcomes [15].
In addition to that the weak value can in general be a complex quantity. What is the physical meaning of the imaginary part of the weak value? It can be shown [16] that the weak measurement causes a translation of the pointer wave function and there is a contribution to the pointer's mean position shift that is proportional to the imaginary part of $\langle\hat{A}\rangle_w$ and the rate at which the pointer is spreading in space as it enters the measurement interaction.

2.2.1. Spin-(1/2) particles and weak measurements

In a theoretical consideration of weak measurements an experiment was found that yields very surprising outcomes: AAV proposed to measure the weak spin value of a spin-(1/2) particle using two sequential Stern-Gerlach magnets [5]. This experiment is now briefly explained:
A beam of spin-(1/2) particles is prepared so that their spins are aligned with the positive z-axis.[b] The particle's spin is now slightly rotated around the y-axis so that it encloses an angle α with the x-axis. After this preparation of the ensemble (the pre selection) the particles spin state is given by

$$|\Psi_i\rangle = \cos\left(\frac{\alpha}{2}\right)|S_x;+\rangle + \sin\left(\frac{\alpha}{2}\right)|S_x;-\rangle \tag{2.20}$$

Its spatial wave function shall have a Gaussian shape of width Δ in the z-direction. Now a weak measurement of the spin's z-component is performed, using a Stern-Gerlach magnet. The interaction Hamiltonian for such a device is represented by

$$\hat{H}_i = -\phi\hat{\sigma}_z^s\hat{z}, \tag{2.21}$$

where the parameter ϕ describes the interaction strength, $\hat{\sigma}_z^s$ is the Pauli spin operator and $\hat{z}$ is the position operator. The condition for weak measurements is met by making ϕ very small. Since the interaction strength of the first Stern-Gerlach apparatus is very small, the beam splitting is also very small. The beam is not sufficiently separate, to distinguish the two spin components. Immediately after the first measurement a second, strong measurement is performed. The beam is split into two components corresponding to $|S_x;+\rangle$ and $|S_x;-\rangle$. The post selection is performed by picking up only the $|S_x;+\rangle$ part, using a position sensitive detector. With the definition of the weak value

$$\begin{aligned}\langle\hat{\sigma}_z^s\rangle_w &\equiv \frac{\langle\Psi_i|\hat{\sigma}_z^s|\Psi_f\rangle}{\langle\Psi_i|\Psi_f\rangle} = \frac{\langle S_x;+|\left[|S_z;+\rangle\langle S_z;+| - |S_z;-\rangle\langle S_z;-|\right]\left[\cos\left(\frac{\alpha}{2}\right)|S_x;+\rangle + \sin\left(\frac{\alpha}{2}\right)|S_x;-\rangle\right]}{\langle S_x;+|\left[\cos\left(\frac{\alpha}{2}\right)|S_x;+\rangle + \sin\left(\frac{\alpha}{2}\right)|S_x;-\rangle\right]} \\ &= \frac{\langle S_x;-|\left[\cos\left(\frac{\alpha}{2}\right)|S_x;+\rangle + \sin\left(\frac{\alpha}{2}\right)|S_x;-\rangle\right]}{\langle S_x;+|\left[\cos\left(\frac{\alpha}{2}\right)|S_x;+\rangle + \sin\left(\frac{\alpha}{2}\right)|S_x;-\rangle\right]} = \frac{\sin\left(\frac{\alpha}{2}\right)}{\cos\left(\frac{\alpha}{2}\right)} = \tan\left(\frac{\alpha}{2}\right)\end{aligned} \tag{2.22}$$

and Eq. (2.18), one gets

$$|\psi'\rangle = \langle p|\Phi_f\rangle = \cos\left(\frac{\alpha}{2}\right)\exp\left[-\Delta^2\left(p_z - \phi\tan\left(\frac{\alpha}{2}\right)\right)^2\right], \tag{2.23}$$

[b] The coordinate system is chosen in the following way: The y-axis coincides with the direction of propagation, the z-axis is parallel to the particle's initial spin direction and the x-axis forms a right handed system with the other two axes.

The distribution of p_z is given by

$$P(p_z) = |\langle\psi'|\psi'\rangle|^2 = |\langle p|\Phi_f\rangle|^2 = \cos\left(\frac{\alpha}{2}\right)^2 \exp\left[-2\Delta^2\left(p_z - \phi\tan\left(\frac{\alpha}{2}\right)\right)^2\right]. \tag{2.24}$$

The position sensitive detector makes it possible to measure this distribution, which will be centered around the value $\langle\hat{\sigma}_z^s\rangle_w$. But if α approaches a value close to π, $\tan\left(\frac{\alpha}{2}\right)$ can become far larger than one and it is possible to obtain an arbitrary large value for the z-spin component of a spin-(1/2) particle!
Not long after AAV published their first paper, a controversy about the physical sense of weak measurements arose [17–19]. Does it really make sense to claim that one is able to measure, say 100, for the a spin-component of a spin-(1/2) particle?
In 2010 Aharonov together with Sandu Popescu and Jeff Tollaksen elucidated the topic with a gedankenexperiment involving spin-(1/2) particles [20]:
At time t_0 it starts with an ensemble of particles whose spin is aligned parallel to the z-axis (preselection). At some later time t_1 a measurement of the x-spin component is performed and only the particles with their spin aligned parallel to the x-axis, i.e. with the spin state $|S_x;+\rangle$, are selected (post selection). Thus it seems that at any time $t_0 < t < t_1$ the spin of the post selected particles has a well defined spin component in both the z- and the x-direction.
The whole problem becomes even more complicated if you ask what happens if you evaluate $\hat{\sigma}^s_{\pi/4}$, the spin of one particle along a direction in the xy-plane making an angle of $\frac{\pi}{4}$ with the axis. The operator for this a measurement is

$$\hat{\sigma}^s_{\pi/4} = \sqrt{\frac{1}{2}}\left(\hat{\sigma}^s_x + \hat{\sigma}^s_z\right). \tag{2.25}$$

In this case, both spin components seem to be well defined and therefore one could naively think that the measurement result will be $\hat{\sigma}^s_{\pi/4} = \sqrt{2}$: This is obviously wrong, since the spin component in any direction can only be 1, if $\hat{\sigma}^s_j$ is evaluated. So where is the mistake?
The answer is rather simple. $\hat{\sigma}^s_x$ and $\hat{\sigma}^s_z$ are noncommuting observables and cannot be well defined at the same time. It is impossible to measure both at the same time. If either $\hat{\sigma}^s_x$ or $\hat{\sigma}^s_z$ are measured the quantum system will be disturbed and we will not find the large value, which we expected.
However, weak measurements make it possible to measure the spin component of a large number N of particles without significantly disturbing the system. Take for example N spin-(1/2) particles all in the $|S_z;+\rangle$ state at t_0 and thanks to a successful post selection all of them are in the $|S_x;+\rangle$ state at some later time t_1. At a time $t_0 < t < t_1$ a nondisturbing measurement of $\hat{\sigma}^s_x$ and $\hat{\sigma}^s_z$ is performed. Since neither measurement disturbs the other, they can be done simultaneously and we will get the result

$$\hat{\sigma}^s_{\pi/4} = \sqrt{\frac{1}{2}}\left(\hat{\sigma}^s_x + \hat{\sigma}^s_z\right) = \sqrt{2}\ N \pm \sqrt{N}. \tag{2.26}$$

So what is the physical meaning of this result? Does it really mean that the ensemble has the impossible large spin value?
The weak measurements are imperfect and hence they are afflicted with a large uncertainty. What we are dealing with is really a measurement error. But, and here comes the interesting point, this error is not random, it has to occur if the post selection succeeds and in every interaction in the weak regime the system does behave as if is has the impossible large value.
In contrast to ideal measurements, weak ones are not able to give any significant information

about a single particle. All they can yield is the ensemble average. However, by choosing a cleverly pre- and post selected ensembles, this ensemble average can behave unexpectedly. It can even lie far outside the region of eigenvalues. At this point it is very important to emphasize, that weak measurements do not contradict quantum mechanics. They are a necessary consequence of quantum mechanic's mathematical structure. As the next section shows, many experiments have been performed, that confirm the predictions made by the theory of weak measurements.

2.3. Associated experiments

This section is devoted to three different experiments dealing with weak values. At the beginning the first realization of a weak measurement is presented, which showed that weak measurements can be used as a means of amplification. The second experiment shows such an amplified weak value measurement. The third experiment makes use of weak measurements in order to extract the average trajectory, i.e. practically the Pointing vector, of an ensemble of photons in a double slit interferometer.

2.3.1. First realization of a weak measurement

In 1991 the first experiment, which was able to confirm the predictions made by the theory of weak measurements was conducted by N. W. M. Ritchie, J.G. Story and Randall G. Hulet at the University of Texas [6]. It is an optical analogue to the experiment proposed by AAV, discussed in section 2.2.
Instead of a beam of spin-(1/2) particles a Gaussian mode laser beam was used. The pre- and post selection are carried out using optical polarizers. The weak measurement was done by a birefringent-crystalline quartz, which caused a very small beam splitting. A schematic diagram of the setup can be seen in Fig. 2.3 The electric field vector of the laser beam after passing through the first polarizer $\vec{E}_i$ (pre selection) is given by

$$\vec{E}_i(x,y) = E_0 \exp\left(-\frac{x^2+y^2}{w_0^2}\right)\left[\cos(\alpha)\,\hat{e}_x + \sin(\alpha)\,\hat{e}_y\right], \tag{2.27}$$

where w_0 describes the width of the laser beam. The coordinate system was chosen such that the direction of propagation coincides with the z-axis, and the polarization is linear with at angle α with respect to the x-axis. Together with the y-axis the two build a right handed coordinate system.
Now the weak measurement is performed, by using a birefringent crystal. The crystal separates the two orthogonal linear polarization components of the field. The condition of a weak measurement is met by making the separation a of the beam very small compared to the beam width, i.e. $a \ll w_0$, making it impossible to distinguish the two beams.[c]. After the weak measurement the electric field vector $\vec{E}_w$ becomes

$$\vec{E}_w(x,y) = E_0 \exp\left(\frac{-x^2}{w_0^2}\right)\left[\cos(\alpha)\exp\left(\frac{-(y+a)^2}{w_0^2}\right)\hat{e}_x + \sin(\alpha)\exp\left(\frac{-y^2}{w_0^2}\right)\hat{e}_y\right]. \tag{2.28}$$

[c]The beam width w_0 was given by $w_0 = 55\mu m$ compared to a beam separation of $a \approx 0.64\mu m$

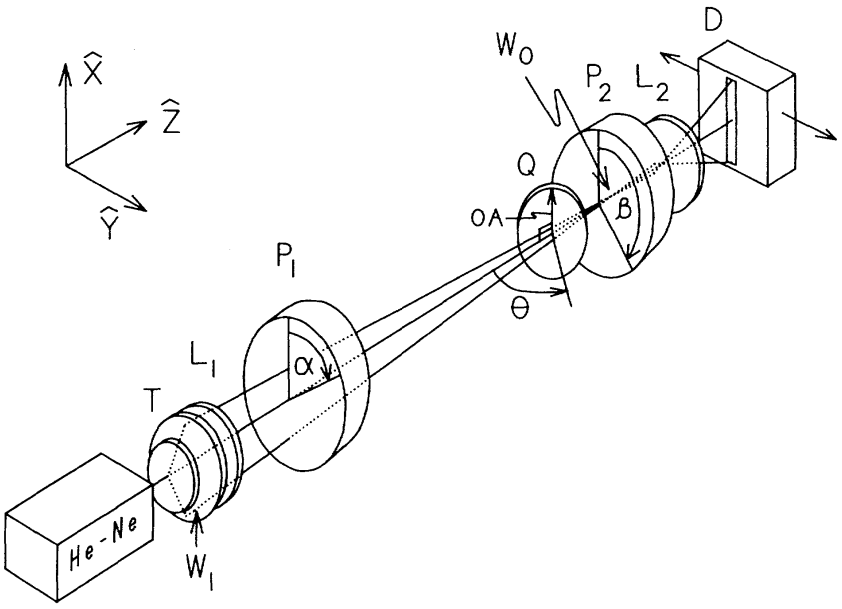

Figure 2.3.: A schematic diagram of the setup, that realized the first weak measurement: The photons are produced by a He-Ne Laser, then collimated by a lens system (T,L1), before they pass through the first polarizer (P1). The weak measurement is done by a birefringent-crystalline quartz (Q). Finally the ensemble is post selected via the second polarizer (P2) and detected (L2,D) [6].

Then the post selection is performed using the second polarizer, which is aligned at an angle β withe respect to the x-axis. The electric field vector after post selection $\vec{E}_f$ is given by

$$\vec{E}_f(x,y) = E_0 \exp\left(\frac{-x^2}{w_0^2}\right)\left[\cos(\alpha)\cos(\beta)\exp\left(\frac{-(y+a)^2}{w_0^2}\right) + \right.$$
$$\left. + \sin(\alpha)\sin(\beta)\exp\left(\frac{-y^2}{w_0^2}\right)\right]\left[\cos(\beta)\,\hat{e}_x + \sin(\beta)\,\hat{e}_y\right] \tag{2.29}$$

Taking the absolute square of the Eq. (2.29) at $x = 0$ yields the intensity distribution along the y-axis.

$$I(y) = I_0\left[\cos^2(\alpha)\cos^2(\beta)\exp\left(\frac{-2(y+a)^2}{w_0^2}\right) + \sin^2(\alpha)\sin^2(\beta)\,exp\left(\frac{-2y^2}{w_0^2}\right) + \right.$$
$$\left. +2\cos(\phi)\cos(\alpha)\cos(\beta)\sin(\alpha)\sin(\beta)\exp\left(\frac{-(y+a)^2+y^2}{w_0^2}\right)\right] \tag{2.30}$$

Looking at Eq. (2.30), three different cases have to be distinguished.

1. If the first and the second polarizer are aligned in the same way, i.e $\alpha = \beta = \frac{\pi}{2}$, the intensity profile is a single broad Gaussian centered at $y = 0$. This single broad profile is really a superposition of two Gaussians that are shifted by the beam separation caused by the birefringent crystal. However, the separation is much smaller than the beam width

and therefore not visible. This situation is plotted in Fig. 2.4.

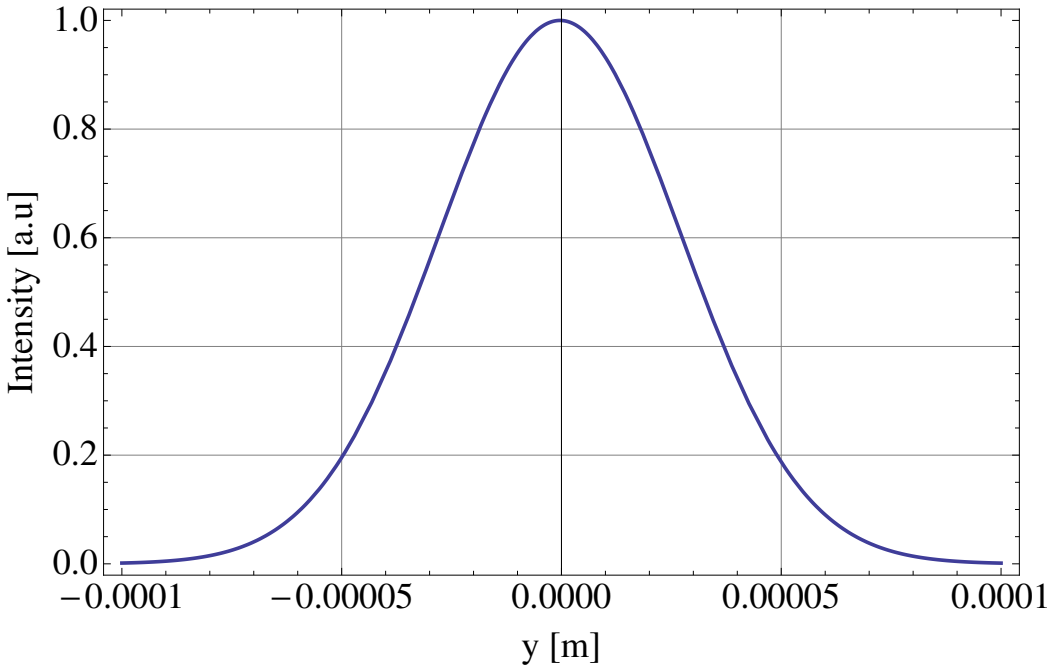

Figure 2.4.: Plot of Eq. (2.30) for $\alpha = \beta = \frac{\pi}{2}$: The intensity profile appears to be one single Gaussian. The small beam separation a is not visible.

2. If the first polarizer is adjusted to an angle of $\alpha = \frac{\pi}{4}$ and the second one to an angle of $\beta = \frac{3\pi}{4} + 0.022$ a measurement of the weak value is performed. Initial and final state are nearly orthogonal. The Gaussian distribution is visible in Fig. 2.5. It is caused by a destructive interference of two Gaussian distributions and is centered around the weak value. Note the small intensity that occur for this case. We will come back to that shortly, but first we want to look at the last case we have to consider.

3. It occurs if $\alpha = \frac{\pi}{4}$ and $\beta = \frac{3\pi}{4}$. Now the final and the initial state are orthogonal and the weak value is no longer defined. As it is clearly visible from Fig. 2.6 the intensity profile shows two separate Gaussians. The separation between the two distributions is much bigger than the actual beam splitting, amplifying a by two orders of magnitude. This behavior shows that the concept of weak measurements can be applied to amplify signals. As with the previous case, the intensity is very low. This is due to the orthogonality of the pre and post selected states and presents a general problem when dealing with weak measurements. The interesting effects occur at very low intensities.

This experiment fully confirmed the predictions made by the theory of weak measurements. It is an impressive demonstration of what this technique is capable of and showed new possibilities for its applications for example as a means of amplification.

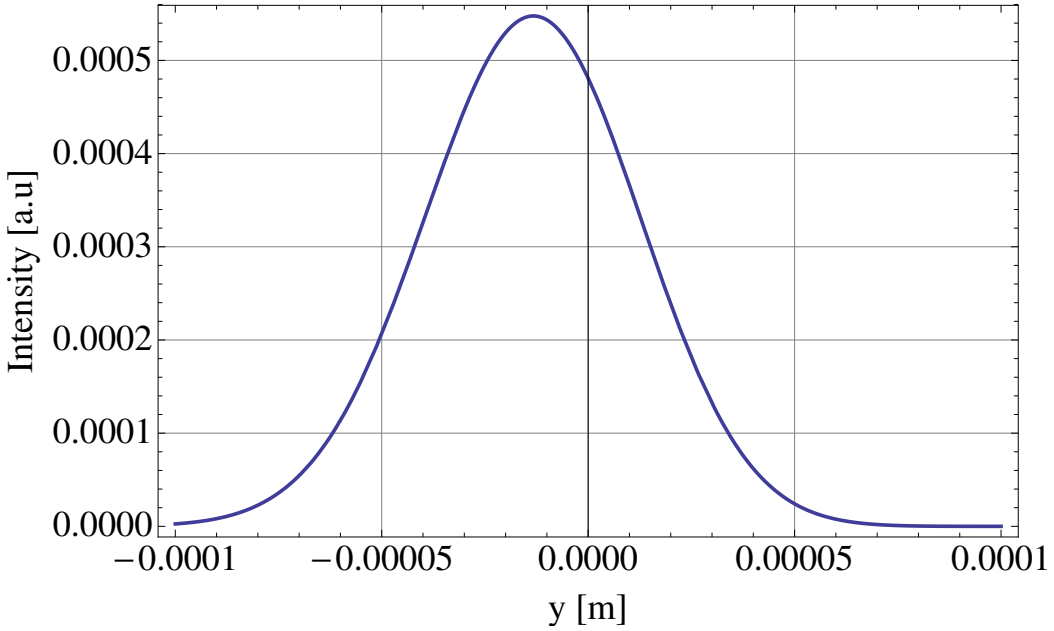

Figure 2.5.: Plot of Eq. (2.30) for $\alpha = \frac{\pi}{4}$ and $\beta = \frac{3\pi}{4} + 0.022$: This situation represents a weak measurement. The intensity profile is a single Gaussian shifted to one side, with a shift that is much greater than the beam separation caused by the birefringent crystal. Note that the intensity is now much lower than compared to the previous case.

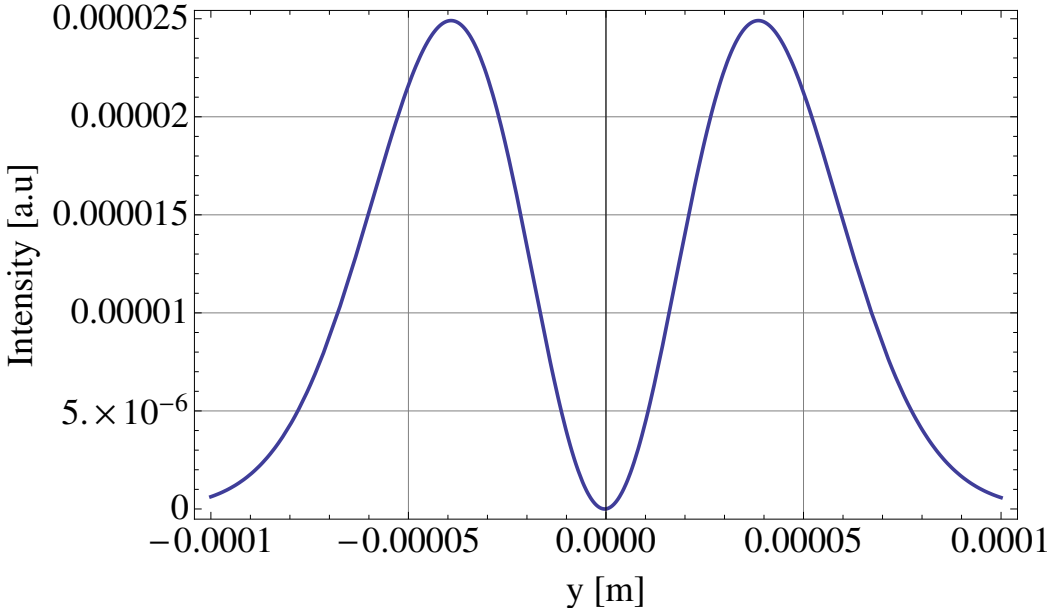

Figure 2.6.: Plot of Eq. (2.30) for $\alpha = \frac{\pi}{4}$ and $\beta = \frac{3\pi}{4}$: Initial and final state are now exactly orthogonal. The weak value is no longer defined. The intensity profile shows two separated beams, with a separation much greater than the one caused by the birefringent crystal, making it possible to use the technique of weak measurements for amplification.

2.3.2. Beam deflection measurement via interferometric weak value amplification

In 2009 P. B. Dixon, D. J. Starling, A. N. Jordan and J. C. Howell from the University of Rochester made use of the amplification effect discussed in the previous section to measure the beam deflection in an interferometer experiment [7].
The experimental setup basically consisted of a Sagnac interferometer and a Piezo driven mirror, that was used to slightly deflect the beams. This deflection is equal to a weak measurement.
A collimated laser beam entered the Sagnac interferometer through a polarizing 50/50 beam splitter. Half of the beam will travel clockwise along path I and the other half counter clockwise along path II. After the beam splitter the polarization is purely horizontal. In addition to that a phase shifter was added into the interferometer. The experimental setup can be seen in Fig. 2.7.

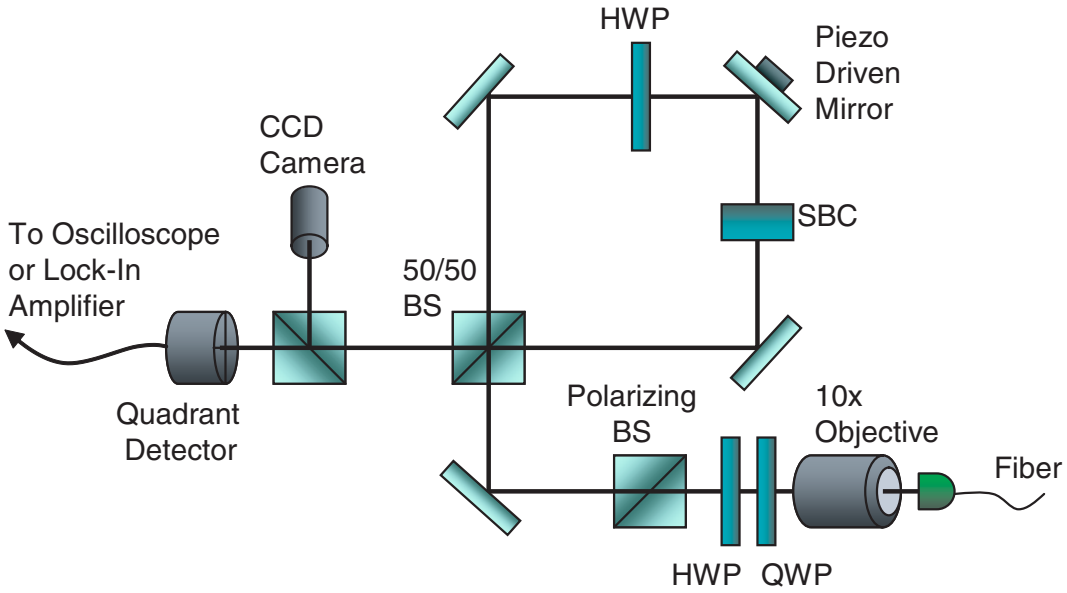

Figure 2.7.: A schematic diagram of the setup of the experiment performed by P. B. Dixon et al. [7]: After passing through polarization optics, the beam enters a Sagnac interferometer consisting of three mirrors and a 50/50 beam splitter arranged in a square. The piezo mirror gives a small beam deflection.

The preselected state is now

$$|\psi\rangle = |P_i\rangle|X\rangle = \sqrt{\frac{1}{2}}\left(\mathrm{e}^{-i\chi/2}|I\rangle + i\mathrm{e}^{i\chi/2}|II\rangle\right)|X\rangle, \tag{2.31}$$

where χ is the additional phase shift caused by the phase shifter and $|X\rangle$ describes the transverse position degree of freedom.
The weak measurement is now performed by slightly tilting the mirror at the symmetric point of the interferometer, using a piezo driven motor. This deflects the beams dependent on their direction of propagation. The condition of a weak measurement is met by making this deflection

very small. The interaction Hamiltonian for this process is given by

$$\hat{H}_i = k\hat{x}\hat{\Pi}_z \tag{2.32}$$

with $\hat{x}$ being the transverse position and k being the transverse momentum shift caused by the mirror. The operator $\hat{\Pi}_z$ is called path operator, which is represented by a Pauli matrix and given by

$$\hat{\Pi}_z = |I\rangle\langle I| - |II\rangle\langle II|. \tag{2.33}$$

The system's wave function $|\psi'\rangle$ after the interaction is

$$|\psi'\rangle = \mathrm{e}^{-ik\hat{x}\hat{\Pi}_z^p}|P_i\rangle|X\rangle = \left(1 - ik\hat{x}\hat{\Pi}_z^p\right)|P_i\rangle|X\rangle. \tag{2.34}$$

Because the condition $ka \ll 1$, with a being the initial beam size, is fulfilled, the measurement is weak. At the exit of the interferometer a projection onto the state $|P_f\rangle = \sqrt{\frac{1}{2}}\left(i|I\rangle + |II\rangle\right)$ is performed. This is the step of post selection.

$$\begin{aligned}\langle P_f|\psi'\rangle &= \langle P_f|\left(1 - ik\hat{x}\hat{\Pi}_z^p\right)|P_i\rangle|X\rangle = \langle P_f|P_i\rangle\left(1 - ik\hat{x}\underbrace{\frac{\langle P_f|\hat{\Pi}_z^p|P_i\rangle}{\langle P_f|P_i\rangle}}_{\equiv\langle\hat{\Pi}_z^p\rangle_w}\right)|X\rangle \\ &= \langle P_f|P_i\rangle \mathrm{e}^{-ik\hat{x}\langle\hat{\Pi}_z^p\rangle_w}|X\rangle\end{aligned} \tag{2.35}$$

The first part in Eq. (2.35) describes the probability that post selection will succeed. It is given by

$$\begin{aligned}P_{ps} = |\langle P_f|P_i\rangle|^2 &= \left|\frac{1}{2}\left(\mathrm{e}^{i\chi/2}\langle I| - i\mathrm{e}^{-i\chi/2}\langle II|\right)\left(i|I\rangle + |II\rangle\right)\right|^2 \\ &= \frac{1}{4}\left|i\mathrm{e}^{i\chi/2} - i\mathrm{e}^{-i\chi/2}\right|^2 = \frac{1}{2}\left(1 - \cos\left(\chi\right)\right) = \sin^2\left(\frac{\chi}{2}\right).\end{aligned} \tag{2.36}$$

The second part describes a momentum shift[d], that depends on the weak value and on the shift caused by the weak measurement. The weak value is

$$\begin{aligned}\langle\hat{\Pi}_z^p\rangle_w = \frac{\langle P_f|\hat{\sigma}_z^p|P_i\rangle}{\langle P_f|P_i\rangle} &= \frac{\left(\langle II| - i\langle I|\right)\left(|I\rangle\langle I| - |II\rangle\langle II|\right)\left(\mathrm{e}^{-i\chi/2}|I\rangle + i\mathrm{e}^{i\chi/2}|II\rangle\right)}{i\mathrm{e}^{i\chi/2} - i\mathrm{e}^{-i\chi/2}} \\ &= \frac{\mathrm{e}^{-i\chi/2} + \mathrm{e}^{i\chi/2}}{\mathrm{e}^{-i\chi/2} - \mathrm{e}^{i\chi/2}} = i\cot\left(\frac{\chi}{2}\right) \approx i\frac{2}{\chi},\end{aligned} \tag{2.38}$$

[d] Why does the term $e^{-ik\hat{x}\langle\hat{\Pi}_z^p\rangle_w}$ describe a momentum shift? This is not obvious at first sight, but the proof is really quite simple. $k\langle\hat{\Pi}_z^p\rangle_w \equiv \zeta$ has the dimension of a momentum. Let $|p\rangle$ be an arbitrary momentum eigenket, then

$$e^{-ix\zeta}|p\rangle = \left(1 + ix\zeta + \cdots\right)|p\rangle = |p\rangle - \zeta\frac{\partial}{\partial p}|p\rangle + \cdots = |p - \zeta\rangle, \tag{2.37}$$

which proves that $e^{-ix\zeta}$ is the translation operator in momentum space.

which can become much bigger than unity for small values of χ.
Even though the beam deflection caused by the mirror is very small, it gets amplified two orders of magnitude by the weak value. This setup made it possible to measure beam deflections of $400 \pm 200 frad$. The travel of the piezo actuator was measured to be $14 \pm 7 fm$, proving quite impressively what weak values are capable of. The experimental results can also be seen in Fig. 2.8.

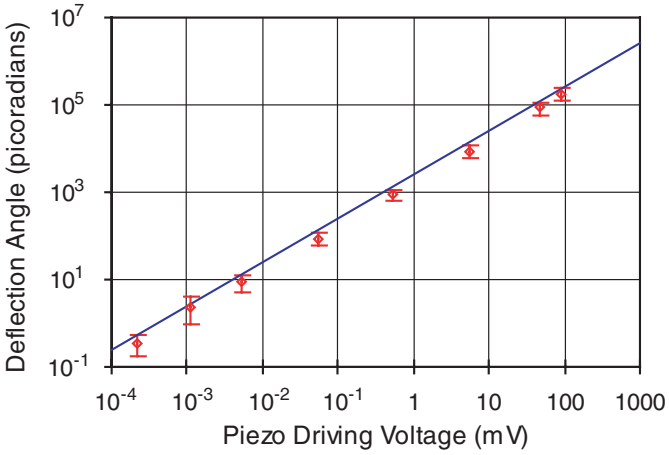

Figure 2.8.: Measurement results of the experiment performed by P. B. Dixon et al. [7]: Beam deflections as small as $400 \pm 200 frad$ were measured.

2.3.3. Average trajectories of single photons

In 2011 a group around Aephraim Steinberg at the Centre for Quantum Information and Control and Institute for Optical Sciences of the University of Toronto performed an experiment observing the average trajectories of single photons, i.e. the pointing vector, in a two-slit interferometer using weak measurements [8].
The basic experimental setup consisted of a quantum dot, that served as a source for single photons, a double slit interferometer, a polarizer used for preparing the states, a birefringent calcite crystal, which performed the weak measurement, a quarter wave plate to project the polarization state onto a certain axis and finally a position sensitive detector. It can be seen in Fig. 2.9.

A single photon was produced at the quantum dot. After passing through the double slit it was sent through a polarizer preparing it in the diagonal polarization state

$$|D\rangle = \sqrt{\frac{1}{2}} \left(|H\rangle + |V\rangle \right), \tag{2.39}$$

where $|H\rangle$ coincides with the horizontal polarization axis and $|V\rangle$ with the vertical one. Hence the photon's total wave function is given by

$$|\psi\rangle = |D\rangle|P\rangle, \tag{2.40}$$

where $|P\rangle$ describes its path.
Now the weak measurement of the photon's transverse moment k_x was performed. The photon's direction of propagation coincided with the z-axis. This was done by inserting a birefringent calcite crystal that changes the polarization of the photons passing through it by introducing a phase shift dependent on k_x. In agreement with the formalism introduced in section 2.2, the Hamiltonian for this interaction is given as $\hat{H}_i = g\hat{k}_x\hat{S}_x$. Therefore the photon's polarization wave function after the weak measurement can be expressed as[e]

$$\begin{aligned}
|\psi'\rangle &= \mathrm{e}^{-ig\hat{H}_i t}|\psi\rangle = \exp\left(\frac{-ig\hat{k}_x t}{2}\underbrace{|H\rangle\langle H| - |V\rangle\langle V|}_{\hat{\sigma}_x^s}\right)|\psi\rangle \\
&\approx \left(1 - \frac{ig\hat{k}_x t}{2}|H\rangle\langle H| - |V\rangle\langle V|\right)\sqrt{\frac{1}{2}}\left(|H\rangle + |V\rangle\right)|P\rangle \\
&= \sqrt{\frac{1}{2}}\left(|H\rangle + |V\rangle\right)|P\rangle - \frac{ig\hat{k}_x t}{2\sqrt{2}}\left(|H\rangle - |V\rangle\right)|P\rangle = \left(|D\rangle - \frac{ig\hat{k}_x t}{2}|A\rangle\right).
\end{aligned} \tag{2.41}$$

This way the weak measurement of the photon's transverse momentum is carried out using the polarization degree of freedom as a pointer. Now the post selection is performed. This is done by performing a strong measurement of the position of the photon, which is of course nothing

[e] $\hbar = 1$

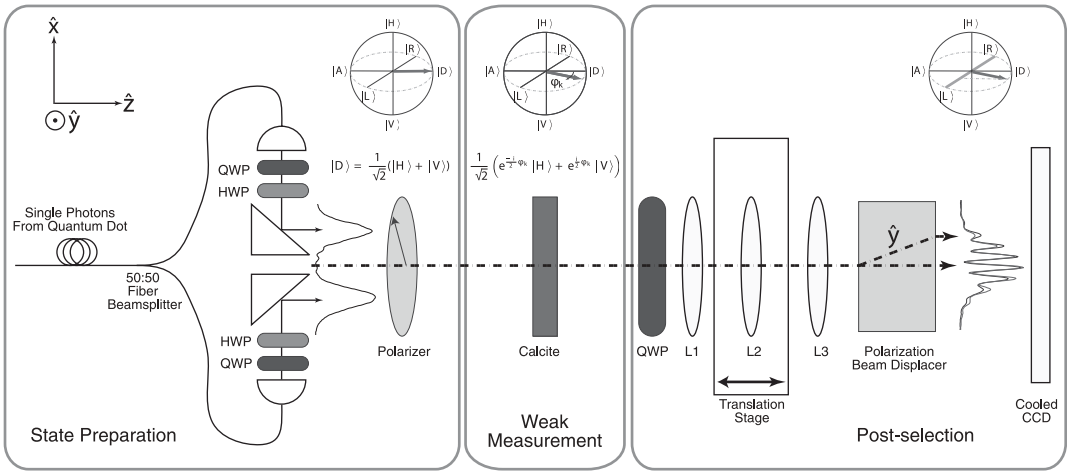

Figure 2.9.: Schematic drawing of the experiment performed by S. Kocsis et al. [8]: A quantum dot served as a source for single photons. A double slit interferometer and a polarizer were used to prepare the states. The birefringent calcite crystal performed the weak measurement and a quarter wave plate projected the polarization state onto a certain axis, which allowed the position sensitive detector to pick up the photons.

else than the detection of the photon on the CCD chip.

$$\begin{aligned}
\langle x_f|\psi'\rangle &= \langle x_f|P\rangle|D\rangle - \frac{igt}{2}\langle x_f|\hat{k}_x|P\rangle|A\rangle = \langle x_f|P\rangle \left(|D\rangle - \frac{igt}{2} \underbrace{\frac{\langle x_f|\hat{k}_x|P\rangle}{\langle x_f|P\rangle}}_{\equiv\langle\hat{k}_x\rangle_w} |A\rangle \right) \\
&\equiv \underbrace{\langle x_f|P\rangle}_{\psi(x_f)} \left(|D\rangle - \frac{igt}{2}\langle\hat{k}_x\rangle_w|A\rangle \right) \\
&= \psi(x_f) \left[\sqrt{\frac{1}{2}} \left(|H\rangle + |V\rangle \right) - \frac{igt}{2\sqrt{2}}\langle\hat{k}_x\rangle_w \left(|H\rangle - |V\rangle \right) \right] \\
&= \frac{\psi(x_f)}{\sqrt{2}} \left(|H\rangle - \frac{igt}{2}\langle\hat{k}_x\rangle_w|H\rangle + |V\rangle + \frac{igt}{2}\langle\hat{k}_x\rangle_w|V\rangle \right) \\
&= \frac{\psi(x_f)}{\sqrt{2}} \left[\mathrm{e}^{-igt/2\langle\hat{k}_x\rangle_w}|H\rangle + \mathrm{e}^{igt/2\langle\hat{k}_x\rangle_w}|V\rangle \right] \\
&= \frac{\psi(x_f)}{\sqrt{2}} \left[\mathrm{e}^{-i\phi(k_x)/2}|H\rangle + \mathrm{e}^{i\phi(k_x)/2}|V\rangle \right], \qquad (2.42)
\end{aligned}$$

where $\phi(k_x)$ is defined as $\phi(k_x) \equiv \frac{\zeta}{|k|}\langle\hat{k}_x\rangle_w$. ζ is a real parameter that describes the interaction strength. Eq. (2.42) shows, that the weak measurement adds a phase to the wave function. To measure this phase the projection onto the y-axis is performed. This is done using a quarter wave plate. Mathematically this means

$$\begin{aligned}
\langle\hat{\sigma}_y^s\rangle = \frac{|\psi(x_f)|^2}{2} &\left[\mathrm{e}^{i\phi(k_x)/2}\langle H| + \mathrm{e}^{-i\phi(k_x)/2}\langle V| \right] \underbrace{\left[|R\rangle\langle R| - |L\rangle\langle L| \right]}_{\hat{\sigma}_y^s} \times \\
&\times \left[\mathrm{e}^{-i\phi(k_x)/2}|H\rangle + \mathrm{e}^{i\phi(k_x)/2}|V\rangle \right] \qquad (2.43)
\end{aligned}$$

Using $|R\rangle = \sqrt{\frac{1}{2}}\left(|H\rangle - i|V\rangle\right)$ and $|L\rangle = \sqrt{\frac{1}{2}}\left(|H\rangle + i|V\rangle\right)$, basic algebra and the fact that $\psi(x_f)$ is normalized to unity yield

$$\langle\hat{\sigma}_y^s\rangle = -\sin\left[\phi(k_x)\right]. \qquad (2.44)$$

$\langle\hat{\sigma}_y^s\rangle$ is now measured using a beam displacer, which spatially separates photons with right hand side and left hand side polarization and allows to observe I_R and I_L separately. Because $\langle\hat{\sigma}_y^s\rangle$ is defined as

$$\langle\hat{\sigma}_y^s\rangle = \frac{I_L - I_R}{I_L + I_R}, \qquad (2.45)$$

the weak value is

$$\langle\hat{k}_x\rangle_w = \frac{|k|}{\zeta}\sin^{-1}\left(\frac{I_R - I_L}{I_R + R_L}\right). \qquad (2.46)$$

It is important to realize that the weak momentum value detected at the position x was already measured at the calcite crystal. The Hamiltonian of a freely propagating particle commutes

with the interaction Hamiltonian and the $\hat{\sigma}_j^s$ operator acts in a different Hilbertspace than the momentum operator. Because of that k_x is not changed in any way after the weak measurement has taken place.
As mentioned previously one weak measurement alone does not yield significant information about the system, because it is afflicted with a very large error. However, by repeating the same weak measurement over and over again, the weak value can be determined by a high degree of certainty. This is the reason why the experiment was performed with an ensemble of over 30,000 photons. The weak momentum value was mapped out for every x-position in a certain z-plane. After that the detector was moved in positive z-direction and the same procedure was performed again. By mapping out $\langle k_x \rangle_w$ at different z-values and connecting the corresponding weak momentum values it was possible to observe the average photon trajectories. The results of this measurement can be seen in Fig. 2.10. It cannot be stressed enough that single particles

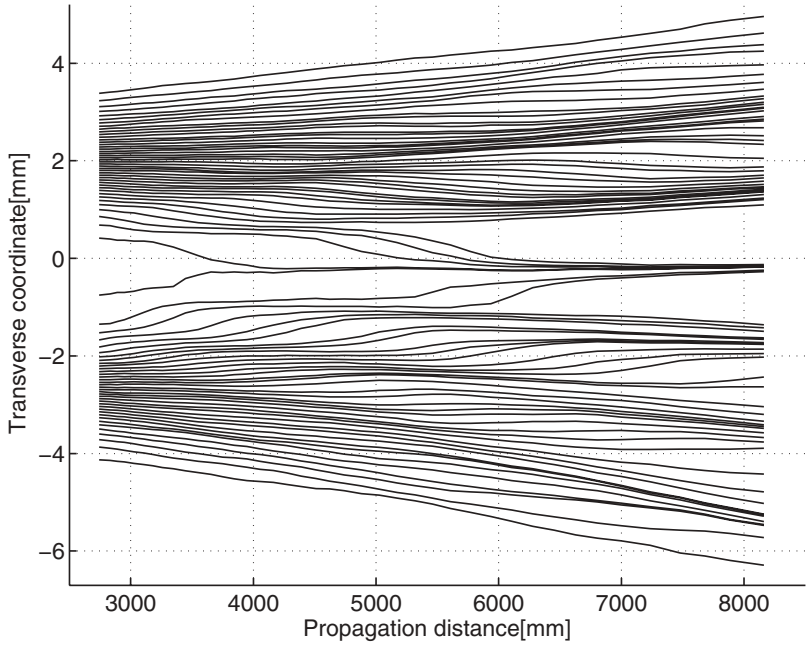

Figure 2.10.: Measurement results of the experiment performed by S. Kocsis et al. [8]: Weak measurements made it possible to map out the average photon trajectories in a double slit experiment.

are not constricted to these trajectories. It is impossible to follow the trajectories of a single particle and observe the interference pattern at the same time. Any attempt to do so would require a strong measurement and therefore alter the system in a way that destroys the interference. The weak momentum measurement does not disturb the system and the interference is still observed, but one measurement alone does not yield any useful information about the photon's momentum. By performing the same measurement over and over again one can map out the average particle trajectories and not more. One cannot simply trick quantum mechanics using weak measurements.
Naturally the question arises what kind of additional information the weak measurement yields that cannot be extracted from the final interference pattern itself. The interference patter alone does not tell us anything about the way the photons took after passing the double slit. It just shows where they are likely to be detected on the screen. The trajectories measured by Stein-

berg and his group tell us where the photons are likely to move, in order to get to the screen where they form the interference pattern. For example the experiment showed, that photons that passed the lower slit are very unlikely to pass the symmetry axis to the upper half of the screen.
As extraordinary the experiment performed by S. Kocsis et al. seems at the first look, there are several issues that are not addressed by them. First of all they repeatedly claim to have measured so called Bohmian trajectories for the photons. However, those trajectories are not defined for bosons. This is due to the fact, that it is not possible to construct a relativistic quantum mechanical theory for bosons with a conserved probability current density with a positive definite time component. All they did was to measure the pointing vector of the photons. In addition to that the system is purely photonic. Quantum mechanics is not needed to perform the calculations necessary for this experiment. Classical electrodynamics suffices. It would be more interesting if the experiment was conducted with matter waves.
Finally S. Kocsis et al. omit the fact that the weak value can be complex. It is not clear whether the real or imaginary part or the absolute of the weak value was measured.

2.4. Technique of neutron polarimeter optics

To gain further insight into the nature of weak measurements and weak values, for example how they come into play with the topic of complementarity and wave particle duality, it is necessary to perform experiments with matter waves. Optical experiments with neutrons are one of the most ideal tool for this kind of studies. At this point a brief overview of the technique and physics of neutron polarimeter optics is given.

2.4.1. Neutron spin

The neutron has a mass m of m = 1.6723×10^{-27} kg and a magnetic moment $|\vec{\mu}|$ of $|\vec{\mu}| = 9.66 \times 10^{-27}$J/T that is coupled to its spin of $\vec{S} = \frac{\hbar}{2}\hat{e}_i$, where $\hat{e}_i$ defines the quantization axis. Its magnetic moment and its spin are related by

$$\vec{\mu} = \gamma \vec{S}, \tag{2.47}$$

where γ is the so called gyromagnetic ratio. It is equal to $\gamma = -1.8301 \times 10^8$ $\mathrm{s}^{-1}\mathrm{T}^{-1}$ [21].
If an external magnetic field $\vec{B}$ acts on the neutron's magnetic moment, it tries to align it. Doing that it exerts a torque, which yields the following equation of motion

$$\frac{d\vec{S}}{dt} = -\gamma \vec{S} \times \vec{B} = \vec{S} \times \vec{\omega}_L, \tag{2.48}$$

where $\vec{\omega}_L = -\gamma \vec{B}$ is the so called Larmor frequency. Equation (2.48) shows that the change of $\vec{S}$ in time is normal to both $\vec{S}$ and $\vec{B}$. This means that $\vec{S}$ and therefore $\vec{\mu}$ precesses around the external field $\vec{B}$.
When the majority of the spins in a neutron beam are aligned in one direction, one is dealing

with polarized neutrons. In general the degree of polarization P is given by

$$P = \frac{I_+ - I_-}{I_+ + I_-}, \tag{2.49}$$

where I_+ is the intensity of neutrons with spin up and I_- is the intensity of spin down neutrons. Magnetic fields are necessary to either keep up or manipulate the direction of neutron's spin vector $\vec{S}$. To prevent depolarization[f] by the earth's magnetic or other stray fields, either a field free region has to be created or a magnetic field that is parallel to $\vec{S}$ has to be applied. Such a field is called guide field.
So what happens if the external magnetic field changes? The answer to this question is rather simple. If the field's direction changes slowly enough the neutron's spin follows the field direction. Slow means that the condition

$$\left| \frac{d}{dt} \left(\frac{\vec{B}}{|\vec{B}|} \right) \right| \ll |\vec{\omega_L}| \,, \tag{2.50}$$

has to be fulfilled. This type of spin change is called adiabatic. Fig. 2.11 shows a schematic visualization of an adiabatic spin change. From (2.50) it is clear that the maximum rate of field

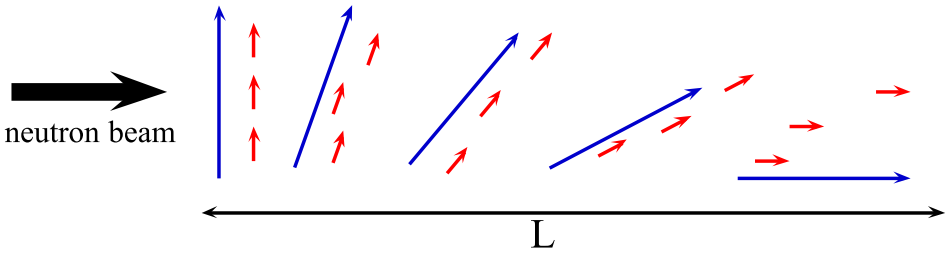

Figure 2.11.: Schematic visualization of an adiabatic spin change: The blue arrows represent the external magnetic field, the red arrows the spin. To fulfill the adiabatic condition, the distance L along which the field changes has to be sufficiently long.

change depends on the neutron's velocity. For thermal neutrons and long distances, even the earth's field change of direction could lead to an adiabatic spin change. Therefore, magnetic guide fields are required to prevent unwanted spin rotations and depolarization of the neutron beam [22].

2.4.2. Polarizing supermirrors

In order to work with polarized neutrons it is first necessary to polarize the neutron beam. This is done by filtering neutrons with one spin component out, which can be achieved by various means. A possible way is to use so called polarizing supermirrors. Their functioning principle is now briefly explained.
Neutrons can be reflected from smooth surfaces. The neutron index of refraction is given by

$$n^2 = 1 - \frac{V}{E}, \tag{2.51}$$

[f] i.e. to conserve the spin direction

where E is the neutron's kinetic energy and V is the potential experienced by them. It is given by

$$V = \frac{2\pi\hbar^2}{m_n} N b_c, \tag{2.52}$$

where m_n is the neutron's mass, N is the density of nuclei and b_c is the nuclear scattering length. Since n depends on E, it is a function of the neutron's wavelength.
For a lot of materials the index of refraction for neutrons is below one. Because of that, neutrons can be totally reflected when they hit a boundary. Total reflection occurs up to a critical angle θ_c, which is given by

$$\theta_c = \lambda\sqrt{\frac{N b_c}{\pi}}, \tag{2.53}$$

where λ is the neutron wavelength [10, 23]. Beyond θ_c the neutron wave penetrates into the material and is partially reflected at boundaries between layers of different materials which usually have a different b_c. In this way, a supermirror and its many layers represent an artificial lattice at which Bragg reflection occurs. The layers are thickest on the surface and become gradually thinner. Every layer adds a Bragg peak and therefore extends the critical angle θ_c.
To polarize neutrons using a supermirror one has to take magnetic scattering into account as well. To put it simply the magnetic interaction adds a magnetic scattering length p to the nuclear one. p depends on the relative orientation of the neutron spin to the magnetization. This means, the total scattering length depends on the neutron spin as well. As we have already seen, the critical angle depends on the scattering length and thus, for magnetic materials, also on the neutron spin.
A supermirror with one type of layers being magnetic, neutrons with spins either parallel or anti parallel to the layer magnetization have a different reflectivity. For the state of the neutron spin parallel to the magnetization the total scattering length is enhanced, for the anti parallel one it is reduced. If the reduced total scattering length is the same as the total scattering length of the non magnetic layers, the total scattering length appears to be constant for one spin component. The supermirror becomes transparent, because the neutrons of one spin component do not see the boundaries any more. Thus only one spin component is reflected and the neutron beam gets polarized [24].

2.4.3. DC-coils

DC-coils can be used to manipulated the neutron's spin. They present an easy way to achieve a neutron spin flip in an external magnetic field and simply consist of two rectangular coils. One of them produces a field $\vec{B}_x$ in x-direction and the other produces a field $\vec{B}_c$ which points in the opposite direction as the guide field in order to compensate it. Thus the total field inside the coil will be $\vec{B}_R = \vec{B}_0 + \vec{B}_x + \vec{B}_c$. A schematic drawing of a DC-coil in an external guide field is given by Fig. 2.12. The change of fields across the winding sheets happens so fast, that the spin is left unaffected. In order to achieve a π-flip, the time for the neutron spent inside the coil has to correspond to one full Larmor precession which gives the flip condition

$$d = \frac{|\vec{v}|\pi}{|\vec{\omega}_L|} = \frac{|\vec{v}|\pi}{|\gamma\vec{B}_r|}, \tag{2.54}$$

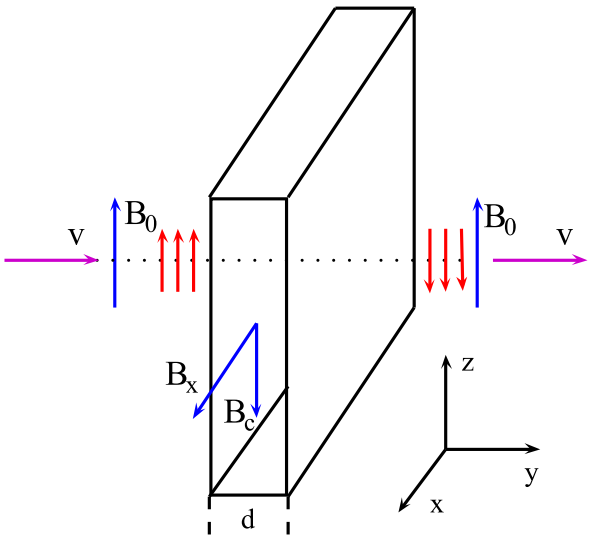

Figure 2.12.: Schematic drawing a π-flip by a DC-coil in an external guide field B_0. The neutron spin (red) is inverted inside the coil. The neutron direction of propagation is marked by v.

where d is the width of the coil, $\vec{v}$ is the neutron speed and $\vec{\omega}_L$ is the Larmor frequency. Thus, for a given coil one can adjust the magnetic fields $\vec{B}_0$, $\vec{B}_x$ and $\vec{B}_c$ in order to perform a π-flip. A spin flip by a DC-coil is only possible for monochromatic neutron beams, monochromatic flippers, i.e. they can only flip the spin of the beam with one specific wavelength. It is also noteworthy that they are not limited to a π-flip. They can be used to turn the neutron spin in any given direction [25].

2.4.4. A polarimeter beamline

With the components described in the previous two subsections it is now possible to construct an apparatus called neutron polarimeter. Such an apparatus is depicted in Fig. 2.13.

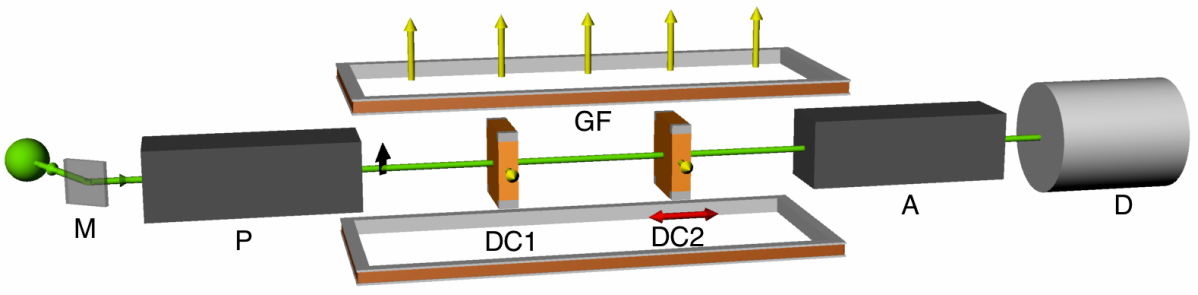

Figure 2.13.: Schematic drawing of a polarimeter beamline: A complete polarimeter beamline consist of a monochromizing crystal (M), a polarizer to prepare the neutron beam (P), at least two DC-coils (DC1 & DC2), a guide field (GF), an analyzer (A) and a detector (D).

Neutrons are produced by some source, usually a nuclear reactor. The spectrum of such a

beam is usually polychromatic, i.e. the energy spreads in a wide range. As we saw, polarizing supermirrors and DC-coils are in principle only available for monochromatic beams. They only work with one specific wave length. It is therefore necessary to monochromize the beam. This is done by a crystal, e.g. by a perfect Si crystal. The monochromator is put into the neutron beam and reflects only neutrons with a certain wave length, that fulfills the Bragg condition. By rotating the crystal and reducing the exit beam's cross section, it is possible to align the polarimeter in a way that only one specific wave length remains in the beam.
After the monochromator the first supermirror is placed. It selects neutrons with one spin component, lets them pass and blocks the neutrons with the other spin component. This supermirror is generally called polarizer. After that at least two DC-coils are placed in the beam. They allow to pre and post select certain states. By mounting several coils on translation stages and supplying them with bipolar power supplies, it is possible to create any initial and final spin state.
At the end of the beamline a second supermirror is placed. It is called analyzer and is usually identical to the polarizer, i.e. the first supermirror. As its name implies the analyzer enables one to analyze the final spin state. It allows only a certain spin component to pass to the detector at the end of the beamline.

3. Weak value measurements using neutrons

As section 2.3 showed, there have been plenty of experiments confirming the predictions by the theory of weak measurements. Nevertheless, all of them used photons. To avoid the ambiguity of the use of classical electrodynamics and to show genuine quantum mechanical treatment by using neutron matter waves, several novel experiments, using neutrons for the extraction of weak values as well as for weak measurements, are proposed in this chapter. With those experiments the theory of weak values can be experimentally validated with matter waves of massive particles for the first time.

3.1. Weak values of the spin operator

In this section several experimental ideas are presented that make it possible to determine the spin operator's weal value.

3.1.1. Determining the absolute of the spin operator's weak value

Here a possibility is shown to extract the square of the absolute of the weak value using a neutron interferometer setup, by making small path dependent spin rotations and observing the intensities at O- and H-beam.
Fig. 3.1 shows a schematic drawing of the setup, which consists of a $\frac{\pi}{2}$-spin turner, the interferometer itself, two spin rotators and a post selector. We start with a completely polarized

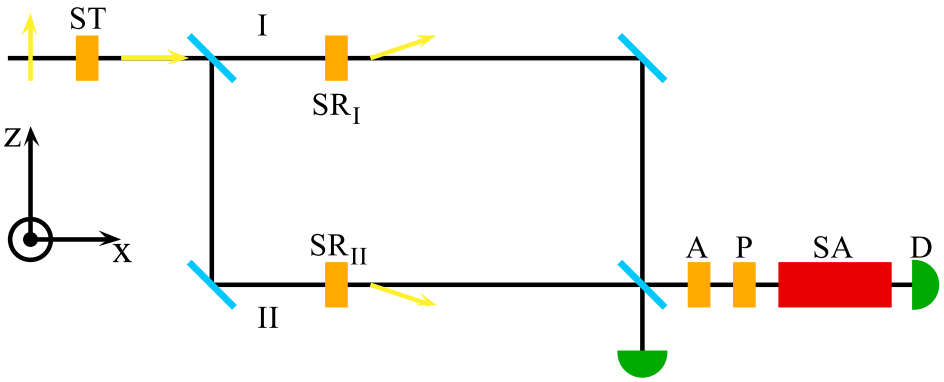

Figure 3.1.: Schematic drawing of neutron interferometer experiment for extracting the absolute of the spin operator's weak value: The complete setup consists of a $\frac{\pi}{2}$-spin turner (ST), the interferometer itself, two spin-rotators (SR$_I$ & SR$_{II}$), a post selector [two coils to select the azimuth and polar angle (A & P) and the red spin analyzer (SA)] and a detector (D).

neutron beam, so that the neutron's spin wave function is $|S_z;+\rangle$. Before entering the interferometer the spin is turned by $\frac{\pi}{2}$, causing its wave function to become $|S_x;+\rangle$.
After the first beam splitter the system's wave function $|\psi\rangle$ has to be extended by a part describing the path:

$$|\psi\rangle = |P\rangle|S\rangle = \sqrt{\frac{1}{2}}\left(|I\rangle + |II\rangle\right)|S_x;+\rangle, \tag{3.1}$$

where $|P\rangle$ and $|S\rangle$ represent the path and the spin part of the wave function. The wave function given by Eq. (3.1) describes the state of the pre selected ensemble. Now a small spin rotation around the z-axis is performed. Here we assume that the spin rotations are strictly positive along path I and negative along path II. The condition of a weak rotation is met by making the angle of rotation α small.

$$|\psi'\rangle = \sqrt{\frac{1}{2}}\mathrm{e}^{-i\alpha\hat{\sigma}_z^s/2}|S_x;+\rangle|I\rangle + \sqrt{\frac{1}{2}}\mathrm{e}^{i\alpha\hat{\sigma}_z^s/2}|S_x;+\rangle|II\rangle \tag{3.2}$$

At the exit of the interferometer the beams are recombined. For the O-beam this yields

$$\begin{aligned}|\Phi_o\rangle &= |P_o\rangle\langle P_o|\psi'\rangle = \frac{1}{2}\left(\langle I| + \langle II|\right)\left[\mathrm{e}^{-i\alpha\hat{\sigma}_z^s/2}|I\rangle + \mathrm{e}^{i\alpha\hat{\sigma}_z^s/2}|II\rangle\right]|S_x;+\rangle|P_o\rangle \\ &= \frac{1}{2}\left[\mathrm{e}^{-i\alpha\hat{\sigma}_z^s/2} + \mathrm{e}^{i\alpha\hat{\sigma}_z^s/2}\right]|S_x;+\rangle|P_o\rangle.\end{aligned} \tag{3.3}$$

Analogously the wave function for the H-beam becomes

$$\begin{aligned}|\Phi_h\rangle &= |P_h\rangle\langle P_h|\psi'\rangle = \frac{1}{2}\left(\langle I| - \langle II|\right)\left[\mathrm{e}^{-i\alpha\hat{\sigma}_z^s/2}|I\rangle + \mathrm{e}^{i\alpha\hat{\sigma}_z^s/2}|II\rangle\right]|S_x;+\rangle|P_h\rangle \\ &= \frac{1}{2}\left[\mathrm{e}^{-i\alpha\hat{\sigma}_z^s/2} - \mathrm{e}^{i\alpha\hat{\sigma}_z^s/2}\right]|S_x;+\rangle|P_h\rangle.\end{aligned} \tag{3.4}$$

Since α is very small, it is possible to expand the exponential functions in Eqs. (3.3) and (3.4):

$$\begin{aligned}|\Phi_o\rangle &= \frac{1}{2}\left[\mathrm{e}^{-i\alpha\hat{\sigma}_z^s/2} + \mathrm{e}^{i\alpha\hat{\sigma}_z^s/2}\right]|S_x;+\rangle|P_o\rangle \\ &\approx \frac{1}{2}\left[\left(1 - \frac{i\alpha\hat{\sigma}_z^s}{2}\right) + \left(1 + \frac{i\alpha\hat{\sigma}_z^s}{2}\right)\right]|S_x;+\rangle|P_o\rangle = |S_x;+\rangle|P_o\rangle \equiv |i\rangle\end{aligned} \tag{3.5}$$

$$\begin{aligned}|\Phi_h\rangle &= \frac{1}{2}\left[\mathrm{e}^{-i\alpha\hat{\sigma}_z^s/2} - \mathrm{e}^{i\alpha\hat{\sigma}_z^s/2}\right]|S_x;+\rangle|P_h\rangle \\ &\approx \frac{1}{2}\left[\left(1 - \frac{i\alpha\hat{\sigma}_z^s}{2}\right) - \left(1 + \frac{i\alpha\hat{\sigma}_z^s}{2}\right)\right]|S_x;+\rangle|P_h\rangle = \frac{-i\alpha\hat{\sigma}_z^s}{2}|S_x;+\rangle|P_h\rangle \equiv \frac{-i\alpha\hat{\sigma}_z^s}{2}|i\rangle\end{aligned} \tag{3.6}$$

Now the post selection is carried out for the O-beam, onto the general spin state

$$|\hat{S}\cdot\hat{n};+\rangle = \cos\left(\frac{\theta}{2}\right)\mathrm{e}^{-i\phi/2}|S_z;+\rangle + \sin\left(\frac{\theta}{2}\right)\mathrm{e}^{i\phi/2}|S_z;-\rangle, \tag{3.7}$$

If we define $|\hat{S}\cdot\hat{n};+\rangle \equiv |f\rangle$ and $|S_x;+\rangle \equiv |i\rangle$, the intensities for the O- and H-beam are given by

$$I_o = \left|\langle \hat{S}\cdot\hat{n};+|\Phi_o\rangle\right|^2 = |\langle f|i\rangle|^2 \tag{3.8}$$

and

$$I_h = \left|\langle \hat{S}\cdot\hat{n};+|\Phi_h\rangle\right|^2 = \left|\left\langle f\left|\frac{-i\alpha\hat{\sigma}_z^s}{2}\right|i\right\rangle\right|^2 = \frac{\alpha^2}{4}\left|\langle f\left|\hat{\sigma}_z^s\right|i\rangle\right|^2. \tag{3.9}$$

From the measurement of the I_o and I_h intensities, it is possible to extract the absolute of the spin operator's weak value

$$|\langle\hat{\sigma}_z^s\rangle_w| \equiv \frac{|\langle f|\hat{\sigma}_z^s|i\rangle|}{|\langle f|i\rangle|} = \frac{2}{\alpha}\sqrt{\frac{I_h}{I_o}} \tag{3.10}$$

Instead of making the experientially difficult observation of I_o and I_h intensities separately, it is simpler to do intensity modulation measurements. For this an additional phase shifter is inserted into the interferometer and the intensities for a phase shift of $\chi = 0$ and $\chi = \pi$ are measured. For fixed $|f\rangle$ and $|i\rangle$ the minimum and maximum intensities correspond to H-beam and O-beam.
It is now possible to calculate the intensities I_o and I_h. With the two matrix elements

$$\begin{aligned}\langle \hat{S}\cdot\hat{n};+|\Phi_o\rangle &= \left[\cos\left(\frac{\theta}{2}\right)\mathrm{e}^{i\phi/2}\langle S_z;+| + \sin\left(\frac{\theta}{2}\right)\mathrm{e}^{-i\phi/2}\langle S_z;-|\right]\sqrt{\frac{1}{2}}\left[|S_z;+\rangle + |S_z;-\rangle\right]|P_o\rangle \\ &= \sqrt{\frac{1}{2}}\left[\cos\left(\frac{\theta}{2}\right)\mathrm{e}^{i\phi/2} + \sin\left(\frac{\theta}{2}\right)\mathrm{e}^{-i\phi/2}\right]|P_o\rangle\end{aligned} \tag{3.11}$$

and

$$\begin{aligned}\langle \hat{S}\cdot\hat{n};+|\Phi_h\rangle &= \left[\cos\left(\frac{\theta}{2}\right)\mathrm{e}^{i\phi/2}\langle S_z;+| + \sin\left(\frac{\theta}{2}\right)\mathrm{e}^{-i\phi/2}\langle S_z;-|\right]\left[-\frac{i\alpha\hat{\sigma}_z^s}{2}\right]\sqrt{\frac{1}{2}}\left[|S_z;+\rangle + |S_z;-\rangle\right]|P_h\rangle \\ &= -\frac{i\alpha}{\sqrt{8}}\left[\cos\left(\frac{\theta}{2}\right)\mathrm{e}^{i\phi/2} - \sin\left(\frac{\theta}{2}\right)\mathrm{e}^{-i\phi/2}\right]|P_h\rangle\end{aligned} \tag{3.12}$$

the intensities can be calculated as

$$\begin{aligned}I_o &= \left|\langle \hat{S}\cdot\hat{n};+|\Phi_o\rangle\right|^2 = \frac{1}{2}\left[\cos\left(\frac{\theta}{2}\right)\mathrm{e}^{i\phi/2} + \sin\left(\frac{\theta}{2}\right)\mathrm{e}^{-\phi/2}\right]\left[\cos\left(\frac{\theta}{2}\right)\mathrm{e}^{-i\phi/2} + \sin\left(\frac{\theta}{2}\right)\mathrm{e}^{i\phi/2}\right] \\ &= \frac{1}{2}\left[\cos^2\left(\frac{\theta}{2}\right) + \sin\left(\frac{\theta}{2}\right)\cos\left(\frac{\theta}{2}\right)\left(\mathrm{e}^{i\phi} + \mathrm{e}^{-i\phi}\right) + \sin^2\left(\frac{\theta}{2}\right)\right] \\ &= \frac{1}{2}\left[1 + \cos(\phi)\sin(\theta)\right]\end{aligned} \tag{3.13}$$

and

$$\begin{aligned} I_h &= \left|\langle \hat{S}\cdot\hat{n};+|\Phi_h\rangle\right|^2 = \left[-\frac{i\alpha}{\sqrt{8}}\right]\left[\cos\left(\frac{\theta}{2}\right)\mathrm{e}^{i\phi/2} - \sin\left(\frac{\theta}{2}\right)\mathrm{e}^{-i\phi/2}\right]\times \\ &\quad\times\left[\frac{i\alpha}{\sqrt{8}}\right]\left[\cos\left(\frac{\theta}{2}\right)\mathrm{e}^{-i\phi/2} - \sin\left(\frac{\theta}{2}\right)\mathrm{e}^{i\phi/2}\right] \\ &= \frac{\alpha^2}{8}\left[\cos^2\left(\frac{\theta}{2}\right) - \sin\left(\frac{\theta}{2}\right)\cos\left(\frac{\theta}{2}\right)\left(\mathrm{e}^{i\phi}+\mathrm{e}^{-i\phi}\right) + \sin^2\left(\frac{\theta}{2}\right)\right] \\ &= \frac{\alpha^2}{8}\left[1-\cos(\phi)\sin(\theta)\right] \end{aligned} \tag{3.14}$$

Inserting Eqs. (3.13) and (3.14) into Eq. (3.10) yields

$$|\langle\hat{\sigma}_z^s\rangle_w|^2 = \frac{1-\cos(\phi)\sin(\theta)}{1+\cos(\phi)\sin(\theta)} \tag{3.15}$$

With given $|i\rangle$ and $|f\rangle$ it is possible to find an analytic solution for $\langle\hat{\sigma}_z^s\rangle_w$:

$$\begin{aligned} \langle\hat{\sigma}_z^s\rangle_w &= \frac{\langle f|\hat{\sigma}_z^s|i\rangle}{\langle f|i\rangle} = \frac{\left[\langle S_z;+|\cos\left(\frac{\theta}{2}\right)\mathrm{e}^{i\phi/2} + \langle S_z;-|\sin\left(\frac{\theta}{2}\right)\mathrm{e}^{-i\phi/2}\right]\left[|S_z;+\rangle - |S_z;-\rangle\right]}{\left[\langle S_z;+|\cos\left(\frac{\theta}{2}\right)\mathrm{e}^{i\phi/2} + \langle S_z;-|\sin\left(\frac{\theta}{2}\right)\mathrm{e}^{-i\phi/2}\right]\left[|S_z;+\rangle + |S_z;-\rangle\right]} \\ &= \frac{\cos\left(\frac{\theta}{2}\right)\mathrm{e}^{i\phi/2} - \sin\left(\frac{\theta}{2}\right)\mathrm{e}^{-i\phi/2}}{\cos\left(\frac{\theta}{2}\right)\mathrm{e}^{i\phi/2} + \sin\left(\frac{\theta}{2}\right)\mathrm{e}^{-i\phi/2}} = 1 - \frac{2}{1+\mathrm{e}^{i\phi}\cot\left(\frac{\theta}{2}\right)} \end{aligned} \tag{3.16}$$

The absolute square of Eq. (3.16) is now given by Eq. (3.15), which shows that an experiment designed as described above, will yield the absolute of the spin operator's weak value, if the pre- and post selection, as well as the small spin rotations, can be realized with high enough precision.

Simplified Version

The experiment presented above can be carried out even easier. Instead of a neutron interferometer a 50:50 beam splitter would do to conduct the experiment, as can be seen in Fig. 3.2.

Pre selection is performed the same way as previously, i.e. we start with $|S_z;+\rangle$ and turn the neutron spin by $\frac{\pi}{2}$, to end up in the $|S_x;+\rangle$ state. At the beam splitter the beam is separated in an upper and a lower part. The upper part is left unaltered and gets post selected onto the state $|\hat{S}\cdot\hat{n};+\rangle$. As in the previous section we define $|i\rangle \equiv |S_x;+\rangle$ and $|f\rangle \equiv |\hat{S}\cdot\hat{n};+\rangle$. Therefore the intensity measured at the end of the upper part is given by

$$I_u = \left|\langle\hat{S}\cdot\hat{n};+|S_x;+\rangle\right|^2 = |\langle f|i\rangle|^2, \tag{3.17}$$

which is of course the same as Eq. (3.8). Along the lower path the neutron spin is rotated by π around the z-axis, which changes the state into

$$\mathrm{e}^{-i\hat{\sigma}_z^s\pi/2}|S_x;+\rangle = \left[\cos\left(\frac{\pi}{2}\right) - i\hat{\sigma}_z^s\sin\left(\frac{\pi}{2}\right)\right]|S_x;+\rangle = -i\hat{\sigma}_z^s|S_x;+\rangle. \tag{3.18}$$

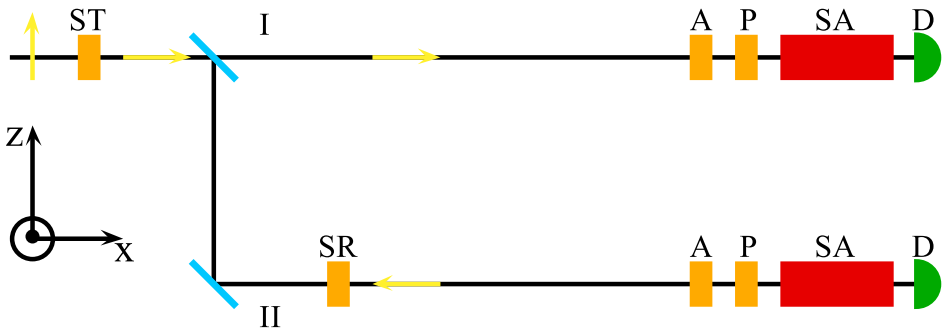

Figure 3.2.: Simplified version of the neutron interferometer experiment for extracting the absolute of the spin operator's weak value: The interferometer is replaced by a 50:50 beam splitter (light blue). Only one spin rotator is necessary (SR). The same post selection is performed on both paths [two coils to select the azimuth and polar angle (A & P), the red spin analyzer (SA) and a detector (D)].

Here the exact formula

$$\exp\left(i\alpha\ \hat{\sigma}_j^s \cdot \hat{n}\right) = \mathbb{1}\cos\left(\alpha\right) + i\ \hat{\sigma}_j^s \cdot \hat{n}\sin\left(\alpha\right) \tag{3.19}$$

where $\hat{\sigma}_j^s$ is a Pauli matrix and $\hat{n}$ marks the axis of rotation, was used. Again post selection onto the state $|\hat{S}\cdot\hat{n};+\rangle$ is done. The intensity measured at the end of the lower path is given by

$$I_l = \left|\langle \hat{S}\cdot\hat{n};+|\hat{\sigma}_z^s|S_x;+\rangle\right|^2 = |\langle f|\hat{\sigma}_z^s|i\rangle|^2\,, \tag{3.20}$$

which is similar to Eq. (3.9). The absolute of the spin operator's weak value can be obtained by measuring the intensities for upper and lower path

$$|\langle\hat{\sigma}_z^s\rangle_w| \equiv \frac{\left|\langle \hat{S}\cdot\hat{n};+|\hat{\sigma}_z^s|S_x;+\rangle\right|}{\left|\langle \hat{S}\cdot\hat{n};+|S_x;+\rangle\right|} = \frac{|\langle f|\hat{\sigma}_z^s|i\rangle|}{|\langle f|i\rangle|} = \sqrt{\frac{I_l}{I_u}} \tag{3.21}$$

Again it is possible to evaluate the matrix elements $\langle\hat{S}\cdot\hat{n};+|\hat{\sigma}_z^s|S_x;+\rangle$ and $\langle\hat{S}\cdot\hat{n};+|S_x;+\rangle$, which are needed to calculate the intensities. They are given by

$$\langle \hat{S}\cdot\hat{n};+|\hat{\sigma}_z^s|S_x;+\rangle = \sqrt{\frac{1}{2}}\left[\cos\left(\frac{\theta}{2}\right)\mathrm{e}^{i\phi/2} - \sin\left(\frac{\theta}{2}\right)\mathrm{e}^{-i\phi/2}\right] \tag{3.22}$$

and

$$\langle \hat{S}\cdot\hat{n};+|S_x;+\rangle = \sqrt{\frac{1}{2}}\left[\cos\left(\frac{\theta}{2}\right)\mathrm{e}^{i\phi/2} + \sin\left(\frac{\theta}{2}\right)\mathrm{e}^{-i\phi/2}\right] \tag{3.23}$$

which leads to the intensities

$$I_l = \left|\langle \hat{S}\cdot\hat{n};+|\hat{\sigma}_z^s|S_x;+\rangle\right|^2 = \frac{1}{2}\left[1-\cos\left(\phi\right)\sin\left(\theta\right)\right] \tag{3.24}$$

and

$$I_u = \left|\langle \hat{S}\cdot\hat{n};+|S_x;+\rangle\right|^2 = \frac{1}{2}\left[1+\cos(\phi)\sin(\theta)\right] \tag{3.25}$$

Inserting Eqs. (3.24) and (3.25) into Eq. (3.21) yields exactly the same solution as for the calculations of the previous experiment, i.e. Eq. (3.15).
It is very interesting to note, that no weak measurement is performed in this experiment. Nevertheless it is possible to extract the absolute of the spin operator's weak value. This sheds a new light onto the nature of the weak value. It was introduced within the context of weak measurements. However, this experiment clearly shows that the weak value itself is accessible without such.

3.1.2. Polarimeter experiment for the determination of the absolute of the spin operator's weak value

If the measurements are performed sequentially, not even a beam splitter is needed. A setup consisting of a polarizer, a DC-coil to turn the spin by $\frac{\pi}{2}$, a second coil to perform the π-rotation around the z-axis and an analyzer that post selects the state $|\hat{S}\cdot\hat{n};+\rangle$, would be enough to extract the absolute of the spin operator's weak value. Fig. 3.3 shows such a setup. The

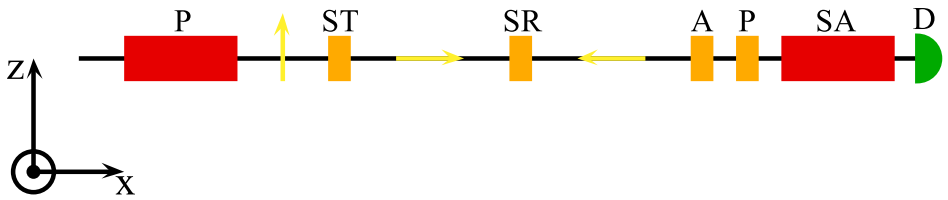

Figure 3.3.: Further simplified version of the neutron experiment for extracting the absolute of the spin operator's weak value: The interferometer is replaced by a polarimeter setup, which consists of a polarizer (P), a $\frac{\pi}{2}$-turner (ST), a π-rotator (SR) and a post selector [two coils to select the azimuth and polar angle (A & P), the red spin analyzer (SA) and a detector (D)].

absolute of the spin operator's weak value would then be given by

$$|\langle\hat{\sigma}_z^s\rangle_w| = \frac{|\langle f|\hat{\sigma}_z^s|i\rangle|}{|\langle f|i\rangle|} = \sqrt{\frac{I_{\text{on}}}{I_{\text{off}}}}, \tag{3.26}$$

where I_{on} is the intensity measured, when the π-rotator is turned on and I_{off} when it is turned off.
If the initial state is given by $|S_x;+\rangle$, it is also possible to perform a π-rotation around the y-axis. Post selection on the $|\hat{S}\cdot\hat{n};+\rangle$ state would then yield the absolute of $\langle\hat{\sigma}_y^s\rangle_w$. Since the operator $\hat{\sigma}_y^s$ is given by

$$\hat{\sigma}_y^s = i|S_z;-\rangle\langle S_z;+| - i|S_z;+\rangle\langle S_z;-| \tag{3.27}$$

its weak value, for this particular set of initial and final state, is

$$\begin{aligned}\langle\hat{\sigma}_y^s\rangle_w &= \frac{\langle f|\hat{\sigma}_z^s|i\rangle}{\langle f|i\rangle} = \frac{\left[\langle S_z;+|\cos\left(\frac{\theta}{2}\right)\mathrm{e}^{i\phi/2} + \langle S_z;-|\sin\left(\frac{\theta}{2}\right)\mathrm{e}^{-i\phi/2}\right]\left[i|S_z;-\rangle - i|S_z;+\rangle\right]}{\left[\langle S_z;+|\cos\left(\frac{\theta}{2}\right)\mathrm{e}^{i\phi/2} + \langle S_z;-|\sin\left(\frac{\theta}{2}\right)\mathrm{e}^{-i\phi/2}\right]\left[|S_z;+\rangle + |S_z;-\rangle\right]} \\ &= \frac{i\sin\left(\frac{\theta}{2}\right)\mathrm{e}^{-i\phi/2} - i\cos\left(\frac{\theta}{2}\right)\mathrm{e}^{i\phi/2}}{\cos\left(\frac{\theta}{2}\right)\mathrm{e}^{i\phi/2} + \sin\left(\frac{\theta}{2}\right)\mathrm{e}^{-i\phi/2}}\end{aligned} \tag{3.28}$$

It is interesting to note that $\mathrm{Re}(\langle\hat{\sigma}_z^s\rangle_w) = -\,\mathrm{Im}(\langle\hat{\sigma}_y^s\rangle_w)$ and $\mathrm{Im}(\langle\hat{\sigma}_z^s\rangle_w) = \mathrm{Re}(\langle\hat{\sigma}_y^s\rangle_w)$, i.e

$$\mathrm{Re}(\langle\hat{\sigma}_z^s\rangle_w) = -\,\mathrm{Im}(\langle\hat{\sigma}_y^s\rangle_w) = \frac{1}{\sec(\theta) + \cos(\phi)\tan(\theta)} \tag{3.29}$$

and

$$\mathrm{Im}(\langle\hat{\sigma}_z^s\rangle_w) = \mathrm{Re}(\langle\hat{\sigma}_y^s\rangle_w) = \frac{1}{\cot(\phi) + \csc(\theta)\csc(\phi)} \tag{3.30}$$

as well as

$$\mathrm{Abs}\left(\langle\hat{\sigma}_z^s\rangle_w\right) = \mathrm{Abs}\left(\langle\hat{\sigma}_y^s\rangle_w\right). \tag{3.31}$$

The weak value of $\hat{\sigma}_z^s$ is constant.
In order to gain a deeper insight into the calculations performed here, the weak value of $\hat{\sigma}_z^s$ is plotted in Fig. 3.4 and that of $\hat{\sigma}_y^s$ in Fig. 3.5.[a] By comparing Figs. 3.4b and 3.5d, Figs. 3.4d and 3.5b, as well as Figs. 3.4f and 3.5f, the statement made by Eqs. (3.29), (3.30) and (3.31) become apparent.
It also possible to perform the experiment with different initial states, to determine other spin operator's weak values. Take for example a system with an initial state quantized along the positive z-axis, so that it is given by $|i\rangle = |S_z;+\rangle$. Now rotations around the x- and y-axis are non trivial. Since the weak values become

$$\begin{aligned}\langle\hat{\sigma}_y^s\rangle_w &= \frac{\langle f|\hat{\sigma}_y^s|i\rangle}{\langle f|i\rangle} = \frac{\left[\langle S_z;+|\cos\left(\frac{\theta}{2}\right)\mathrm{e}^{i\phi/2} + \langle S_z;-|\sin\left(\frac{\theta}{2}\right)\mathrm{e}^{-i\phi/2}\right] i|S_z;+\rangle}{\left[\langle S_z;+|\cos\left(\frac{\theta}{2}\right)\mathrm{e}^{i\phi/2} + \langle S_z;-|\sin\left(\frac{\theta}{2}\right)\mathrm{e}^{-i\phi/2}\right]|S_z;+\rangle} \\ &= \frac{i\sin\left(\frac{\theta}{2}\right)\mathrm{e}^{-i\phi/2}}{\cos\left(\frac{\theta}{2}\right)\mathrm{e}^{i\phi/2}} = i\tan\left(\frac{\theta}{2}\right)\mathrm{e}^{-i\phi}\end{aligned} \tag{3.32}$$

and

$$\begin{aligned}\langle\hat{\sigma}_x^s\rangle_w &= \frac{\langle f|\hat{\sigma}_x^s|i\rangle}{\langle f|i\rangle} = \frac{\left[\langle S_z;+|\cos\left(\frac{\theta}{2}\right)\mathrm{e}^{i\phi/2} + \langle S_z;-|\sin\left(\frac{\theta}{2}\right)\mathrm{e}^{-i\phi/2}\right]|S_z;-\rangle}{\left[\langle S_z;+|\cos\left(\frac{\theta}{2}\right)\mathrm{e}^{i\phi/2} + \langle S_z;-|\sin\left(\frac{\theta}{2}\right)\mathrm{e}^{-i\phi/2}\right]|S_z;+\rangle} \\ &= \frac{\sin\left(\frac{\theta}{2}\right)\mathrm{e}^{-i\phi/2}}{\cos\left(\frac{\theta}{2}\right)\mathrm{e}^{i\phi/2}} = \tan\left(\frac{\theta}{2}\right)\mathrm{e}^{-i\phi}.\end{aligned} \tag{3.33}$$

the same relation as in the previous case can be found between them.

$$\mathrm{Re}(\langle\hat{\sigma}_y^s\rangle_w) = -\,\mathrm{Im}(\langle\hat{\sigma}_x^s\rangle_w) = \sin(\phi)\tan\left(\frac{\theta}{2}\right) \tag{3.34}$$

[a] For each case the initial state is given by $|S_x;+\rangle$, the final one by $|\hat{S}\cdot\hat{n};+\rangle$.

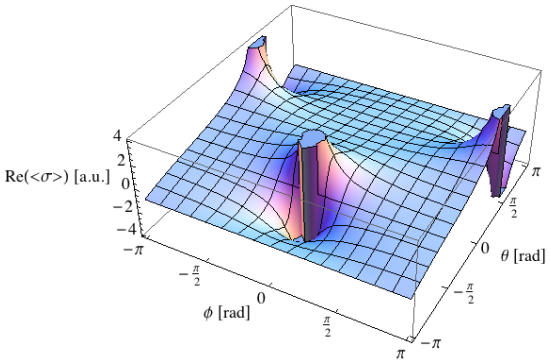

(a) 3D plot of $\mathrm{Re}\left(\langle\hat{\sigma}_z^s\rangle_w\right)$ [real part of Eq. (3.16)]

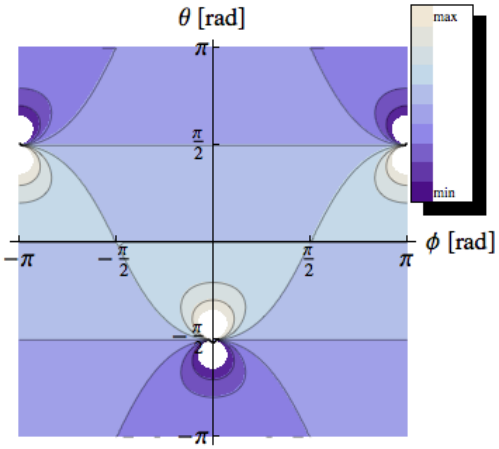

(b) Contour plot of $\mathrm{Re}\left(\langle\hat{\sigma}_z^s\rangle_w\right)$ [real part of Eq. (3.16)]

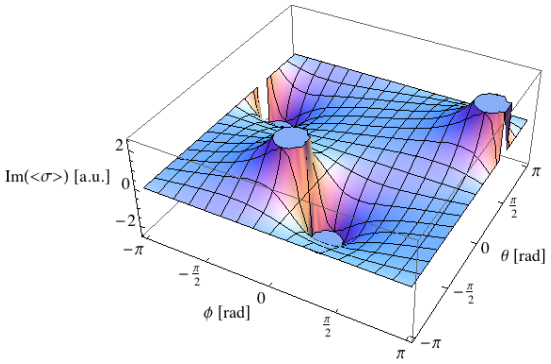

(c) 3D plot of $\mathrm{Im}\left(\langle\hat{\sigma}_z^s\rangle_w\right)$ [imaginary part of Eq. (3.16)]

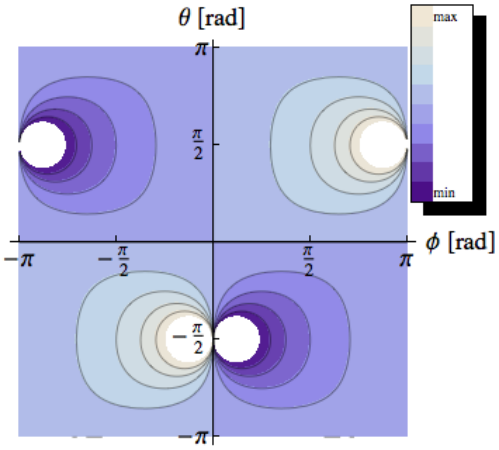

(d) Contour plot of $\mathrm{Im}\left(\langle\hat{\sigma}_z^s\rangle_w\right)$ [imaginary part of Eq. (3.16)]

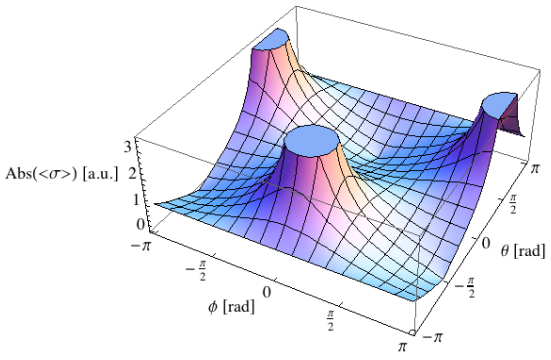

(e) 3D plot of $\mathrm{Abs}\left(\langle\hat{\sigma}_z^s\rangle_w\right)$ [absolute of Eq. (3.16)]

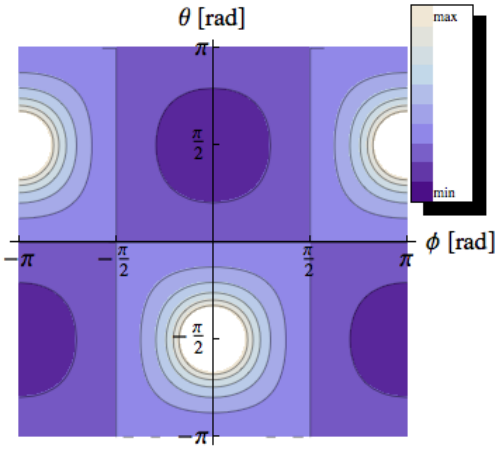

(f) Contour plot of $\mathrm{Abs}\left(\langle\hat{\sigma}_z^s\rangle_w\right)$ [absolute of Eq. (3.16)]

Figure 3.4.: Visualization of $\langle\hat{\sigma}_z^s\rangle$, for both, real and imaginary part, as well as its absolute

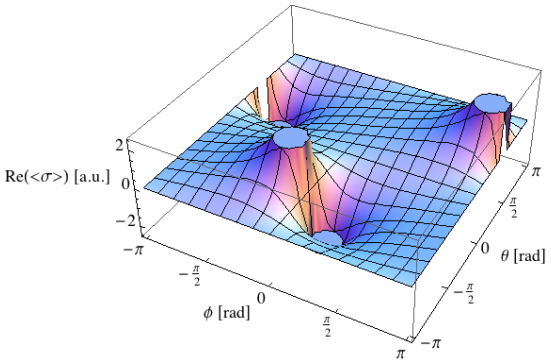

(a) 3D plot of Re $\left(\langle\hat{\sigma}_y^s\rangle_w\right)$ [real part of Eq. (3.28)]

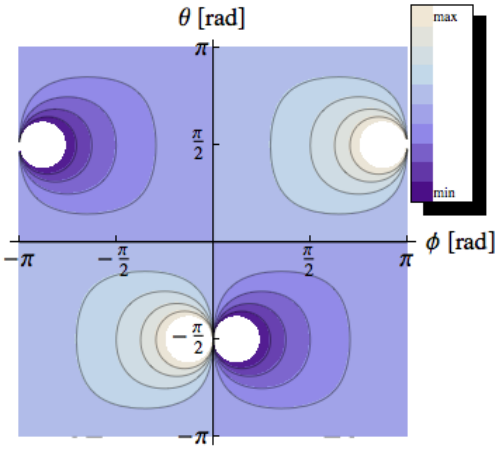

(b) Contour plot of Re $\left(\langle\hat{\sigma}_y^s\rangle_w\right)$ [real part of Eq. (3.28)]

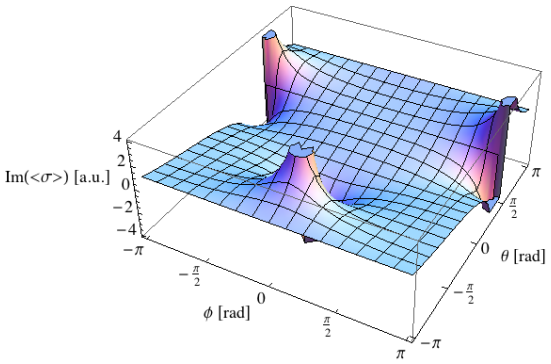

(c) 3D plot of Im $\left(\langle\hat{\sigma}_y^s\rangle_w\right)$ [imaginary part of Eq. (3.28)]

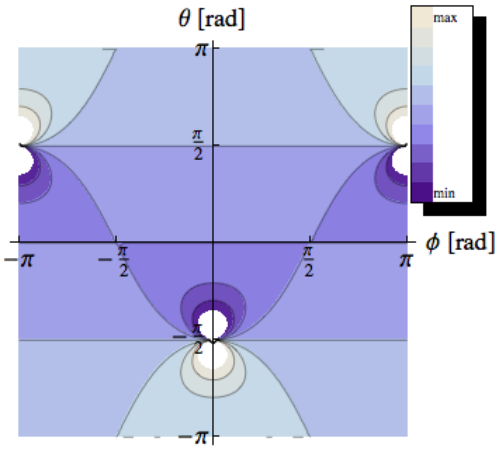

(d) Contour plot of Im $\left(\langle\hat{\sigma}_y^s\rangle_w\right)$ [imaginary part of Eq. (3.28)]

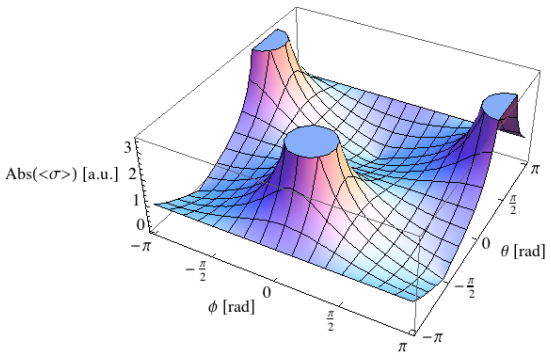

(e) 3D plot of Abs $\left(\langle\hat{\sigma}_y^s\rangle_w\right)$ [absolute of Eq. (3.28)]

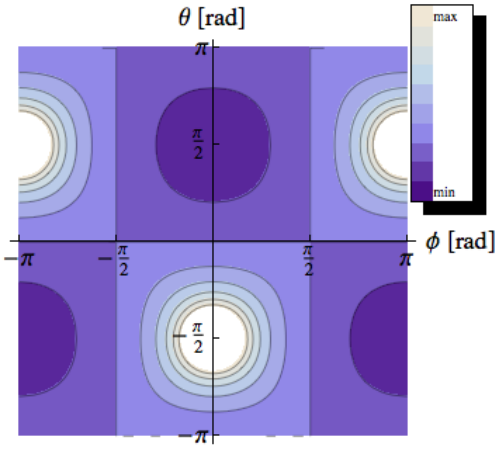

(f) Contour plot of Abs $\left(\langle\hat{\sigma}_y^s\rangle_w\right)$ [absolute of Eq. (3.28)]

Figure 3.5.: Visualization of $\langle\hat{\sigma}_y^s\rangle$, for both, real and imaginary part, as well as its absolute

and

$$\mathrm{Im}(\langle\hat{\sigma}_y^s\rangle_w) = \mathrm{Re}(\langle\hat{\sigma}_x^s\rangle_w) = \cos(\phi)\tan\left(\frac{\theta}{2}\right), \tag{3.35}$$

as well as

$$\mathrm{Abs}(\langle\hat{\sigma}_z^s\rangle_w) = \mathrm{Abs}(\langle\hat{\sigma}_y^s\rangle_w). \tag{3.36}$$

Here $\langle\hat{\sigma}_z^s\rangle_w$ is constant, since $|i\rangle$ is an eigenstate of $\hat{\sigma}_z^s$.
For completeness sake it is worth looking into the last possible case, that is the initial state quantized along the positive y-axis ($|i\rangle = |S_y;+\rangle$). The weak values $\langle\hat{\sigma}_x^s\rangle_w$ and $\langle\hat{\sigma}_z^s\rangle_w$ then become

$$\begin{aligned}\langle\hat{\sigma}_x^s\rangle_w &= \frac{\langle f|\hat{\sigma}_x^s|i\rangle}{\langle f|i\rangle} = \frac{\left[\langle S_z;+|\cos\left(\frac{\theta}{2}\right)\mathrm{e}^{i\phi/2} + \langle S_z;-|\sin\left(\frac{\theta}{2}\right)\mathrm{e}^{-i\phi/2}\right]\left[i|S_z;+\rangle + |S_z;-\rangle\right]}{\left[\langle S_z;+|\cos\left(\frac{\theta}{2}\right)\mathrm{e}^{i\phi/2} + \langle S_z;-|\sin\left(\frac{\theta}{2}\right)\mathrm{e}^{-i\phi/2}\right]\left[|S_z;+\rangle + i|S_z;-\rangle\right]} \\ &= \frac{\sin\left(\frac{\theta}{2}\right)\mathrm{e}^{-i\phi/2} + i\cos\left(\frac{\theta}{2}\right)\mathrm{e}^{i\phi/2}}{\cos\left(\frac{\theta}{2}\right)\mathrm{e}^{i\phi/2} + i\sin\left(\frac{\theta}{2}\right)\mathrm{e}^{-i\phi/2}} = \frac{2}{i + \mathrm{e}^{i\phi}\cot\left(\frac{\theta}{2}\right)} + i\end{aligned} \tag{3.37}$$

and

$$\begin{aligned}\langle\hat{\sigma}_z^s\rangle_w &= \frac{\langle f|\hat{\sigma}_z^s|i\rangle}{\langle f|i\rangle} = \frac{\left[\langle S_z;+|\cos\left(\frac{\theta}{2}\right)\mathrm{e}^{i\phi/2} + \langle S_z;-|\sin\left(\frac{\theta}{2}\right)\mathrm{e}^{-i\phi/2}\right]\left[|S_z;+\rangle - i|S_z;-\rangle\right]}{\left[\langle S_z;+|\cos\left(\frac{\theta}{2}\right)\mathrm{e}^{i\phi/2} + \langle S_z;-|\sin\left(\frac{\theta}{2}\right)\mathrm{e}^{-i\phi/2}\right]\left[|S_z;+\rangle + i|S_z;-\rangle\right]} \\ &= \frac{\cos\left(\frac{\theta}{2}\right)\mathrm{e}^{i\phi/2} - i\sin\left(\frac{\theta}{2}\right)\mathrm{e}^{-i\phi/2}}{\cos\left(\frac{\theta}{2}\right)\mathrm{e}^{i\phi/2} + i\sin\left(\frac{\theta}{2}\right)\mathrm{e}^{-i\phi/2}} = \frac{2}{i\mathrm{e}^{i\phi}\cot\left(\frac{\theta}{2}\right) - 1} + 1\end{aligned} \tag{3.38}$$

It is not surprising to find

$$\mathrm{Re}(\langle\hat{\sigma}_x^s\rangle_w) = -\,\mathrm{Im}(\langle\hat{\sigma}_z^s\rangle_w) = \frac{1}{\csc(\theta)\sec(\phi) + \tan(\phi)} \tag{3.39}$$

and

$$\mathrm{Im}(\langle\hat{\sigma}_x^s\rangle_w) = \mathrm{Re}(\langle\hat{\sigma}_z^s\rangle_w) = \frac{1}{\sec(\theta) + \sin(\phi) + \tan(\phi)}, \tag{3.40}$$

as well as

$$\mathrm{Abs}(\langle\hat{\sigma}_x^s\rangle_w) = \mathrm{Abs}(\langle\hat{\sigma}_z^s\rangle_w) \tag{3.41}$$

and $\langle\hat{\sigma}_y^s\rangle_w = 1$.
It would be very interesting to perform a polarimeter experiment test the validity of the relations given by Eqs. (3.31), (3.36) and (3.41) within a limited degree of polarization in a practical experiment. One might object that such an experiment would have the flaw that sequential measurements would be needed. However, since the neutrons are indistinguishable from each other, it can be argued that such measurements would still yield important information. In addition it can be realized very easily from an experimental point of view and is therefore worth looking into.

3.1.3. Determining the spin operator's complete weak value

All of the above experiments have the limitation, that it is only possible to extract the absolute of the spin operator's weak value. So, it would be very interesting to measure its real and imaginary part separately, to check out their relation, which was stated in the previous section. If both experiments are combined in a clever way, theory predicts a possible measurement of all the desired variables. The basic setup for such an experiment can be seen in Fig. 3.6. It

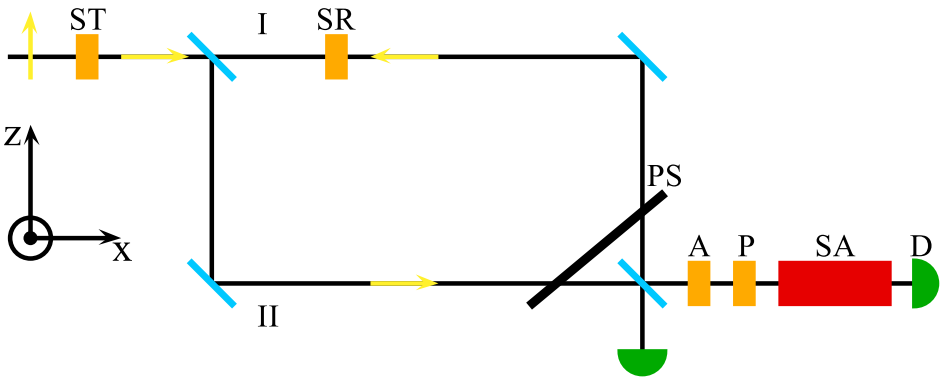

Figure 3.6.: Interferometer experiment for extracting the complete weak value of $\hat{\sigma}_z^s$: The setup consists of a $\frac{\pi}{2}$-turner (ST), a neutron interferometer, a phase shifter (PS), a π-spin rotator (SR) and a post selector [two coils to select the azimuth and polar angle (A & P), the red spin analyzer (SA) and a detector (D)].

consists of a $\frac{\pi}{2}$-turner, which pre selects the spin state, a neutron interferometer, a phase shifter, a π-spin rotator, and an analyzer that performs the post selection onto the final spin state. As in the previous experiments the initial spin state is prepared in $|S_x;+\rangle$. At the first beam splitter the beam is separated into two paths.

$$|\psi\rangle = \sqrt{\frac{1}{2}}\left(|I\rangle + |II\rangle\right)|S_x;+\rangle \tag{3.42}$$

Now a phase shifter shall be put into the beam only along path I. In addition to that a π-rotation of the spin around the z-axis, also only on path I, is performed. This causes $|\psi\rangle$ to become

$$|\psi'\rangle = \sqrt{\frac{1}{2}}\left[\mathrm{e}^{i\chi}\mathrm{e}^{i\hat{\sigma}_z^s\pi/2}|I\rangle + |II\rangle\right]|S_x;+\rangle \tag{3.43}$$

At the second beam splitter the beams are recombined

$$\begin{aligned}|\Phi_o\rangle = |P_o\rangle\langle P_o|\psi'\rangle &= \frac{1}{2}\left(\langle I| + \langle II|\right)\left[\mathrm{e}^{i\chi}\mathrm{e}^{i\hat{\sigma}_z^s\pi/2}|I\rangle + |II\rangle\right]|S_x;+\rangle|P_o\rangle \\ &= \frac{1}{2}\left(1 - i\mathrm{e}^{i\chi}\hat{\sigma}_z^s\right)|S_x;+\rangle|P_o\rangle\end{aligned} \tag{3.44}$$

After the recombination, the post selection onto the final spin state, which is given by Eq. (3.7), is performed. Let this spin state be our final one, $|\hat{S}\cdot\hat{n};+\rangle \equiv |f\rangle$, and $|S_x;+\rangle \equiv |i\rangle$ our initial

one. Therefore the intensity for the O-beam of the interferometer becomes

$$I_o = \left|\frac{1}{2}\langle f|\left(1 - i\mathrm{e}^{i\chi}\hat{\sigma}_z^s\right)|i\rangle\right|^2 = \frac{1}{4}\left|\langle f|i\rangle - i\mathrm{e}^{i\chi}\langle f|\hat{\sigma}_z^s|i\rangle\right|^2 \tag{3.45}$$

In general $\langle f|i\rangle$ and $\langle f|\hat{\sigma}_z^s|i\rangle$ are complex numbers, which can be written as

$$\langle f|i\rangle \equiv A_1\mathrm{e}^{i\gamma_1} \tag{3.46}$$

and

$$\langle f|\hat{\sigma}_z^s|i\rangle \equiv A_2\mathrm{e}^{i\gamma_2}. \tag{3.47}$$

Using these two definitions, Eq. (3.45) becomes

$$\begin{aligned}
I_o &= \frac{1}{4}\left|A_1\mathrm{e}^{i\gamma_1} - i\mathrm{e}^{i\chi}A_2\mathrm{e}^{i\gamma_2}\right|^2 = \frac{1}{4}\left|A_1\mathrm{e}^{i\gamma_1}\right|^2\left|1 - \frac{A_2}{A_1}i\mathrm{e}^{i[\chi+(\gamma_2-\gamma_1)]}\right|^2 \\
&= \frac{1}{4}|A_1|^2\left\{1 - i\frac{A_2}{A_1}\mathrm{e}^{i[\chi+(\gamma_2-\gamma_1)]}\right\}\left\{1 + i\frac{A_2}{A_1}\mathrm{e}^{-i[\chi+(\gamma_2-\gamma_1)]}\right\} \\
&= \frac{|A_1|^2}{4}\left\{1 + \left|\frac{A_2}{A_1}\right|^2 - i\frac{A_2}{A_1}\mathrm{e}^{i[\chi+(\gamma_2-\gamma_1)]} + i\frac{A_2}{A_1}\mathrm{e}^{-i[\chi+(\gamma_2-\gamma_1)]}\right\} \\
&= \frac{|A_1|^2}{4}\left\{1 + \left|\frac{A_2}{A_1}\right|^2 + 2\frac{A_2}{A_1}\sin\left[\chi + (\gamma_2 - \gamma_1)\right]\right\} \\
&= \frac{|A_1|^2}{4}\left\{1 + \left|\frac{A_2}{A_1}\right|^2 + 2\frac{A_2}{A_1}\cos\left[\chi + (\gamma_2 - \gamma_1) - \frac{\pi}{2}\right]\right\}
\end{aligned} \tag{3.48}$$

For the empty interferometer, i.e. with the π-rotator turned off, the O-beam's intensity is

$$I_o = \frac{1}{4}\left|\langle f|\left(\mathrm{e}^{i\chi} + 1\right)|i\rangle\right|^2 = \frac{1}{4}|\langle f|i\rangle|^2\left(\mathrm{e}^{i\chi} + 1\right)\left(\mathrm{e}^{-i\chi} + 1\right) = \frac{|A_1|^2}{2}\left[1 + \cos\left(\chi\right)\right] \tag{3.49}$$

Using Eqs. (3.46) and (3.47) the weak value is

$$\langle\hat{\sigma}_z^s\rangle_w \equiv \frac{\langle f|\hat{\sigma}_z^s|i\rangle}{\langle f|i\rangle} = \frac{A_2}{A_1}\mathrm{e}^{i(\gamma_2-\gamma_1)}. \tag{3.50}$$

Combining Eqs. (3.48), (3.49) and (3.50) it is possible to extract the weak value. In comparison to the empty interferometer, an additional phase shift of $(\gamma_2 - \gamma_1) - \frac{\pi}{2}$ is expected, when the π-rotator is turned on. In addition to that the amplitude of the oscillation is modified by $\frac{A_2}{A_1}$. By making an intensity modulation measurement for a fixed $|f\rangle$, that is for fixed ϕ and θ, first with the π-rotator turned on, and then turned off, and comparing both, it is possible to measure $(\gamma_2 - \gamma_1) - \frac{\pi}{2}$ and $\frac{A_2}{A_1}$ and thus extract the weak value.

3.1.4. Experimental value range

To find the experimentally relevant values of ϕ and θ for all the experiments presented so far[b], one has to look at Fig. 3.4. The most interesting cases occur for the following sets of variables

1. Fixed θ at $\pm\frac{\pi}{2}$ and a scan of ϕ.
2. Fixed ϕ at 0 and a scan of θ.

The first case represents the final spin state on which post selection is performed lying in the xy-plane, rotated around the z-axis with angle θ. In the second one the final state is fixed in the xz-plane and rotated around the y-axis by the angle ϕ. The singularities in the plots occur whenever $|f\rangle$ and $|i\rangle$ become orthogonal. The two cases can also be plotted on the Bloch sphere, as one can see in Fig. 3.7. The red circle represents the first case, the blue circle the latter one. Two possible value ranges for an experiment can be found in Tab. 3.1. From the experimental

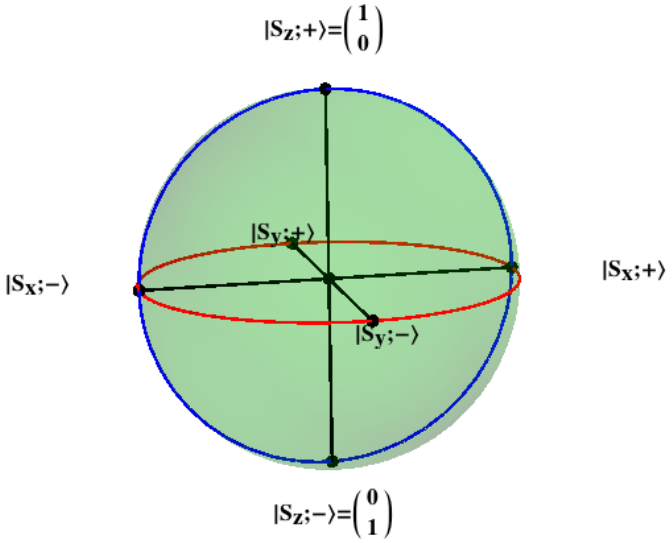

Figure 3.7.: Cases one and two on the Bloch sphere: The first case represents the final spin state on which post selection is performed lying in the xy-plane, rotated around the z-axis with angle θ (red circle). In the second one the final state is fixed in the xz-plane and rotated around the y-axis by the angle ϕ (blue circle).

point of view one has to bear in mind, that for orthogonal states the detected intensity becomes very low. It is proportional to:

$$I_o \propto \frac{1}{2}\left[1 + \cos(\phi)\sin(\theta)\right] \tag{3.51}$$

and plotted in Fig. 3.8. Comparing the regions of interest in Figs. 3.4a-3.4d to the intensities in Figs. 3.8a-3.8b the dilemma appears: Physically interesting values of θ and ϕ are related

[b] If initial and final state are given by $|S_x;+\rangle$ and $|\hat{S}\cdot\hat{n};+\rangle$.

to low intensities. Long measurement times and a stable experimental setup are necessary in order to get statistically significant results.

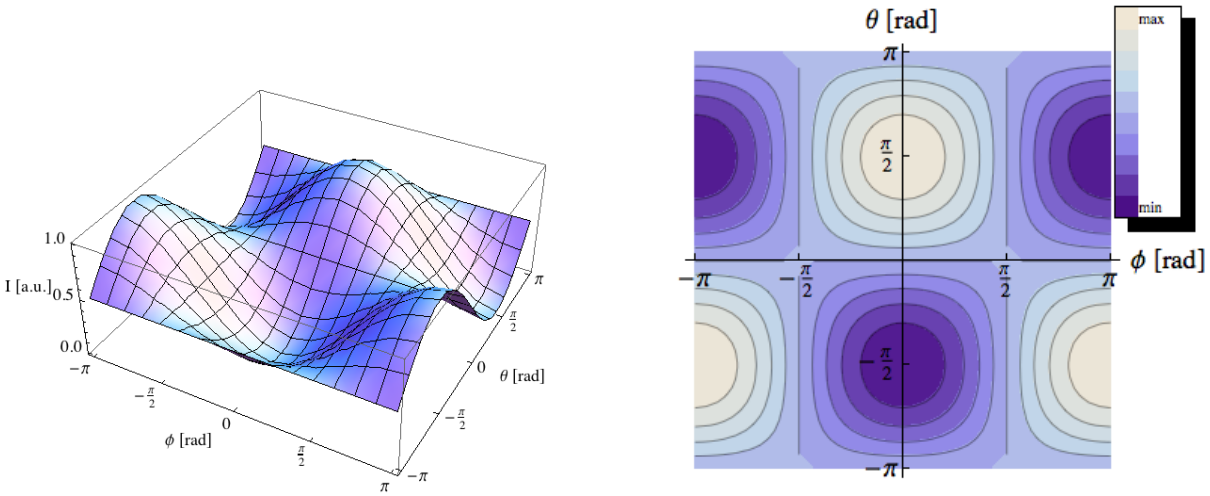

(a) 3D plot of the detected intensity [Eq. (3.51)]

(b) Contour plot of the detected intensity [Eq. (3.51)]

Figure 3.8.: Visualization of the expected intensity given by Eq. (3.51).

3.2. Weak values of the path operator

All the novel experiments presented so far, extract the weak value of the spin operator. In contrast to that, a different experiment is proposed in this section, which uses a weak spin rotation to measure the weak value of the path operator. This would help to develop a new insight of the complementarity relation and the wave-particle duality.
Fig. 3.9 shows the experimental setup. A neutron beam is prepared in a way that all neutron spins are aligned parallel to the z-axis. After that the spin is turned by $\frac{\pi}{2}$, aligning it along the positive x-axis. The neutron beam is split into two paths as it enters the interferometer and

$\theta = \frac{\pi}{2} = 90°$	$\phi = 0$
$\phi = 0°$	$\theta = 90°$
$\phi = \pm 45° \left(\pm\frac{\pi}{4}\right)$	$\theta = 90° \pm 45° \left(\frac{\pi}{2} \pm \frac{\pi}{4}\right)$
$\phi = \pm 90° \left(\pm\frac{\pi}{2}\right)$	$\theta = 90° \pm 90° \left(\frac{\pi}{2} \pm \frac{\pi}{2}\right)$
$\phi = \pm 120° \left(\pm\frac{2\pi}{3}\right)$	$\theta = 90° \pm 120° \left(\frac{\pi}{2} \pm \frac{2\pi}{3}\right)$
$\phi = \pm 135° \left(\pm\frac{3\pi}{4}\right)$	$\theta = 90° \pm 135° \left(\frac{\pi}{2} \pm \frac{3\pi}{4}\right)$
$\phi = \pm 150° \left(\pm\frac{5\pi}{6}\right)$	$\theta = 90° \pm 150° \left(\frac{\pi}{2} \pm \frac{5\pi}{6}\right)$
$\phi = \pm 165° \left(\pm\frac{11\pi}{12}\right)$	$\theta = 90° \pm 165° \left(\frac{\pi}{2} \pm \frac{11\pi}{12}\right)$
$\phi = \pm 175° \left(\pm\frac{35\pi}{36}\right)$	$\theta = 90° \pm 175° \left(\frac{\pi}{2} \pm \frac{35\pi}{36}\right)$

Table 3.1.: Possible value ranges for an experiment

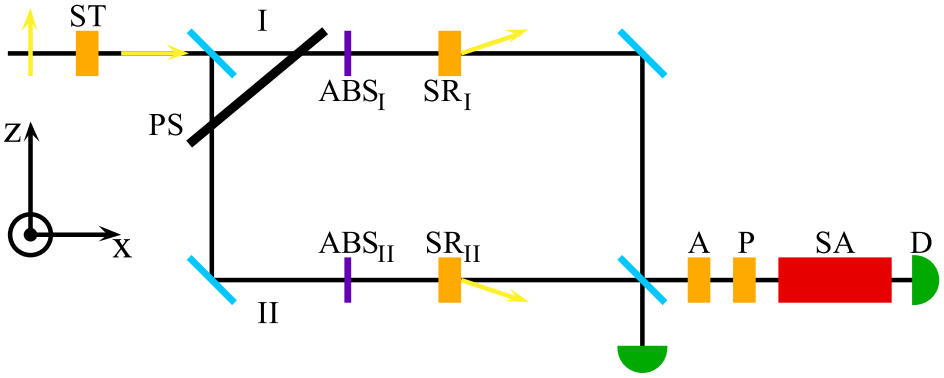

Figure 3.9.: Interferometer experiment for a weak measurement of the path operator: The setup consists of the interferometer itself, a $\frac{\pi}{2}$-turner (ST), two variable absorbers (ABS$_I$ & ABS$_{II}$), two spin rotators (SR$_I$ & SR$_{II}$) and a spin analyzer [two coils to select the azimuth and polar angle (A & P), the red supermirror (SA) and a detector (D)].

experiences a path dependent phase shift. In addition to that, variable absorbers are placed in both paths, which complete the pre selection of the ensemble. Now the weak measurement is performed. This is done by rotating the spin in the xy-plane. By making the angle of rotation very small, it is guaranteed that the system is not disturbed significantly. At the exit of the interferometer the beams are recombined. This is equal to post selecting the ensemble. Finally $\langle\hat{\sigma}_x^s\rangle$ is evaluated. Here it is explained, how this setup allows to perform a weak measurement of the path operator.
As long as the neutron spin is aligned parallel to the z-axis its spin wave function is given by $|S_z;+\rangle$. After the $\frac{\pi}{2}$-turn it can be described by

$$|S\rangle = \sqrt{\frac{1}{2}}\left(|S_z;+\rangle + |S_z;-\rangle\right). \tag{3.52}$$

When the neutron beam enters the interferometer, it is split into two paths. The spin wave function has to be extended by a part describing the path, so that the combined wave function $|\psi\rangle$ becomes

$$|\psi\rangle = |P\rangle|S\rangle = \sqrt{\frac{1}{2}}\left(|I\rangle + |II\rangle\right)\sqrt{\frac{1}{2}}\left(|S_z;+\rangle + |S_z;-\rangle\right), \tag{3.53}$$

where $|I\rangle$ and $|II\rangle$ describe path I and path II respectively. After that a phase shifter is put into the beam. This adds a path dependent phase ($\mathrm{e}^{-i\chi/2}$ for path I and $\mathrm{e}^{i\chi/2}$ for path II). Additionally variable absorbers are placed in both paths. This enables the pre selection of the ensemble. The normalized wave function $|\psi\rangle$ describing the system is now

$$|\psi\rangle = \underbrace{\left[\mathrm{e}^{-i\chi/2}\sqrt{b}|I\rangle + \mathrm{e}^{i\chi/2}\sqrt{a}|II\rangle\right]}_{|P_i\rangle}\underbrace{\sqrt{\frac{1}{2}}\left[|S_z;+\rangle + |S_z;-\rangle\right]}_{|S_x;+\rangle}, \tag{3.54}$$

with a and $b = 1 - a$ describing the effect of the absorber present in the paths.[c] At this point the pre selection of the ensemble is completed.
Now the weak measurement is performed. This is done by rotating the spin in the xy-plane. By making the rotation path dependent, it is possible to 'mark' the path the neutron took. The angle of rotation is kept small. Therefore the system's wave function is not disturbed significantly and the condition for a weak measurement is fulfilled. The interaction Hamiltonian for such a measurement is given by

$$\hat{H}_i = -\vec{\mu}\vec{B}\hat{\Pi}_z = -\gamma\hat{S}\vec{B}\hat{\Pi}_z \equiv \frac{-\alpha\hat{\sigma}_z^s\hat{\Pi}_z}{2}, \tag{3.55}$$

where $\vec{\mu}$ is the neutron's magnetic moment and $\vec{B}$ an externally applied magnetic field. $\vec{\mu}$ is directly proportional to the neutron's spin via the so called gyromagnetic ratio γ. $\vec{B}$ and γ can be combined into the parameter α, which describes the angle of rotation and therefore the interaction strength of the measurement. $\hat{\sigma}_z^s$ is the operator describing the rotation around the z-axis and $\hat{\Pi}_z$ is the operator which represents the neutron's path. It is given by a Pauli matrix as $\hat{\Pi}_z = |I\rangle\langle I| - |II\rangle\langle II|$. This experiment is designed to extract the weak value of $\hat{\Pi}_z$. After the weak measurement the wave function evolves.

$$\begin{aligned}
|\psi'\rangle &= \mathrm{e}^{i\alpha\hat{\sigma}_z^s\hat{\Pi}_z/2}|\psi\rangle \approx \left(1 + \frac{i\alpha\hat{\sigma}_z^s\hat{\Pi}_z}{2}\right)|\psi\rangle \\
&= |P_i\rangle|S_x;+\rangle + \frac{i\alpha\hat{\Pi}_z}{2}|P_i\rangle\hat{\sigma}_z^s|S_x;+\rangle \\
&= |P_i\rangle|S_x;+\rangle + \frac{i\alpha\hat{\Pi}_z}{2}|P_i\rangle\left(|S_z;+\rangle\langle S_z;+| - |S_z;-\rangle\langle S_z;-|\right)|S_x;+\rangle \\
&= |P_i\rangle|S_x;+\rangle + \frac{i\alpha\hat{\Pi}_z}{2}|P_i\rangle|S_x;-\rangle.
\end{aligned} \tag{3.56}$$

At the exit of the interferometer the neutrons are post selected by recombining the beams. Mathematically this is done by multiplying the projector $|P_f\rangle\langle P_f|$ with the the final state

[c] a ranges from 0 to 1. For $a = 0$ path II is completely blocked, for 1 path I. At $a = 0.5$ the absorber is equally strong for path I and II.

$|P_f\rangle = \sqrt{\frac{1}{2}}\left(|I\rangle + |II\rangle\right)$ from the left onto $|\psi\rangle$.

$$
\begin{aligned}
|\Phi\rangle &= |P_f\rangle\langle P_f|\psi'\rangle = |P_f\rangle\langle P_f|P_i\rangle|S_x;+\rangle + \frac{i\alpha}{2}|P_f\rangle\langle P_f|\hat{\Pi}_z|P_i\rangle|S_x;-\rangle \\
&= \langle P_f|P_i\rangle \left(|S_x;+\rangle + \frac{i\alpha}{2} \underbrace{\frac{\langle P_f|\hat{\Pi}_z|P_i\rangle}{\langle P_f|P_i\rangle}}_{\equiv\langle\hat{\Pi}_z\rangle_w} |S_x;-\rangle \right) |P_f\rangle \\
&= \underbrace{\sqrt{\frac{1}{2}}\left[\sqrt{1-a}\ \mathrm{e}^{-i\chi/2} + \sqrt{a}\ \mathrm{e}^{i\chi/2}\right]}_{\equiv\epsilon} \sqrt{\frac{1}{2}}\left[\left(|S_z;+\rangle + |S_z;-\rangle\right) + \frac{i\alpha}{2}\langle\hat{\Pi}_z\rangle_w \left(|S_z;+\rangle - |S_z;-\rangle\right)\right] |P_f\rangle \\
&= \frac{\epsilon}{\sqrt{2}}\left[\left(1 + \frac{i\alpha}{2}\langle\hat{\Pi}_z\rangle_w\right)|S_z;+\rangle + \left(1 - \frac{i\alpha}{2}\langle\hat{\Pi}_z\rangle_w\right)|S_z;-\rangle \right] |P_f\rangle \\
&\approx \frac{\epsilon}{\sqrt{2}}\left(\mathrm{e}^{i\alpha\langle\hat{\Pi}_z\rangle_w/2}|S_z;+\rangle + \mathrm{e}^{-i\alpha\langle\hat{\Pi}_z\rangle_w/2}|S_z;-\rangle \right) |P_f\rangle
\end{aligned}
\tag{3.57}
$$

The weak value is now defined as $\langle\hat{\Pi}_z\rangle_w$ and acts as an additional phase in the wave function. After post selection $\langle\hat{\sigma}_x^s\rangle$ is evaluated

$$
\begin{aligned}
\langle\hat{\sigma}_x^s\rangle &= \frac{\langle\Phi\,|\hat{\sigma}_x^s|\,\Phi\rangle}{\langle\Phi|\Phi\rangle} = \frac{\langle P_f|P_f\rangle}{2}\frac{\epsilon\epsilon^*}{\langle\Phi|\Phi\rangle}\left(\mathrm{e}^{-i\alpha\langle\hat{\Pi}_z\rangle_w/2}\langle S_z;+| + \mathrm{e}^{i\alpha\langle\hat{\Pi}_z\rangle_w/2}\langle S_z;-|\right)\times \\
&\qquad \times \left(|S_z;+\rangle\langle S_z;-| + |S_z;-\rangle\langle S_z;+|\right)\left(\mathrm{e}^{i\alpha\langle\hat{\Pi}_z\rangle_w/2}|S_z;+\rangle + \mathrm{e}^{-i\alpha\langle\hat{\Pi}_z\rangle_w/2}|S_z;-\rangle\right) \\
&= \frac{1}{2}\frac{|\epsilon|^2}{\langle\Phi|\Phi\rangle}\left(\mathrm{e}^{-i\alpha\langle\hat{\Pi}_z\rangle_w/2}\langle S_z;-| + \mathrm{e}^{i\alpha\langle\hat{\Pi}_z\rangle_w/2}\langle S_z;+|\right)\left(\mathrm{e}^{i\alpha\langle\hat{\Pi}_z\rangle_w/2}|S_z;+\rangle + \mathrm{e}^{-i\alpha\langle\hat{\Pi}_z\rangle_w/2}|S_z;-\rangle\right) \\
&= \frac{1}{2}\frac{|\epsilon|^2}{\langle\Phi|\Phi\rangle}\left(\mathrm{e}^{i\alpha\langle\hat{\Pi}_z\rangle_w} + \mathrm{e}^{-i\alpha\langle\hat{\Pi}_z\rangle_w}\right) = \frac{|\epsilon|^2}{\langle\Phi|\Phi\rangle}\cos\left(\alpha\langle\hat{\Pi}_z\rangle_w\right).
\end{aligned}
\tag{3.58}
$$

Since

$$
\begin{aligned}
|\epsilon|^2 &= \sqrt{\frac{1}{2}}\left[\sqrt{1-a}\ \mathrm{e}^{-i\chi/2} + \sqrt{a}\ \mathrm{e}^{i\chi/2}\right]\sqrt{\frac{1}{2}}\left[\sqrt{1-a}\ \mathrm{e}^{i\chi/2} + \sqrt{a}\ \mathrm{e}^{-i\chi/2}\right] \\
&= \frac{1}{2} + \sqrt{a\,(1-a)}\ \cos(\chi)\,,
\end{aligned}
\tag{3.59}
$$

and

$$
\begin{aligned}
\langle\Phi|\Phi\rangle &= \frac{\langle P_f|P_f\rangle}{2}\left[\sqrt{1-a}\ \mathrm{e}^{i\chi/2} + \sqrt{a}\ \mathrm{e}^{-i\chi/2}\right]\left[\langle S_z;+|\mathrm{e}^{-i\alpha\langle\hat{\Pi}_z\rangle_w/2} + \langle S_z;-|\mathrm{e}^{i\alpha\langle\hat{\Pi}_z\rangle_w/2}\right]\times \\
&\qquad \times \left[\mathrm{e}^{i\alpha\langle\hat{\Pi}_z\rangle_w/2}|S_z;+\rangle + \mathrm{e}^{-i\alpha\langle\hat{\Pi}_z\rangle_w/2}|S_z;-\rangle\right]\frac{1}{2}\left[\sqrt{1-a}\ \mathrm{e}^{-i\chi/2} + \sqrt{a}\ \mathrm{e}^{i\chi/2}\right] \\
&= \frac{1}{2} + \sqrt{a\,(1-a)}\ \cos(\chi)
\end{aligned}
\tag{3.60}
$$

are equal, i.e. $|\epsilon|^2 = \langle\Phi|\Phi\rangle$, Eq. (3.58) becomes

$$
\langle\hat{\sigma}_x^s\rangle = \cos\left(\alpha\langle\hat{\Pi}_z\rangle_w\right) \tag{3.61}
$$

The left hand side of Eq. (3.61) is now given by $\langle\hat{\sigma}_x^s\rangle = \frac{I_+ - I_-}{I_+ + I_-}$ and the weak value can be determined by measuring the two different intensities for I_+ and I_-.

$$\langle\hat{\Pi}_z\rangle_w(\alpha, I_+, I_-) = \frac{1}{\alpha}\arccos\left(\left[\frac{I_+ - I_-}{I_+ + I_-}\right]\right) \tag{3.62}$$

I_+ and I_- are the intensities for the neutron spin aligned parallel and anti parallel to the x-axis. In Eq. (3.56) a Taylor expansion of the exponential function has been performed according to the theory of weak measurements, making use of the fast that $\alpha \ll 1$. Let us try a slightly different approach now, which uses the exact formula $\exp\left(i\alpha\ \hat{\sigma}_j^s \cdot \hat{n}\right) = \mathbb{1}\cos(\alpha) + i\ \hat{\sigma}_j^s \cdot \hat{n}\sin(\alpha)$[d].

$$\begin{aligned}
|\psi'\rangle = \mathrm{e}^{i\alpha\hat{\sigma}_z^s\hat{\Pi}_z/2}|\psi\rangle &= \left[\cos\left(\frac{\alpha}{2}\right) + i\hat{\sigma}_z^s\hat{\Pi}_z\sin\left(\frac{\alpha}{2}\right)\right]|P_i\rangle|S_x;+\rangle \\
&= \cos\left(\frac{\alpha}{2}\right)|P_i\rangle|S_x;+\rangle + i\hat{\sigma}_z^s\hat{\Pi}_z\sin\left(\frac{\alpha}{2}\right)|P_i\rangle|S_x;+\rangle \\
&= \cos\left(\frac{\alpha}{2}\right)|P_i\rangle|S_x;+\rangle + i\sin\left(\frac{\alpha}{2}\right)\hat{\Pi}_z|P_i\rangle|S_x;-\rangle.
\end{aligned} \tag{3.63}$$

Again post selection is performed.

$$\begin{aligned}
|\Phi\rangle = |P_f\rangle\langle P_f|\psi'\rangle &= \cos\left(\frac{\alpha}{2}\right)|P_f\rangle\langle P_f|P_i\rangle|S_x;+\rangle + i\sin\left(\frac{\alpha}{2}\right)|P_f\rangle\langle P_f|\hat{\Pi}_z|P_i\rangle|S_x;-\rangle \\
&= \langle P_f|P_i\rangle\left[\cos\left(\frac{\alpha}{2}\right)|S_x;+\rangle + i\sin\left(\frac{\alpha}{2}\right)\underbrace{\frac{\langle P_f|\hat{\Pi}_z|P_i\rangle}{\langle P_f|P_i\rangle}}_{\equiv\langle\hat{\Pi}_z\rangle_w}|S_x;-\rangle\right]|P_f\rangle \\
&= \frac{\sqrt{1-a}\ \mathrm{e}^{-i\chi/2} + \sqrt{a}\ \mathrm{e}^{i\chi/2}}{\sqrt{2}}\left[\cos\left(\frac{\alpha}{2}\right)|S_x;+\rangle + i\sin\left(\frac{\alpha}{2}\right)\langle\hat{\Pi}_z\rangle_w|S_x;-\rangle\right]|P_f\rangle \\
&= \frac{\sqrt{1-a}\ \mathrm{e}^{-i\chi/2} + \sqrt{a}\ \mathrm{e}^{i\chi/2}}{2}\left\{\left[\cos\left(\frac{\alpha}{2}\right) + i\sin\left(\frac{\alpha}{2}\right)\langle\hat{\Pi}_z\rangle_w\right]|S_z;+\rangle + \right. \\
&\quad \left. + \left[\cos\left(\frac{\alpha}{2}\right) - i\sin\left(\frac{\alpha}{2}\right)\langle\hat{\Pi}_z\rangle_w\right]|S_z;-\rangle\right\}|P_f\rangle,
\end{aligned} \tag{3.64}$$

and finally $\langle\hat{\sigma}_x^s\rangle$ is evaluated

$$\begin{aligned}
\langle\hat{\sigma}_x^s\rangle = \frac{\langle\Phi\,|\hat{\sigma}_x^s|\,\Phi\rangle}{\langle\Phi|\Phi\rangle} &= \frac{\langle P_f|P_f\rangle}{2}\frac{\epsilon\epsilon^*}{\langle\Phi|\Phi\rangle}\left[\left(\mathrm{c} - i\mathrm{s}\langle\hat{\Pi}_z\rangle_w\right)\langle S_z;+| + \left(\mathrm{c} + i\mathrm{s}\langle\hat{\Pi}_z\rangle_w\right)\langle S_z;-|\right]\times \\
&\quad \times\left[|S_z;+\rangle\langle S_z;-| + |S_z;-\rangle\langle S_z;+|\right]\left[\left(\mathrm{c} + i\mathrm{s}\langle\hat{\Pi}_z\rangle_w\right)|S_z;+\rangle + \left(\mathrm{c} - i\mathrm{s}\langle\hat{\Pi}_z\rangle_w\right)|S_z;-\rangle\right] \\
&= \frac{1}{2}\frac{|\epsilon|^2}{\langle\Phi|\Phi\rangle}\left[\left(\mathrm{c} - i\mathrm{s}\langle\hat{\Pi}_z\rangle_w\right)^2 + \left(\mathrm{c} + i\mathrm{s}\langle\hat{\Pi}_z\rangle_w\right)^2\right] \\
&= \frac{|\epsilon|^2}{\langle\Phi|\Phi\rangle}\left[\cos^2\left(\frac{\alpha}{2}\right) - \langle\hat{\Pi}_z\rangle_w^2\sin^2\left(\frac{\alpha}{2}\right)\right],
\end{aligned} \tag{3.65}$$

[d] Mathematically this means that we consider all orders of α, instead of just the first.

where the abbreviations $\mathrm{s} \equiv \sin(\frac{\alpha}{2})$ and $\mathrm{c} \equiv \cos(\frac{\alpha}{2})$ were used. With the same abbreviations the normalization factor $\langle\Phi|\Phi\rangle$ is

$$\begin{aligned}\langle\Phi|\Phi\rangle &= \frac{\langle P_f|P_f\rangle}{2}\left[\sqrt{1-a}\,\mathrm{e}^{i\chi/2}+\sqrt{a}\,\mathrm{e}^{-i\chi/2}\right]\left[\langle S_z;+|\left(\mathrm{c}-i\mathrm{s}\langle\hat{\Pi}_z\rangle_w\right)+\langle S_z;-|\left(\mathrm{c}+i\mathrm{s}\langle\hat{\Pi}_z\rangle_w\right)\right\}\times\\ &\quad\times\left[\left(\mathrm{c}+i\mathrm{s}\langle\hat{\Pi}_z\rangle_w\right)|S_z;+\rangle+\left(\mathrm{c}-i\mathrm{s}\langle\hat{\Pi}_z\rangle_w\right)|S_z;-\rangle\right]\frac{1}{2}\left[\sqrt{1-a}\,\mathrm{e}^{-i\chi/2}+\sqrt{a}\,\mathrm{e}^{i\chi/2}\right]\\ &= \left[1+2\sqrt{a\,(1-a)}\cos(\chi)\right]\left[\cos^2\left(\frac{\alpha}{2}\right)+\langle\hat{\Pi}_z\rangle_w^2\sin\left(\frac{\alpha}{2}\right)\right] \qquad (3.66)\end{aligned}$$

so that Eq. (3.65) simplifies to

$$\langle\hat{\sigma}_x^s\rangle = \frac{\cos^2\left(\frac{\alpha}{2}\right)-\langle\hat{\Pi}_z\rangle_w^2\sin\left(\frac{\alpha}{2}\right)}{\cos^2\left(\frac{\alpha}{2}\right)+\langle\hat{\Pi}_z\rangle_w^2\sin\left(\frac{\alpha}{2}\right)} \qquad (3.67)$$

and the weak value $\langle\hat{\Pi}_z\rangle_w$ becomes

$$\begin{aligned}\frac{I_+-I_-}{I_++I_-} &= \frac{\cos^2\left(\frac{\alpha}{2}\right)-\langle\hat{\Pi}_z\rangle_w^2\sin^2\left(\frac{\alpha}{2}\right)}{\cos^2\left(\frac{\alpha}{2}\right)+\langle\hat{\Pi}_z\rangle_w^2\sin^2\left(\frac{\alpha}{2}\right)}\\ \Rightarrow\qquad \left|\langle\hat{\Pi}_z\rangle_w\right| &= \sqrt{\frac{\cos^2\left(\frac{\alpha}{2}\right)-\frac{I_+-I_-}{I_++I_-}\cos^2\left(\frac{\alpha}{2}\right)}{\sin^2\left(\frac{\alpha}{2}\right)+\frac{I_+-I_-}{I_++I_-}\sin^2\left(\frac{\alpha}{2}\right)}} = \sqrt{\frac{I_-}{I_+}\cot^2\left(\frac{\alpha}{2}\right)} \qquad (3.68)\end{aligned}$$

Per definition the weak value can be calculated as follows

$$\begin{aligned}\langle\hat{\Pi}_z\rangle_w &\equiv \frac{\langle P_f|\hat{\Pi}_z|P_i\rangle}{\langle P_f|P_i\rangle} = \frac{\left[\langle I|+\langle II|\right]\left[\mathrm{e}^{-i\chi/2}\sqrt{1-a}|I\rangle-\mathrm{e}^{i\chi/2}\sqrt{a}|II\rangle\right]}{\left[\langle I|+\langle II|\right]\left[\mathrm{e}^{-i\chi/2}\sqrt{1-a}|I\rangle+\mathrm{e}^{i\chi/2}\sqrt{a}|II\rangle\right]}\\ &= \frac{\sqrt{1-a}-\sqrt{a}\,\mathrm{e}^{i\chi}}{\sqrt{1-a}+\sqrt{a}\,\mathrm{e}^{i\chi}} \qquad (3.69)\end{aligned}$$

The plot of Eq. (3.69) in Fig. 3.10 exhibits very interesting features. In some sense the information about the absorber is stored in the real part of $\langle\hat{\Pi}_z\rangle_w$, whereas the information about the phase shifter is found in the imaginary part.
For $a = 0$ path II is completely blocked and all neutrons have to go through path I. For this case $\mathrm{Re}(\langle\hat{\Pi}_z\rangle_w)$ becomes 1. The opposite limit is $a = 1$. Now path I is completely blocked and $\mathrm{Re}(\langle\hat{\Pi}_z\rangle_w)$ equals -1. For any case between those two limits, i.e. both parts are partially blocked, $\mathrm{Re}(\langle\hat{\Pi}_z\rangle_w)$ is $-1 < \mathrm{Re}(\langle\hat{\Pi}_z\rangle_w) < 1$.
It is also possible to model the absorber in a different way, using

$$|P_i\rangle = \mathrm{e}^{-i\chi/2}\cos(a)\,|I\rangle + \mathrm{e}^{i\chi/2}\sin(a)\,|II\rangle. \qquad (3.70)$$

Now a ranges from 0 to $\frac{\pi}{2}$. Again, for $a = 0$ path II is completely blocked, for $\frac{\pi}{2}$ path I. At $a = \frac{\pi}{4}$ the absorber is equally strong for path I and II. Equations (3.62) and (3.68) do not change. However, the weak value itself becomes:

$$\begin{aligned}\langle\hat{\Pi}_z\rangle_w &\equiv \frac{\langle P_f|\hat{\Pi}_z|P_i\rangle}{\langle P_f|P_i\rangle} = \frac{\left[\langle I|+\langle II|\right]\left[\mathrm{e}^{-i\chi/2}\cos(a)\,|I\rangle-\mathrm{e}^{i\chi/2}\sin(a)\,|II\rangle\right]}{\left[\langle I|+\langle II|\right]\left[\mathrm{e}^{-i\chi/2}\cos(a)\,|I\rangle+\mathrm{e}^{i\chi/2}\sin(a)\,|II\rangle\right]}\\ &= \frac{\cos(a)-\sin(a)\,\mathrm{e}^{i\chi}}{\cos(a)+\sin(a)\,\mathrm{e}^{i\chi}} \qquad (3.71)\end{aligned}$$

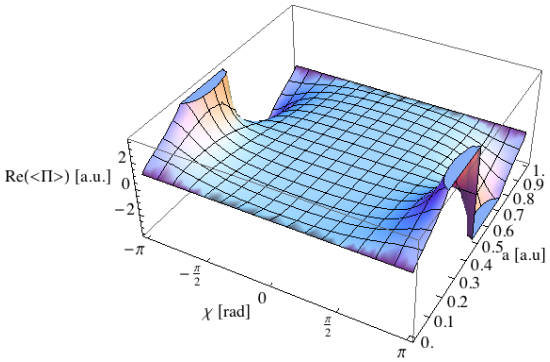

(a) 3D plot of $\mathrm{Re}(\langle\hat{\Pi}_z\rangle_w)$ [real part of Eq. (3.69)]

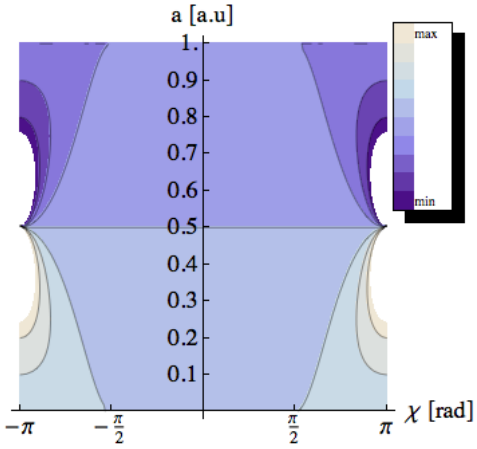

(b) Contour plot of $\mathrm{Re}(\langle\hat{\Pi}_z\rangle_w)$ [real part of Eq. (3.69)]

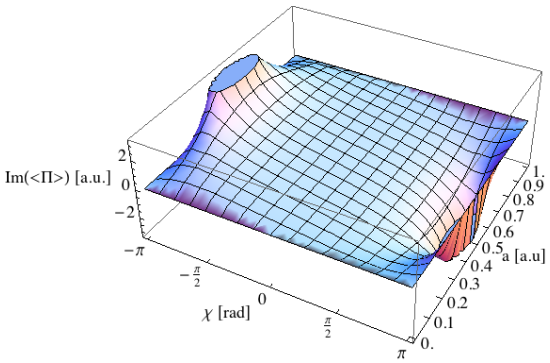

(c) 3D plot of $\mathrm{Im}(\langle\hat{\Pi}_z\rangle_w)$ [imaginary part of Eq. (3.69)]

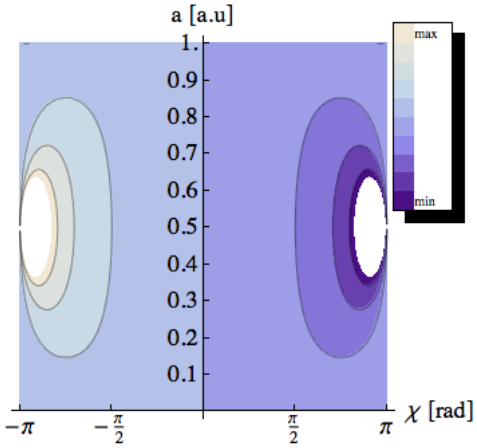

(d) Contour plot of $\mathrm{Im}(\langle\hat{\Pi}_z\rangle_w)$ [imaginary part of Eq. (3.69)]

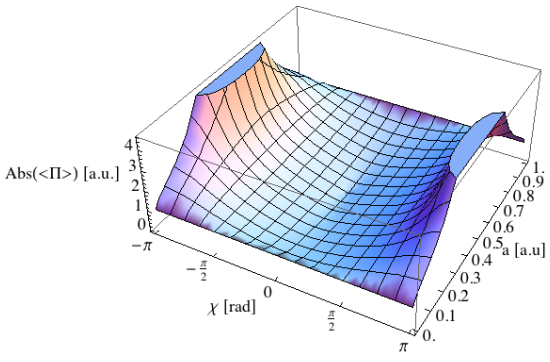

(e) 3D plot of $\mathrm{Abs}(\langle\hat{\Pi}_z\rangle_w)$ [absolute of Eq. (3.69)]

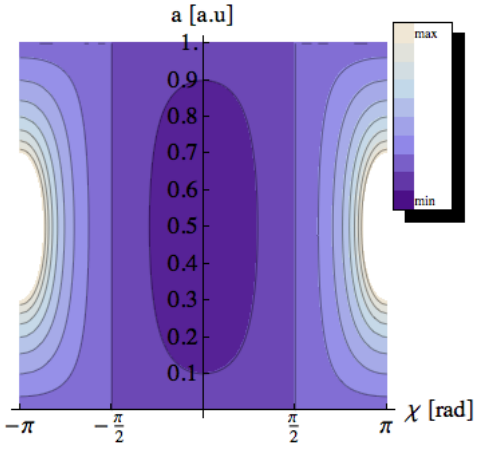

(f) Contour plot of $\mathrm{Abs}(\langle\hat{\Pi}_z\rangle_w)$ [absolute of Eq. (3.69)]

Figure 3.10.: Visualization of the weak value, for real and imaginary part, as well as for the absolute of the weak value. The absorber is modeled as $|P_i\rangle = \mathrm{e}^{-i\chi/2}\sqrt{b}|I\rangle + \mathrm{e}^{i\chi/2}\sqrt{a}|II\rangle$ with $b = 1 - a$.

Real and imaginary parts of Eq. (3.71), as well as its absolute value are plotted in Fig. 3.11. The different parametrization of the absorber in the calculation induces no big effect on the weak value itself. The maxima and minima are more compact, but the overall shape stays roughly the same.

3.2.1. Estimates of the measurement strength's influence

To get a better understanding of the system it is possible to perform an analytical evaluation of the factor $\frac{I_+ - I_-}{I_+ + I_-}$. For this we start with the system's wave function which is given by Eq. (3.54) and let the evolution operator $\hat{U} = \exp\left(\frac{i\alpha\hat{\Pi}_z\hat{\sigma}_z^s}{2}\right)$ act upon it.

$$\begin{aligned}
|\psi'\rangle &= \mathrm{e}^{i\alpha\hat{\Pi}_z\hat{\sigma}_z^s/2}|\psi\rangle = \mathrm{e}^{i\alpha\hat{\Pi}_z\hat{\sigma}_z^s/2}\left(\mathrm{e}^{-i\chi/2}\sqrt{1-a}|I\rangle + \mathrm{e}^{i\chi/2}\sqrt{a}|II\rangle\right)\sqrt{\frac{1}{2}}\left(|S_z;+\rangle + |S_z;-\rangle\right) \\
&= \sqrt{\frac{1}{2}}\mathrm{e}^{i\alpha\hat{\Pi}_z\hat{\sigma}_z^s/2}\Big(\mathrm{e}^{-i\chi/2}\sqrt{1-a}|I\rangle|S_z;+\rangle + \mathrm{e}^{-i\chi/2}\sqrt{1-a}|I\rangle|S_z;-\rangle + \\
&\quad + \mathrm{e}^{i\chi/2}\sqrt{a}|II\rangle|S_z;+\rangle + \mathrm{e}^{i\chi/2}\sqrt{a}|II\rangle|S_z;-\rangle\Big) \\
&= \sqrt{\frac{1}{2}}\Big(\mathrm{e}^{-i\chi/2}\sqrt{1-a}\ \mathrm{e}^{i\alpha/2}|I\rangle|S_z;+\rangle + \mathrm{e}^{-i\chi/2}\sqrt{1-a}\ \mathrm{e}^{-i\alpha/2}|I\rangle|S_z;-\rangle + \\
&\quad + \mathrm{e}^{i\chi/2}\sqrt{a}\ \mathrm{e}^{-i\alpha/2}|II\rangle|S_z;+\rangle + \mathrm{e}^{i\chi/2}\sqrt{a}\ \mathrm{e}^{i\alpha/2}|II\rangle|S_z;-\rangle\Big)
\end{aligned} \tag{3.72}$$

Now we post select onto $|P_f\rangle\langle P_f|$ with $|P_f\rangle = \sqrt{\frac{1}{2}}\left(|I\rangle + |II\rangle\right)$ and get

$$\begin{aligned}
|\Phi\rangle = |P_f\rangle\langle P_f|\psi\rangle &= \frac{1}{2}\Big(\mathrm{e}^{-i\chi/2}\sqrt{1-a}\ \mathrm{e}^{i\alpha/2}|S_z;+\rangle + \mathrm{e}^{-i\chi/2}\sqrt{1-a}\ \mathrm{e}^{-i\alpha/2}|S_z;-\rangle + \\
&\quad + \mathrm{e}^{i\chi/2}\sqrt{a}\ \mathrm{e}^{-i\alpha/2}|S_z;+\rangle + \mathrm{e}^{i\chi/2}\sqrt{a}\ \mathrm{e}^{i\alpha/2}|S_z;-\rangle\Big)|P_f\rangle \\
&= \Bigg\{\frac{1}{2}\left[\mathrm{e}^{-i(\chi-\alpha)/2}\sqrt{1-a} + \mathrm{e}^{i(\chi-\alpha)/2}\sqrt{a}\right]|S_z;+\rangle + \\
&\quad + \frac{1}{2}\left[\mathrm{e}^{-i(\chi+\alpha)/2}\sqrt{1-a} + \mathrm{e}^{i(\chi+\alpha)/2}\sqrt{a}\right]|S_z;-\rangle\Bigg\}|P_f\rangle
\end{aligned} \tag{3.73}$$

The next step is to perform the projection onto the negative and positive spin state, which yields

$$\begin{aligned}
\langle S_x;-|\Phi\rangle &= \sqrt{\frac{1}{2}}\left\{\langle S_z;+| - \langle S_z;-|\right\}\Bigg\{\frac{1}{2}\left[\mathrm{e}^{-i(\chi-\alpha)/2}\sqrt{1-a} + \mathrm{e}^{i(\chi-\alpha)/2}\sqrt{a}\right]|S_z;+\rangle + \\
&\quad + \frac{1}{2}\left[\mathrm{e}^{-i(\chi+\alpha)/2}\sqrt{1-a} + \mathrm{e}^{i(\chi+\alpha)/2}\sqrt{a}\right]|S_z;-\rangle\Bigg\}|P_f\rangle \\
&= \sqrt{\frac{1}{8}}\left\{\left[\mathrm{e}^{-i(\chi-\alpha)/2}\sqrt{1-a} + \mathrm{e}^{i(\chi-\alpha)/2}\sqrt{a}\right] - \left[\mathrm{e}^{-i(\chi+\alpha)/2}\sqrt{1-a} + \mathrm{e}^{i(\chi+\alpha)/2}\sqrt{a}\right]\right\}|P_f\rangle
\end{aligned} \tag{3.74}$$

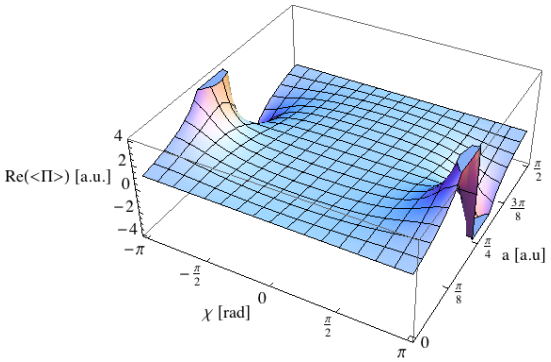

(a) 3D plot of $\mathrm{Re}(\langle\hat{\Pi}_z\rangle_w)$ [real part of Eq. (3.71)]

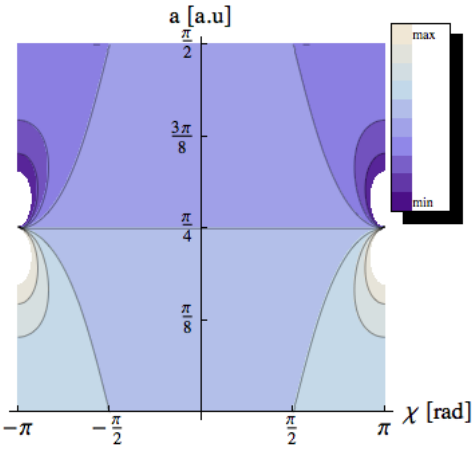

(b) Contour plot of $\mathrm{Re}(\langle\hat{\Pi}_z\rangle_w)$ [real part of Eq. (3.71)]

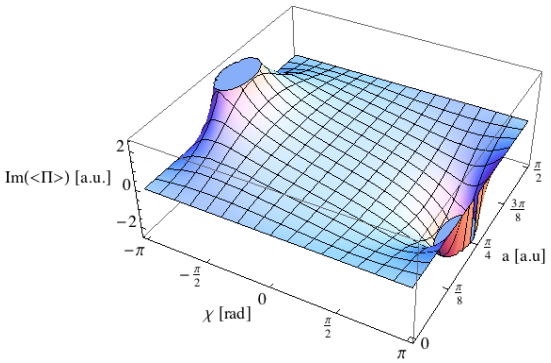

(c) 3D plot of $\mathrm{Im}(\langle\hat{\Pi}_z\rangle_w)$ [imaginary part of Eq. (3.71)]

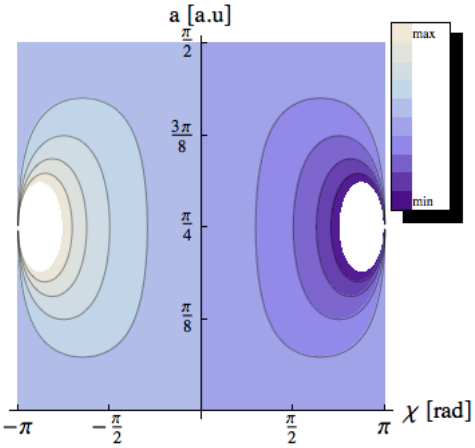

(d) Contour plot of $\mathrm{Im}(\langle\hat{\Pi}_z\rangle_w)$ [imaginary part of Eq. (3.71)]

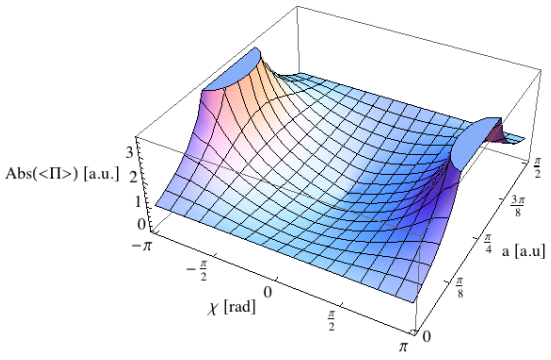

(e) 3D plot of $\mathrm{Abs}(\langle\hat{\Pi}_z\rangle_w)$ [absolute of Eq. (3.71)]

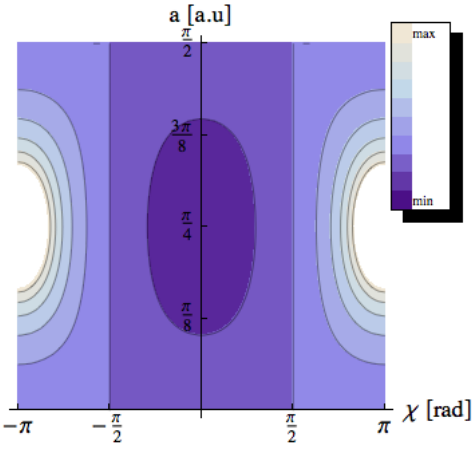

(f) Contour plot of $\mathrm{Abs}(\langle\hat{\Pi}_z\rangle_w)$ [absolute of Eq. (3.71)]

Figure 3.11.: Visualization of the weak value, for real and imaginary part, as well as for the absolute of the weak value. The absorber is modeled as $|P_i\rangle = \mathrm{e}^{-i\chi/2}\cos(a)\,|I\rangle + \mathrm{e}^{i\chi/2}\sin(a)\,|II\rangle$

and analogously

$$\langle S_x;+|\Phi\rangle = \sqrt{\frac{1}{8}}\left\{\left[\mathrm{e}^{-i(\chi-\alpha)/2}\sqrt{1-a}+\mathrm{e}^{i(\chi-\alpha)/2}\sqrt{a}\right]+\left[\mathrm{e}^{-i(\chi+\alpha)/2}\sqrt{1-a}+\mathrm{e}^{i(\chi+\alpha)/2}\sqrt{a}\right]\right\}|P_f\rangle \tag{3.75}$$

With Eqs. (3.74) and (3.75) it is possible to calculate the intensities I_- and I_+

$$I_- = |\langle S_x;-|\Phi\rangle|^2 = \frac{1}{2}\left[1-2\sqrt{a\,(1-a)}\cos(\chi)\right]\sin^2\left(\frac{\alpha}{2}\right) \tag{3.76}$$

$$I_+ = |\langle S_x;+|\Phi\rangle|^2 = \frac{1}{2}\left[1+2\sqrt{a\,(1-a)}\cos(\chi)\right]\cos^2\left(\frac{\alpha}{2}\right) \tag{3.77}$$

Finally we get

$$\frac{I_+ - I_-}{I_+ + I_-} = \frac{\cos(\alpha)+2\sqrt{a\,(1-a)}\cos(\chi)}{1+2\sqrt{a\,(1-a)}\cos(\alpha)\cos(\chi)} \tag{3.78}$$

Now it is possible to directly evaluate the expectation value of the operator $\hat{\sigma}_x^s$ to check the result.

$$\begin{aligned}\langle\hat{\sigma}_x^s\rangle &= \frac{\langle\Phi|\left(|S_z;+\rangle\langle S_z;-|+|S_z;-\rangle\langle S_z;+|\right)|\Phi\rangle}{\langle\Phi|\Phi\rangle}\\ &= \frac{\langle\Phi|S_z;+\rangle\langle S_z;-|\Phi\rangle+\langle\Phi|S_z;-\rangle\langle S_z;+|\Phi\rangle}{\langle\Phi|\Phi\rangle}\end{aligned} \tag{3.79}$$

With

$$\begin{aligned}\langle\Phi|S_z;+\rangle\langle S_z;-|\Phi\rangle &= \frac{1}{4}\left[\mathrm{e}^{i(\chi-\alpha)/2}\sqrt{1-a}+\mathrm{e}^{-i(\chi-\alpha)/2}\sqrt{a}\right]\left[\mathrm{e}^{-i(\chi+\alpha)/2}\sqrt{1-a}+\mathrm{e}^{i(\chi+\alpha)/2}\sqrt{a}\right]+\\ &= \frac{1}{4}\left[\cos(\alpha)+2\sqrt{a\,(1-a)}\cos(\chi)+i\,(2a-1)\sin(\alpha)\right],\end{aligned} \tag{3.80}$$

$$\begin{aligned}\langle\Phi|S_z;-\rangle\langle S_z;+|\Phi\rangle &= \frac{1}{4}\left[\mathrm{e}^{i(\chi+\alpha)/2}\sqrt{1-a}+\mathrm{e}^{-i(\chi+\alpha)/2}\sqrt{a}\right]\left[\mathrm{e}^{-i(\chi-\alpha)/2}\sqrt{1-a}+\mathrm{e}^{i(\chi-\alpha)/2}\sqrt{a}\right]\\ &= \frac{1}{4}\left[\cos(\alpha)+2\sqrt{a\,(1-a)}\cos(\chi)+i\,(1-2a)\sin(\alpha)\right],\end{aligned} \tag{3.81}$$

and

$$\begin{aligned}\langle\Phi|\Phi\rangle &= \frac{1}{4}\left[\mathrm{e}^{i(\chi-\alpha)/2}\sqrt{1-a}+\mathrm{e}^{-i(\chi-\alpha)/2}\sqrt{a}\right]\left[\mathrm{e}^{-i(\chi-\alpha)/2}\sqrt{1-a}+\mathrm{e}^{i(\chi-\alpha)/2}\sqrt{a}\right]+\\ &\quad+\frac{1}{4}\left[\mathrm{e}^{i(\chi+\alpha)/2}\sqrt{1-a}+\mathrm{e}^{-i(\chi+\alpha)/2}\sqrt{a}\right]\left[\mathrm{e}^{-i(\chi+\alpha)/2}\sqrt{1-a}+\mathrm{e}^{i(\chi+\alpha)/2}\sqrt{a}\right]\\ &= \frac{1}{4}\left[1+2\sqrt{a\,(1-a)}\cos(\alpha-\chi)+1+2\sqrt{a\,(1-a)}\cos(\alpha+\chi)\right]\\ &= \frac{1}{4}\left\{2+2\sqrt{a\,(1-a)}\left[\cos(\alpha+\chi)+\cos(\alpha-\chi)\right]\right\}\\ &= \frac{1}{4}\left[2+4\sqrt{a\,(1-a)}\cos(\alpha)\cos(\chi)\right] = \frac{1}{2}+\sqrt{a\,(1-a)}\cos(\alpha)\cos(\chi),\end{aligned} \tag{3.82}$$

we get

$$\langle \hat{\sigma}_x^s \rangle = \frac{\frac{1}{2}\cos(\alpha) + \sqrt{a(1-a)}\cos(\chi)}{\frac{1}{2} + \sqrt{a(1-a)}\cos(\alpha)\cos(\chi)} = \frac{\cos(\alpha) + 2\sqrt{a(1-a)}\cos(\chi)}{1 + 2\sqrt{a(1-a)}\cos(\alpha)\cos(\chi)}, \tag{3.83}$$

which is just the same as Eq. (3.78). The degree of polarization is plotted in Fig. 3.12. A fixed value of $a = 0.5$ has been used. Having obtained this result, it is possible to further develop the

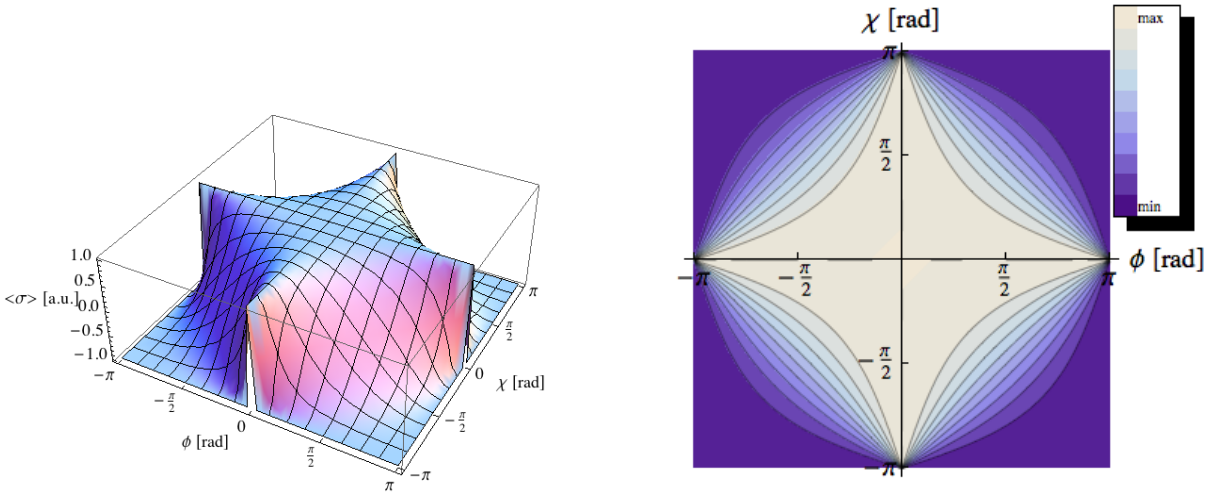

(a) 3D plot of the degree of polarization for a fixed value of $a = 0.5$ [Eq. (3.83)]

(b) Contour plot of the degree of polarization for a fixed value of $a = 0.5$ [Eq. (3.83)]

Figure 3.12.: Visualization of the degree of polarization. The absorber is set to a fixed value of $a = 0.5$. As expected the degree of polarization ranges from 1 to -1 one.

theoretical analysis of the experiment. Eq. (3.62) now becomes

$$\left|\langle \hat{\Pi}_z \rangle_w\right|(a, \alpha, \chi) = \frac{1}{\alpha}\arccos\left(\frac{\cos(\alpha) + 2\sqrt{a(1-a)}\ \cos(\chi)}{1 + 2\sqrt{a(1-a)}\ \cos(\alpha)\cos(\chi)}\right) \tag{3.84}$$

and Eq. (3.68) simplifies to

$$\left|\langle \hat{\Pi}_z \rangle_w\right|(a, \chi) = \sqrt{\frac{1 - 2\sqrt{a(1-a)}\ \cos(\chi)}{1 + 2\sqrt{a(1-a)}\ \cos(\chi)}}. \tag{3.85}$$

The same calculation can be performed for the second absorber model. For this case the intensities I_- and I_+ become

$$I_- = |\langle S_x; -|\Phi\rangle|^2 = \frac{1}{2}\left[1 - \sin(2a)\cos(\chi)\right]\sin^2\left(\frac{\alpha}{2}\right) \tag{3.86}$$

and

$$I_+ = |\langle S_x; +|\Phi\rangle|^2 = \frac{1}{2}\left[1 + \sin(2a)\cos(\chi)\right]\cos^2\left(\frac{\alpha}{2}\right). \tag{3.87}$$

The calculation using the approximation to extract the weak value then yields

$$\left|\langle\hat{\Pi}_z\rangle_w\right|(a,\alpha,\chi) = \frac{1}{\alpha}\arccos\left(\frac{\cos(\alpha)+\sin(2a)\cos(\chi)}{1+\sin(2a)\cos(\chi)\cos(\alpha)}\right), \tag{3.88}$$

whereas the one that considers all orders of α yields

$$\left|\langle\hat{\Pi}_z\rangle_w\right|(a,\chi) = \sqrt{\frac{1-\sin(2a)\cos(\chi)}{1+\sin(2a)\cos(\chi)}}. \tag{3.89}$$

At first glance it seems, that the exact calculation and the use of a Taylor expansion of the exponential function lead to two fundamentally different results. Eqs. (3.84) and (3.88) depend on α and their results can be a complex number. In comparison to that, Eqs. (3.85) and (3.89) are independent of α and always real. For any given value of a and χ the result will never be imaginary. But they are exactly the absolute of the analytic solutions given by Eqs. (3.69) and (3.71)!
Now the question arises, if there exists a certain value of α, for which Eqs. (3.84) and (3.88) reproduce the weak value's analytic solution. First of all, one has to notice, that the solutions obtained by using a Taylor expansion are practically the arccosine of the degree of polarization. As we showed earlier the degree of polarization always varies between -1 and 1. So we have $\langle\hat{\Pi}_z\rangle_w(x) \propto \arccos(x)$ with $-1 \leq x \leq 1$. For this value range the arccosine function is always real! This means that also the calculational method using approximations will never yield the weak value's imaginary part.
The next step is quite simple. We perform 'simulations' of the actual measurement. Equations (3.84) and (3.88) tell us what we will measure, if the experiment is performed at an ideal setup, for given values of α, a and χ. All we have to do is to pick values and compare the analytic solutions given by Eqs. (3.69) and (3.71) with what we expect from the experiment. The results of such a 'simulation' can be seen in Fig. 3.13 to 3.17. In Eq. (3.84) a has been set to 0.5 and its result is plotted for four different values of α dependent on the phase shifter position χ.

Fig. 3.13 shows the plot of Eq. (3.84) for $a = b = 0.5$ and $\alpha_a = \frac{\pi}{4}$. For $-\frac{\pi}{2} \leq \chi \leq \frac{\pi}{2}$ the two curves match. However, for larger values of χ the analytic solution rises more steeply than the measured solution.
If the angle of rotation is now reduced the curves begin to match better and better. This can be seen in Fig. 3.14 to 3.16, in which the values of α are reduced to $\alpha_b = \frac{\pi}{8}$, $\alpha_c = \frac{\pi}{20}$ and $\alpha_d = \frac{\pi}{36}$. For values of α that are smaller than $\frac{\pi}{36}$, the curves are nearly identical.
This tells us several very important things. Firstly Eqs. (3.62) and (3.68) are equivalent for small values of α, even though the first one is derived using an approximation and the second one is obtained by using exact formulas only.
Moreover we now know what small values of α means. As soon as the Eq.(3.62) reproduces the weak value's absolute, α is small enough. Fig. 3.13 to 3.16 tells us, that this happens at $\alpha \leq \frac{\pi}{36}$, i.e. for a angles of rotation that are smaller than or equal than 5°. This means that the interaction strength, described by the parameter α is at the order of magnitude of $\alpha \sim 0.1$. This also means that higher orders of α are already very small, i.e. $\mathcal{O}(\alpha^2) \sim 0.01$. Clearly rotations that are smaller than this fulfill the condition of a weak measurement and the approximations made in Eq. (3.56) are justified.
In addition to that, it is now clear that the experiment will only yield the absolute of the path operator's weak value. This is a bit of a setback, because to this point it was believed that the experiment would allow to extract 'which-way-information' from the interferometer, but one

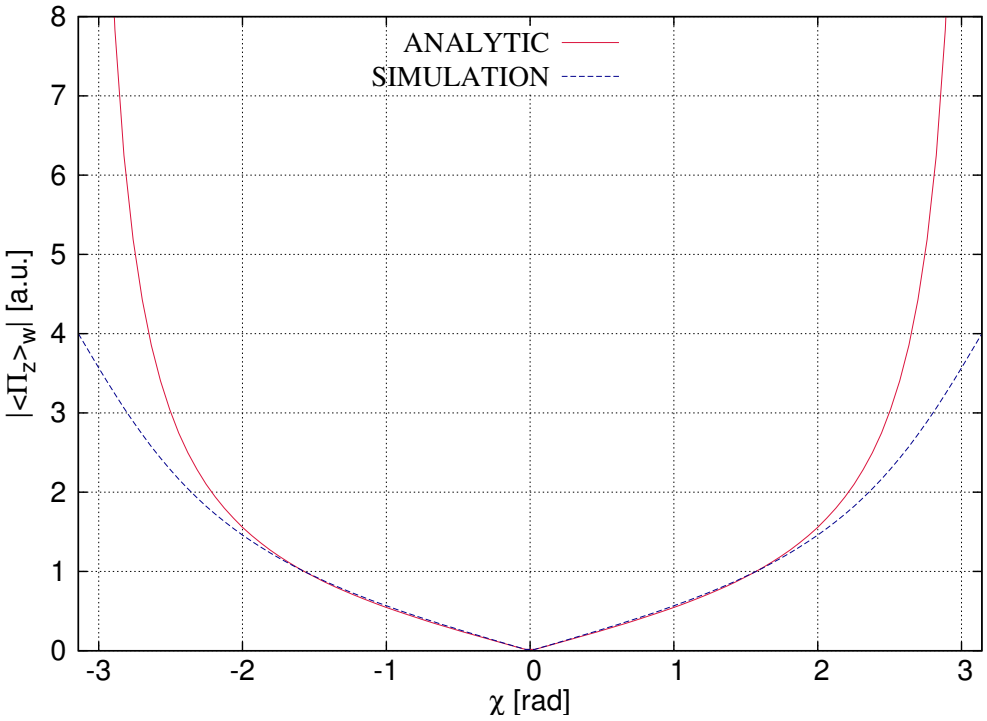

Figure 3.13.: Simulation [Eq. (3.84)] and the absolute of the weak value's analytic solution [absolute of Eq. (3.69)]. The absorber is modeled as $|P_i\rangle = \mathrm{e}^{-i\chi/2}\sqrt{1-a}|I\rangle + \mathrm{e}^{i\chi/2}\sqrt{a}|II\rangle$ with $a = 0.5$ and $\alpha = \pi/4$.

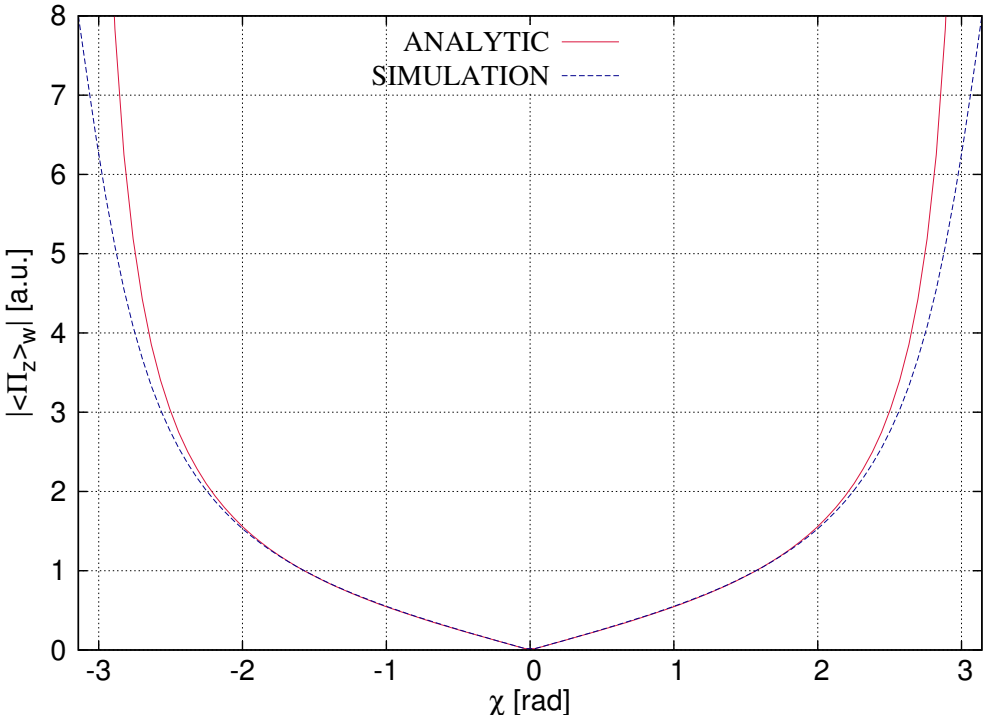

Figure 3.14.: Simulation [Eq. (3.84)] and the absolute of the weak value's analytic solution [absolute of Eq. (3.69)]. The absorber is modeled as $|P_i\rangle = \mathrm{e}^{-i\chi/2}\sqrt{1-a}|I\rangle + \mathrm{e}^{i\chi/2}\sqrt{a}|II\rangle$ with $a = 0.5$ and $\alpha = \pi/8$.

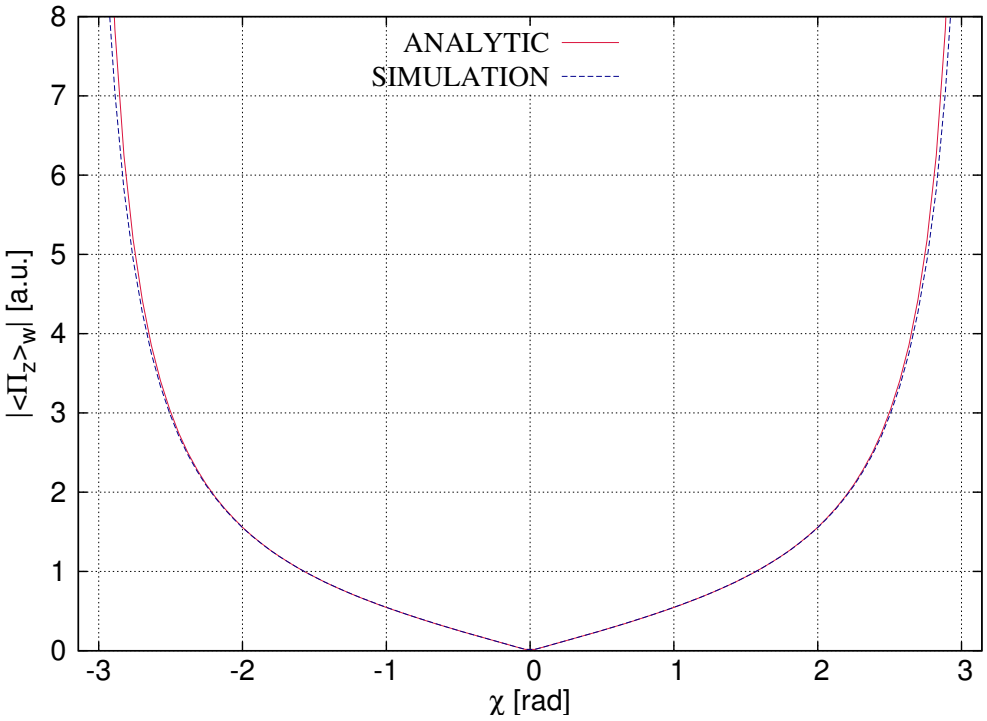

Figure 3.15.: Simulation [Eq. (3.84)] and the absolute of the weak value's analytic solution [absolute of Eq. (3.69)]. The absorber is modeled as $|P_i\rangle = \mathrm{e}^{-i\chi/2}\sqrt{1-a}|I\rangle + \mathrm{e}^{i\chi/2}\sqrt{a}|II\rangle$ with $a = 0.5$ and $\alpha = \pi/20$.

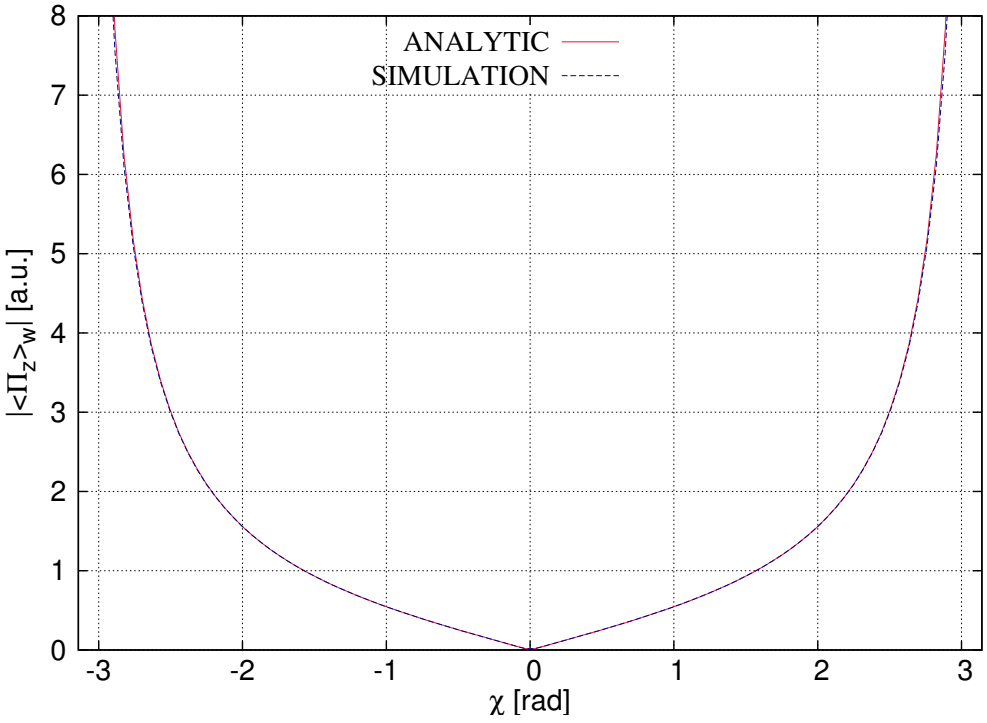

Figure 3.16.: Simulation [Eq. (3.84)] and the absolute of the weak value's analytic solution [absolute of Eq. (3.69)]. The absorber is modeled as $|P_i\rangle = \mathrm{e}^{-i\chi/2}\sqrt{1-a}|I\rangle + \mathrm{e}^{i\chi/2}\sqrt{a}|II\rangle$ with $a = 0.5$ and $\alpha = \pi/36$.

does not know if the neutron took path I or II. The problem is made clear by Fig. 3.17[e]. The

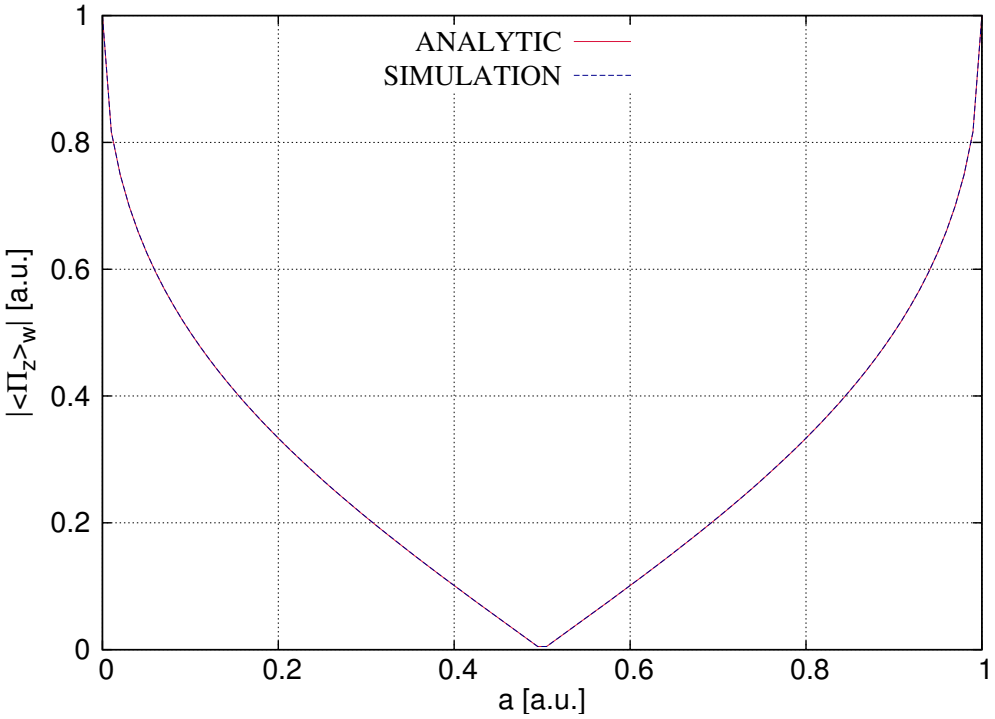

Figure 3.17.: Simulation and the weak value's analytic solution [Eq. (3.84)] for $\chi = 0$: It ranges from 0 if both paths are equally blocked ($a = 0.5$) to 1 if one path is completely blocked ($a = 1$ or $a = 0$). While Abs $\left(\langle\hat{\Pi}_z\rangle_w\right)$ tells us that the ensemble went through one path rather than another, it does not tell us which one and therefore makes it impossible to extract pure 'which-way-information'. It is noteworthy that the approximation made by Eq. (3.84) works very well for small values of χ. The simulation was performed with an angle of $\alpha = 5°$ and there is no notable difference to the analytic solution.

absolute of $\langle\hat{\Pi}_z\rangle_w$ ranges from 0 to 1. If both paths are equally blocked ($a = 0.5$), Abs $\left(\langle\hat{\Pi}_z\rangle_w\right)$ becomes 0. One half of the ensemble goes through path I, the other through path II. If one path is completely blocked ($a = 1$ or $a = 0$) the weak value becomes 1. This tells us that the ensemble went through one path. However, it does not tell us which one. To extract pure 'which-way-information', it is at least necessary to measure the real, or even better also the imaginary part of $\langle\hat{\Pi}_z\rangle_w$, as well as its absolute.

3.2.2. Influences of imperfect experimental circumstances

The calculations presented so far, are approximations for an ideal system. However, it would be close to impossible to recreate this ideal system in an experiment and therefore some changes have to be made to get a more realistic description.

[e]For Fig. 3.17 and the considerations thereafter, let the absorber be modelled as in Eq. (3.54).

For this the system's pre selected wave function has to be

$$|\psi\rangle = \underbrace{\frac{1}{\sqrt{a+b}}\left[\mathrm{e}^{-i\chi/2}\sqrt{b}|I\rangle + \mathrm{e}^{i\chi/2}\sqrt{a}|II\rangle\right]}_{|P_i\rangle}\underbrace{\sqrt{\frac{1}{1-2p+2p^2}}\;\left[(1-p)\,|S_x;+\rangle + p|S_x;-\rangle\right]}_{|S\rangle}. \quad (3.90)$$

The factor p ($0 \leq p \leq 1$) takes into account, that the neutron beam's polarization might not be perfect. For $p = 0$ Eq. (3.90) describes a totally polarized beam along the positive x-axis. As p becomes bigger the degree of polarization becomes smaller, till it becomes zero for $p = 0.5$. For $p = 1$ the polarization is again complete, but now with respect to the anti parallel direction.
In addition to that the absorbers in path I and path II are now modeled completely arbitrary using the two factors $\sqrt{b}$ and $\sqrt{a}$, which can both vary between 0 and 1, i.e. $0 \leq \sqrt{b} \leq 1$ and $0 \leq \sqrt{a} \leq 1$.
For completeness sake the same calculations as above shall now be made using the system's 'new' wave function. Eq. (3.90) describes the system after pre selection. After the weak interaction the system evolves into

$$\begin{aligned}
|\psi'\rangle &= \mathrm{e}^{i\alpha\hat{\sigma}_z^s\hat{\Pi}_z/2}|\psi\rangle \approx \left(1 + \frac{i\alpha\hat{\sigma}_z^s\hat{\Pi}_z}{2}\right)|\psi\rangle \\
&= \left(1 + \frac{i\alpha\hat{\sigma}_z^s\hat{\Pi}_z}{2}\right)|P_i\rangle\underbrace{\sqrt{\frac{1}{1-2p+2p^2}}}_{\equiv\sqrt{n}}\left[(1-p)\,|S_x;+\rangle + p|S_x;-\rangle\right] \\
&= |P_i\rangle\sqrt{n}\;\left[(1-p)\,|S_x;+\rangle + p|S_x;-\rangle\right] + \frac{i\alpha}{2}\hat{\Pi}_z|P_i\rangle\sqrt{n}\;\left[(1-p)\,\hat{\sigma}_z^s|S_x;+\rangle + p\hat{\sigma}_z^s|S_x;-\rangle\right] \\
&= |P_i\rangle\sqrt{n}\;\left[(1-p)\,|S_x;+\rangle + p|S_x;-\rangle\right] + \frac{i\alpha}{2}\hat{\Pi}_z|P_i\rangle\sqrt{n}\;\left[(1-p)\,|S_x;-\rangle + p|S_x;+\rangle\right] \\
&= |P_i\rangle\sqrt{\frac{n}{2}}\left[|S_z;+\rangle + (1-2p)\,|S_z;-\rangle\right] + \frac{i\alpha}{2}\hat{\Pi}_z|P_i\rangle\sqrt{\frac{n}{2}}\left[|S_z;+\rangle - (1-2p)\,|S_z;-\rangle\right], \quad (3.91)
\end{aligned}$$

where the exponential function has been Taylor expanded. The exact calculation shall be put forward later. After the weak measurement the ensemble is post selected onto the final state $|P_f\rangle = \sqrt{\frac{1}{2}}\left(|I\rangle + |II\rangle\right)$, so that the system's wave function becomes

$$\begin{aligned}
|\Phi\rangle &= |P_f\rangle\langle P_f|P_i\rangle\sqrt{\frac{n}{2}}\left[|S_z;+\rangle + (1-2p)\,|S_z;-\rangle\right] + \frac{i\alpha}{2}\langle P_f|\hat{\Pi}_z|P_i\rangle\sqrt{\frac{n}{2}}\left[|S_z;+\rangle - (1-2p)\,|S_z;-\rangle\right] \\
&= \sqrt{\frac{n}{2}}\underbrace{\langle P_f|P_i\rangle}_{\equiv\epsilon}\left\{\left[|S_z;+\rangle + (1-2p)\,|S_z;-\rangle\right] + \frac{i\alpha}{2}\langle\hat{\Pi}_z\rangle_w\left[|S_z;+\rangle - (1-2p)\,|S_z;-\rangle\right]\right\}|P_f\rangle \\
&= \epsilon\sqrt{\frac{n}{2}}\left[\left(1 + \frac{i\alpha}{2}\langle\hat{\Pi}_z\rangle_w\right)|S_z;+\rangle + (1-2p)\left(1 - \frac{i\alpha}{2}\langle\hat{\Pi}_z\rangle_w\right)|S_z;-\rangle\right]|P_f\rangle \\
&= \epsilon\sqrt{\frac{n}{2}}\left[\mathrm{e}^{i\alpha\langle\hat{\Pi}_z\rangle_w/2}|S_z;+\rangle + (1-2p)\,\mathrm{e}^{-i\alpha\langle\hat{\Pi}_z\rangle_w/2}|S_z;-\rangle\right]|P_f\rangle \quad (3.92)
\end{aligned}$$

with

$$\epsilon \equiv \langle P_f|P_i\rangle = \frac{1}{\sqrt{2\,(a+b)}}\left[\sqrt{b}\;\mathrm{e}^{-i\chi/2} + \sqrt{a}\;\mathrm{e}^{i\chi/2}\right] \quad (3.93)$$

To extract the weak value, the expectation value of $\hat{\sigma}_x^s$ is evaluated. With

$$\begin{aligned}
\langle\Phi|\hat{\sigma}_x^s|\Phi\rangle &= \epsilon\epsilon^*\langle P_f|P_f\rangle\frac{n}{2}\left[\mathrm{e}^{-i\alpha\langle\hat{\Pi}_z\rangle_w/2}\langle S_z;+| + (1-2p)\,\mathrm{e}^{i\alpha\langle\hat{\Pi}_z\rangle_w/2}\langle S_z;-|\right]\times \\
&\quad\times\left[|S_z;+\rangle\langle S_z;-| + |S_z;-\rangle\langle S_z;+|\right]\left[\mathrm{e}^{i\alpha\langle\hat{\Pi}_z\rangle_w/2}|S_z;+\rangle + (1-2p)\,\mathrm{e}^{-i\alpha\langle\hat{\Pi}_z\rangle_w/2}|S_z;-\rangle\right] \\
&= \frac{n|\epsilon|^2}{2}\left[\mathrm{e}^{-i\alpha\langle\hat{\Pi}_z\rangle_w/2}\langle S_z;+| + (1-2p)\,\mathrm{e}^{i\alpha\langle\hat{\Pi}_z\rangle_w/2}\langle S_z;-|\right]\times \\
&\quad\times\left[\mathrm{e}^{i\alpha\langle\hat{\Pi}_z\rangle_w/2}|S_z;-\rangle + (1-2p)\,\mathrm{e}^{-i\alpha\langle\hat{\Pi}_z\rangle_w/2}|S_z;+\rangle\right] \\
&= \frac{n|\epsilon|^2}{2}\left[\mathrm{e}^{-i\alpha\langle\hat{\Pi}_z\rangle_w}(1-2p) + \mathrm{e}^{i\alpha\langle\hat{\Pi}_z\rangle_w}(1-2p)\right] = |\epsilon|^2\frac{(1-2p)}{1-2p+2p^2}\cos\left(\alpha\langle\hat{\Pi}_z\rangle_w\right)
\end{aligned} \tag{3.94}$$

and

$$\begin{aligned}
\langle\Phi|\Phi\rangle &= \frac{n\epsilon\epsilon^*}{2}\left[\mathrm{e}^{-i\alpha\langle\hat{\Pi}_z\rangle_w/2}\langle S_z;+| + (1-2p)\,\mathrm{e}^{i\alpha\langle\hat{\Pi}_z\rangle_w/2}\langle S_z;-|\right]\times \\
&\quad\times\left[\mathrm{e}^{i\alpha\langle\hat{\Pi}_z\rangle_w/2}|S_z;+\rangle + (1-2p)\,\mathrm{e}^{-i\alpha\langle\hat{\Pi}_z\rangle_w/2}|S_z;-\rangle\right] \\
&= |\epsilon|^2
\end{aligned} \tag{3.95}$$

we get

$$\langle\hat{\sigma}_x^s\rangle = \frac{\langle\Phi|\hat{\sigma}_x^s|\Phi\rangle}{\langle\Phi|\Phi\rangle} = \frac{(1-2p)}{1-2p+2p^2}\cos\left(\alpha\langle\hat{\Pi}_z\rangle_w\right), \tag{3.96}$$

which leads to

$$\left|\langle\hat{\Pi}_z\rangle_w\right| = \frac{1}{\alpha}\arccos\left[\frac{1+2p\,(p-1)}{1-2p}\frac{I_+ - I_-}{I_+ + I_-}\right]. \tag{3.97}$$

In contrast the same calculation without using the Taylor expansion gives

$$\begin{aligned}
|\psi'\rangle &= \mathrm{e}^{i\alpha\hat{\sigma}_z^s\hat{\Pi}_z/2}|\psi\rangle = \mathrm{e}^{i\alpha\hat{\sigma}_z^s\hat{\Pi}_z/2}\sqrt{n}\left[(1-p)\,|S_x;+\rangle + p|S_x;-\rangle\right]|P_i\rangle \\
&= \sqrt{\frac{n}{2}}\left\{(1-p)\left[\mathrm{e}^{i\alpha\hat{\sigma}_z^s\hat{\Pi}_z/2}|S_z;+\rangle + \mathrm{e}^{i\alpha\hat{\sigma}_z^s\hat{\Pi}_z/2}|S_z;-\rangle\right] + \right. \\
&\quad\left. + p\left[\mathrm{e}^{i\alpha\hat{\sigma}_z^s\hat{\Pi}_z/2}|S_z;+\rangle - \mathrm{e}^{i\alpha\hat{\sigma}_z^s\hat{\Pi}_z/2}|S_z;-\rangle\right]\right\}|P_i\rangle \\
&= \sqrt{\frac{n}{2}}\left\{(1-p)\left[\mathrm{e}^{i\alpha\hat{\Pi}_z/2}|S_z;+\rangle + \mathrm{e}^{-i\alpha\hat{\Pi}_z/2}|S_z;-\rangle\right] + p\left[\mathrm{e}^{i\alpha\hat{\Pi}_z/2}|S_z;+\rangle - \mathrm{e}^{-i\alpha\hat{\Pi}_z/2}|S_z;-\rangle\right]\right\}|P_i\rangle \\
&= \sqrt{\frac{n}{2}}\left[\mathrm{e}^{i\alpha\hat{\Pi}_z/2}|S_z;+\rangle + (1-2p)\,\mathrm{e}^{-i\alpha\hat{\Pi}_z/2}|S_z;-\rangle\right]|P_i\rangle \\
&= \sqrt{\frac{n}{2}}\left\{\left[\cos\left(\frac{\alpha}{2}\right) + i\hat{\Pi}_z\sin\left(\frac{\alpha}{2}\right)\right]|S_z;+\rangle + (1-2p)\left[\cos\left(\frac{\alpha}{2}\right) - i\hat{\Pi}_z\sin\left(\frac{\alpha}{2}\right)\right]|S_z;-\rangle\right\}|P_i\rangle \\
&= \sqrt{\frac{n}{2}}\left\{\cos\left(\frac{\alpha}{2}\right)\left[|S_z;+\rangle + (1-2p)\,|S_z;-\rangle\right] + i\hat{\Pi}_z\sin\left(\frac{\alpha}{2}\right)\left[|S_z;+\rangle - (1-2p)\,|S_z;-\rangle\right]\right\}|P_i\rangle.
\end{aligned} \tag{3.98}$$

After post selection the system's wave function $|\Phi\rangle$ becomes

$$\begin{aligned}|\Phi\rangle &= \sqrt{\frac{n}{2}}\Big\{\langle P_f|P_i\rangle\cos\left(\frac{\alpha}{2}\right)[|S_z;+\rangle + (1-2p)\,|S_z;-\rangle] + \\ &\quad + i\langle P_f|\hat{\Pi}_z|P_i\rangle\sin\left(\frac{\alpha}{2}\right)[|S_z;+\rangle - (1-2p)\,|S_z;-\rangle]\Big\}\,|P_f\rangle \\ &= \epsilon\sqrt{\frac{n}{2}}\Big\{\cos\left(\frac{\alpha}{2}\right)[|S_z;+\rangle + (1-2p)\,|S_z;-\rangle] + i\langle\hat{\Pi}_z\rangle_w\sin\left(\frac{\alpha}{2}\right)[|S_z;+\rangle - (1-2p)\,|S_z;-\rangle]\Big\}\,|P_f\rangle.\end{aligned} \tag{3.99}$$

Evaluating $\langle\hat{\sigma}_x^s\rangle$, using

$$\begin{aligned}\langle\Phi|\hat{\sigma}_x^s|\Phi\rangle &= |\epsilon|^2\frac{n}{2}\langle P_f|P_f\rangle\Big\{\cos\left(\frac{\alpha}{2}\right)[\langle S_z;+| + (1-2p)\,\langle S_z;-|] - \\ &\quad - i\langle\hat{\Pi}_z\rangle_w\sin\left(\frac{\alpha}{2}\right)[\langle S_z;+| - (1-2p)\,\langle S_z;-|]\Big\}\Big\{\cos\left(\frac{\alpha}{2}\right)[|S_z;-\rangle + (1-2p)\,|S_z;+\rangle] + \\ &\quad + i\langle\hat{\Pi}_z\rangle_w\sin\left(\frac{\alpha}{2}\right)[|S_z;-\rangle - (1-2p)\,|S_z;+\rangle]\Big\} \\ &= |\epsilon|^2\frac{n}{2}\Big\{(1-2p)\cos^2\left(\frac{\alpha}{2}\right) + i\langle\hat{\Pi}_z\rangle_w(1-2p)\cos\left(\frac{\alpha}{2}\right)\sin\left(\frac{\alpha}{2}\right) + (1-2p)\cos^2\left(\frac{\alpha}{2}\right) - \\ &\quad - i\langle\hat{\Pi}_z\rangle_w(1-2p)\cos\left(\frac{\alpha}{2}\right)\sin\left(\frac{\alpha}{2}\right) + i\langle\hat{\Pi}_z\rangle_w(1-2p)\cos\left(\frac{\alpha}{2}\right)\sin\left(\frac{\alpha}{2}\right) - \\ &\quad - \langle\hat{\Pi}_z\rangle_w^2(1-2p)\sin^2\left(\frac{\alpha}{2}\right) - i\langle\hat{\Pi}_z\rangle_w(1-2p)\cos\left(\frac{\alpha}{2}\right)\sin\left(\frac{\alpha}{2}\right) - \\ &\quad - \langle\hat{\Pi}_z\rangle_w^2(1-2p)\sin^2\left(\frac{\alpha}{2}\right)\Big\} \\ &= |\epsilon|^2\frac{1-2p}{1-2p+2p^2}\left[\cos^2\left(\frac{\alpha}{2}\right) - \langle\hat{\Pi}_z\rangle_w^2\sin^2\left(\frac{\alpha}{2}\right)\right]\end{aligned} \tag{3.100}$$

and

$$\begin{aligned}\langle\Phi|\Phi\rangle &= |\epsilon|^2\frac{n}{2}\langle P_f|P_f\rangle\Big\{\cos\left(\frac{\alpha}{2}\right)[\langle S_z;+| + (1-2p)\,\langle S_z;-|] - \\ &\quad - i\langle\hat{\Pi}_z\rangle_w\sin\left(\frac{\alpha}{2}\right)[\langle S_z;+| - (1-2p)\,\langle S_z;-|]\Big\}\Big\{\cos\left(\frac{\alpha}{2}\right)[|S_z;+\rangle + (1-2p)\,|S_z;-\rangle] + \\ &\quad + i\langle\hat{\Pi}_z\rangle_w\sin\left(\frac{\alpha}{2}\right)[|S_z;+\rangle - (1-2p)\,|S_z;-\rangle]\Big\} \\ &= |\epsilon|^2\frac{n}{2}\Big[\cos^2\left(\frac{\alpha}{2}\right) - i\langle\hat{\Pi}_z\rangle_w\cos\left(\frac{\alpha}{2}\right)\sin\left(\frac{\alpha}{2}\right) + (1-2p)^2\cos^2\left(\frac{\alpha}{2}\right) + \\ &\quad + i\langle\hat{\Pi}_z\rangle_w(1-2p)^2\cos\left(\frac{\alpha}{2}\right)\sin\left(\frac{\alpha}{2}\right) + i\langle\hat{\Pi}_z\rangle_w\cos\left(\frac{\alpha}{2}\right)\sin\left(\frac{\alpha}{2}\right) + \\ &\quad + \langle\hat{\Pi}_z\rangle_w^2\sin^2\left(\frac{\alpha}{2}\right) - i\langle\hat{\Pi}_z\rangle_w(1-2p)^2\cos\left(\frac{\alpha}{2}\right)\sin\left(\frac{\alpha}{2}\right) + \langle\hat{\Pi}_z\rangle_w^2(1-2p)^2\sin^2\left(\frac{\alpha}{2}\right)\Big\} \\ &= |\epsilon|^2\left[\cos^2\left(\frac{\alpha}{2}\right) + \langle\hat{\Pi}_z\rangle_w^2\sin^2\left(\frac{\alpha}{2}\right)\right]\end{aligned} \tag{3.101}$$

yields

$$\langle\hat{\sigma}_x^s\rangle = \frac{2(1-2p)}{1+(1-2p)^2}\,\frac{\cos^2\left(\frac{\alpha}{2}\right) - \langle\hat{\Pi}_z\rangle_w^2\sin^2\left(\frac{\alpha}{2}\right)}{\cos^2\left(\frac{\alpha}{2}\right) + \langle\hat{\Pi}_z\rangle_w^2\sin^2\left(\frac{\alpha}{2}\right)}, \tag{3.102}$$

which leads to the weak value

$$\left|\langle\hat{\Pi}_z\rangle_w\right| = \sqrt{\cot^2\left(\frac{\alpha}{2}\right)\frac{1-\frac{1+(1-2p)^2}{2(1-2p)}\,\frac{I_+-I_-}{I_++I_-}}{1+\frac{1+(1-2p)^2}{2(1-2p)}\,\frac{I_+-I_-}{I_++I_-}}} = \sqrt{\cot^2\left(\frac{\alpha}{2}\right)\frac{(p-1)^2 I_- - p^2 I_+}{(p-1)^2 I_+ - p^2 I_-}} \tag{3.103}$$

Since $|P_i\rangle$ has been altered the analytic solution for the weak value has to change as well.

$$\langle\hat{\Pi}_z\rangle_w = \frac{\langle P_f|\hat{\Pi}_z|P_i\rangle}{\langle P_f|P_i\rangle} = \frac{[\langle I| + \langle II|]\left[\mathrm{e}^{-i\chi/2}\sqrt{b}|I\rangle - \mathrm{e}^{i\chi/2}\sqrt{a}|II\rangle\right]}{[\langle I| + \langle II|]\left[\mathrm{e}^{-i\chi/2}\sqrt{b}|I\rangle + \mathrm{e}^{i\chi/2}\sqrt{a}|II\rangle\right]} = \frac{\sqrt{b}-\sqrt{a}\;\mathrm{e}^{i\chi}}{\sqrt{b}+\sqrt{a}\;\mathrm{e}^{i\chi}} \tag{3.104}$$

As previously the next step is to calculate the expected intensities. Again we let the evolution operator act upon the pre selected system to gain the wave function $|\Phi\rangle$.

$$\begin{aligned}
|\psi'\rangle &= \mathrm{e}^{i\alpha\hat{\sigma}_z^s\hat{\Pi}_z/2}|\psi\rangle = e^{i\alpha\hat{\sigma}_z^s\hat{\Pi}_z/2}\left\{\sqrt{\frac{n}{(a+b)}}\left[\mathrm{e}^{-i\chi/2}\sqrt{b}|I\rangle + \mathrm{e}^{i\chi/2}\sqrt{a}|II\rangle\right][(1-p)\,|S_x;+\rangle + p|S_x;-\rangle]\right\} \\
&= \sqrt{\frac{n}{2\,(a+b)}}\left[\mathrm{e}^{-i\chi/2}\sqrt{b}\;\mathrm{e}^{i\alpha/2}|I\rangle|S_z;+\rangle + \mathrm{e}^{i\chi/2}\sqrt{a}\;\mathrm{e}^{-i\alpha/2}|II\rangle|S_z;+\rangle + \right. \\
&\quad \left. + \mathrm{e}^{-i\chi/2}\,(1-2p)\,\sqrt{b}\;\mathrm{e}^{-i\alpha/2}|I\rangle|S_z;-\rangle + \mathrm{e}^{i\chi/2}\,(1-2p)\,\sqrt{a}\;\mathrm{e}^{i\alpha/2}|II\rangle|S_z;-\rangle\right],
\end{aligned} \tag{3.105}$$

and post select onto $|P_f\rangle\langle P_f|$ to get the final wave function $|\Phi\rangle$

$$\begin{aligned}
|\Phi\rangle = |P_f\rangle\langle P_f|\psi'\rangle &= \frac{1}{2}\sqrt{\frac{n}{(a+b)}}\left[\mathrm{e}^{-i\chi/2}\sqrt{b}\;\mathrm{e}^{i\alpha/2}|S_z;+\rangle + \mathrm{e}^{i\chi/2}\sqrt{a}\;\mathrm{e}^{-i\alpha/2}|S_z;+\rangle + \right. \\
&\quad \left. + \mathrm{e}^{-i\chi/2}\,(1-2p)\,\sqrt{b}\;\mathrm{e}^{-i\alpha/2}|S_z;-\rangle + \mathrm{e}^{i\chi/2}\,(1-2p)\,\sqrt{a}\;\mathrm{e}^{i\alpha/2}|S_z;-\rangle\right]|P_f\rangle \\
&= \frac{1}{2}\sqrt{\frac{n}{(a+b)}}\left[\left(\mathrm{e}^{-i(\chi-\alpha)/2}\sqrt{b} + \mathrm{e}^{i(\chi-\alpha)/2}\sqrt{a}\right)|S_z;+\rangle + \right. \\
&\quad \left. + \left(\mathrm{e}^{-i(\chi+\alpha)/2}\sqrt{b} + \mathrm{e}^{i(\chi+\alpha)/2}\sqrt{a}\right)(1-2p)\,|S_z;-\rangle\right]|P_f\rangle.
\end{aligned} \tag{3.106}$$

Using Eq. (3.106) we obtain the intensities I_- and I_+ by calculating $\langle S_x;-|\Phi\rangle$ and $\langle S_x;+|\Phi\rangle$.

$$\begin{aligned}
\langle S_x;-|\Phi\rangle &= \sqrt{\frac{n}{8\,(a+b)}}\,[\langle S_z;+| - \langle S_z;-|]\left[\left(\mathrm{e}^{-i(\chi-\alpha)/2}\sqrt{b} + \mathrm{e}^{i(\chi-\alpha)/2}\sqrt{a}\right)|S_z;+\rangle + \right. \\
&\quad \left. + \left(\mathrm{e}^{-i(\chi+\alpha)/2}\sqrt{b} + \mathrm{e}^{i(\chi+\alpha)/2}\sqrt{a}\right)(1-2p)\,|S_z;-\rangle\right]|P_f\rangle \\
&= \sqrt{\frac{n}{8\,(a+b)}}\left[\left(\mathrm{e}^{-i(\chi-\alpha)/2}\sqrt{b} + \mathrm{e}^{i(\chi-\alpha)/2}\sqrt{a}\right) - \right. \\
&\quad \left. - \left(\mathrm{e}^{-i(\chi+\alpha)/2}\sqrt{b} + \mathrm{e}^{i(\chi+\alpha)/2}\sqrt{a}\right)(1-2p)\right]|P_f\rangle
\end{aligned} \tag{3.107}$$

and

$$\begin{aligned}\langle S_x;+|\Phi\rangle &= \sqrt{\frac{n}{8\,(a+b)}}\,[\langle S_z;+|+\langle S_z;-|]\left[\left(\mathrm{e}^{-i(\chi-\alpha)/2}\sqrt{b}+\mathrm{e}^{i(\chi-\alpha)/2}\sqrt{a}\right)|S_z;+\rangle+\right.\\ &\quad\left.+\left(\mathrm{e}^{-i(\chi+\alpha)/2}\sqrt{b}+\mathrm{e}^{i(\chi+\alpha)/2}\sqrt{a}\right)(1-2p)\,|S_z;-\rangle\right]|P_f\rangle\\ &= \sqrt{\frac{n}{8\,(a+b)}}\left[\left(\mathrm{e}^{-i(\chi-\alpha)/2}\sqrt{b}+\mathrm{e}^{i(\chi-\alpha)/2}\sqrt{a}\right)+\right.\\ &\quad\left.+\left(\mathrm{e}^{-i(\chi+\alpha)/2}\sqrt{b}+\mathrm{e}^{i(\chi+\alpha)/2}\sqrt{a}\right)(1-2p)\right]|P_f\rangle \end{aligned} \tag{3.108}$$

lead to the intensities

$$\begin{aligned}I_- = |\langle S_x;-|\Phi\rangle|^2 &= \frac{n}{8\,(a+b)}\left[\left(\mathrm{e}^{-i(\chi-\alpha)/2}\sqrt{b}+\mathrm{e}^{i(\chi-\alpha)/2}\sqrt{a}\right)-\right.\\ &\quad\left.-\left(\mathrm{e}^{-i(\chi+\alpha)/2}\sqrt{b}+\mathrm{e}^{i(\chi+\alpha)/2}\sqrt{a}\right)(1-2p)\right]\left[\left(\mathrm{e}^{i(\chi-\alpha)/2}\sqrt{b}+\mathrm{e}^{-i(\chi-\alpha)/2}\sqrt{a}\right)-\right.\\ &\quad\left.-\left(\mathrm{e}^{i(\chi+\alpha)/2}\sqrt{b}+\mathrm{e}^{-i(\chi+\alpha)/2}\sqrt{a}\right)(1-2p)\right]\\ &= \frac{1}{4\,(a+b)}\frac{1}{1-2p+p^2}\left\{[a+b]\left[1-2p+2p^2-(1-2p)\cos(\alpha)\right]-\right.\\ &\quad\left.-4\sqrt{ab}\;p\,[p-1]\sin(\alpha)\sin(\chi)+2\sqrt{ab}\left[2p-1+\left(1-2p+2p^2\right)\cos(\alpha)\right]\cos(\chi)\right\}\end{aligned} \tag{3.109}$$

and

$$\begin{aligned}I_+ = |\langle S_x;+|\Phi\rangle|^2 &= \frac{n}{8\,(a+b)}\left[\left(\mathrm{e}^{-i(\chi-\alpha)/2}\sqrt{b}+\mathrm{e}^{i(\chi-\alpha)/2}\sqrt{a}\right)+\right.\\ &\quad\left.+\left(\mathrm{e}^{-i(\chi+\alpha)/2}\sqrt{b}+\mathrm{e}^{i(\chi+\alpha)/2}\sqrt{a}\right)(1-2p)\right]\left[\left(\mathrm{e}^{i(\chi-\alpha)/2}\sqrt{b}+\mathrm{e}^{-i(\chi-\alpha)/2}\sqrt{a}\right)+\right.\\ &\quad\left.+\left(\mathrm{e}^{i(\chi+\alpha)/2}\sqrt{b}+\mathrm{e}^{-i(\chi+\alpha)/2}\sqrt{a}\right)(1-2p)\right]\\ &= \frac{1}{4\,(a+b)}\frac{1}{1-2p+p^2}\left\{[a+b]\left[1-2p+2p^2+(1-2p)\cos(\alpha)\right]-\right.\\ &\quad\left.-4\sqrt{ab}\;p\,[p-1]\sin(\alpha)\sin(\chi)+2\sqrt{ab}\left[1-2p+\left(1-2p+2p^2\right)\cos(\alpha)\right]\cos(\chi)\right\}\end{aligned} \tag{3.110}$$

Putting Eqs. (3.109) and (3.110) into Eq. (3.97), we get the experimentally expected weak value, using the calculational method of the Taylor expansion including arbitrary absorbers and taking into account a non perfect degree of polarization.

$$\left|\langle\hat{\Pi}_z\rangle_w\right| = \frac{1}{\alpha}\arccos\left\{\frac{[1-2p]\left[(a+b)\cos(\alpha)+2\sqrt{ab}\;\cos(\chi)\right]}{(a+b)\,[1+2p\,(p-1)]+\sqrt{ab}\left[\cos(\alpha-\chi)+(1-2p)^2\cos(\alpha+\chi)\right]}\right\}. \tag{3.111}$$

For $p=0$, that is for a perfect degree of polarization, it simplifies to

$$\left|\langle\hat{\Pi}_z\rangle_w\right| = \frac{1}{\alpha}\arccos\left[\frac{(a+b)\cos(\alpha)+2\sqrt{ab}\cos(\chi)}{a+b+2\sqrt{ab}\;\cos(\alpha)\cos(\chi)}\right], \tag{3.112}$$

which is just what we would expect considering the previous calculations[f]. For the exact approach the weak value turns out to be

$$\left|\langle\hat{\Pi}_z\rangle_w\right| = \sqrt{\cot^2\left(\frac{\alpha}{2}\right)\frac{N}{D}}, \tag{3.113}$$

where N and D are given by

$$N = [a+b]\left[1-2p+2p^2+(2p-1)\cos(\alpha)\right] + 2\sqrt{ab}\left[2p-1+\left(1-2p+2p^2\right)\cos(\alpha)\right]\cos(\chi) - \\ - 4\sqrt{ab}(p-1)p\sin(\alpha)\sin(\chi) \tag{3.114}$$

and

$$D = [a+b]\left[1-2p+2p^2+(1-2p)\cos(\alpha)\right] + 2\sqrt{ab}\left[1-2p+\left(1-2p+2p^2\right)\cos(\alpha)\right]\cos(\chi) - \\ - 4\sqrt{ab}\,(p-1)\,p\sin(\alpha)\sin(\chi) \tag{3.115}$$

which becomes

$$\left|\langle\hat{\Pi}_z\rangle_w\right| = \sqrt{\frac{a+b-2\sqrt{ab}\ \cos(\chi)}{a+b+2\sqrt{ab}\ \cos(\chi)}} \tag{3.116}$$

for $p = 0$. This is the absolute of the weak value calculated in Eq. (3.104) and shows that the calculations performed so far are consistent.
Unfortunately we are still not at our goal. We want to describe the real system as accurately as possible. Because of that we have to take one more factor into account: the contrast of the neutron interferometer. It was considered to be 100% in all calculations so far. In practice it will not be unity, but less. To take this effect into account all intensity obtained by oscillations dependent on χ have to be weighted by a factor $\mathfrak{C}$. Equation (3.111) then becomes

$$\left|\langle\hat{\Pi}_z\rangle_w\right| = \frac{1}{\alpha}\arccos\left\{\frac{[1-2p]\left[(a+b)\cos(\alpha)+2\sqrt{ab}\ \mathfrak{C}\cos(\chi)\right]}{(a+b)\left[1+2p\,(p-1)\right]+\sqrt{ab}\ \mathfrak{C}\left[\cos(\alpha-\chi)+(1-2p)^2\cos(\alpha+\chi)\right]}\right\} \tag{3.117}$$

Equations (3.114) and (3.115) are then given by

$$N = [a+b]\left[1-2p+2p^2+(2p-1)\cos(\alpha)\right] + 2\sqrt{ab}\left[2p-1+\left(1-2p+2p^2\right)\cos(\alpha)\right]\mathfrak{C}\cos(\chi) - \\ - 4\sqrt{ab}(p-1)p\sin(\alpha)\,\mathfrak{C}\sin(\chi) \tag{3.118}$$

and

$$D = [a+b]\left[1-2p+2p^2+(1-2p)\cos(\alpha)\right] + 2\sqrt{ab}\left[1-2p+\left(1-2p+2p^2\right)\cos(\alpha)\right]\mathfrak{C}\cos(\chi) - \\ - 4\sqrt{ab}\,(p-1)\,p\sin(\alpha)\,\mathfrak{C}\sin(\chi) \tag{3.119}$$

A closer look at Eq. (3.117) shows that the experimental imperfections have mainly two effects:

1. If the degree of polarization is not perfect, i.e. if $p \neq 0$, then the curve that one would

[f] See for example Eq. (3.84).

expect to measure for the path operators weak value becomes asymmetric. At one edge the curve's flank falls off more steeply than on the other side, which causes the minima and maxima of the graph to shift into the negative direction of χ.

2. If the contrast of the interferometer is less than unity, the expected curve becomes damped. The weak value does not reach zero any more and the points of discontinuities at which the final and initial state are orthogonal vanish.

Figure 3.18 shows Eq. (3.84) and Eq. (3.117) for $a = b = 0.5$, $\mathfrak{C} = 0.8$, $p = 0.02$ and $\alpha = \pi/36$. The weak value's curve, that can be retrieved by an experiment will look much more like the

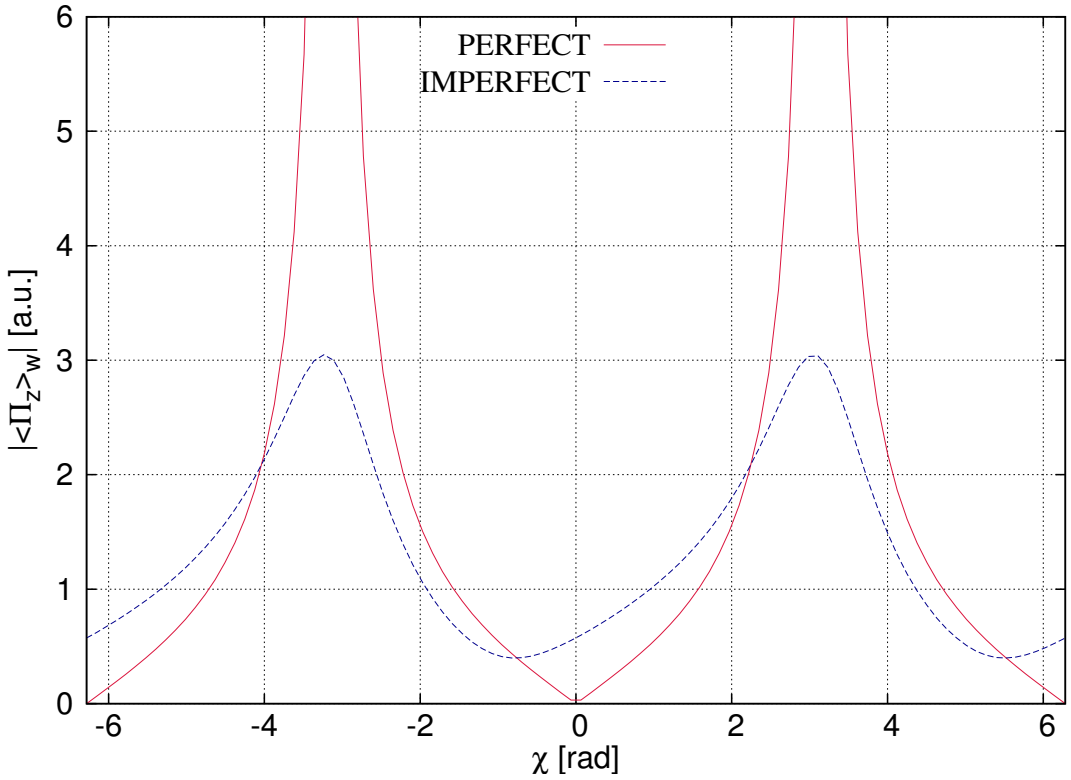

Figure 3.18.: Plot of the expected measurement results for a perfect setup [Eq. (3.84)] and for a realistic one [Eq. (3.117)] with $a = b = 0.5$, $\mathfrak{C} = 0.8$, $p = 0.02$ and $\alpha = \pi/36$: The imperfect degree of polarization causes the curve to become asymmetric, the imperfect contrast causes a compression of the graph's amplitude.

blue dashed line in Fig. 3.18 than the red solid one.

3.2.3. Other path operators

It is also worth looking at other path operators, for instance, $\hat{\Pi}_x = |I\rangle\langle II| + |II\rangle\langle I|$ and $\hat{\Pi}_y = i|II\rangle\langle I| - i|I\rangle\langle II|$. For the initial and final state, $|P_i\rangle = \frac{1}{\sqrt{a+b}}\left[\mathrm{e}^{-i\chi/2}\sqrt{b}|I\rangle + \mathrm{e}^{i\chi/2}\sqrt{a}|II\rangle\right]$

and $|P_f\rangle = \sqrt{\frac{1}{2}}\left(|I\rangle + |II\rangle\right)$, they are

$$\begin{aligned}\langle\hat{\Pi}_x\rangle_w &= \frac{\langle P_f|\hat{\Pi}_x|P_i\rangle}{\langle P_f|P_i\rangle} = \frac{\left[\langle I| + \langle II|\right]\left[\mathrm{e}^{-i\chi/2}\sqrt{b}|I\rangle + \mathrm{e}^{i\chi/2}\sqrt{a}|II\rangle\right]}{\left[\langle I| + \langle II|\right]\left[\mathrm{e}^{-i\chi/2}\sqrt{b}|I\rangle + \mathrm{e}^{i\chi/2}\sqrt{a}|II\rangle\right]} \\ &= \frac{\sqrt{b} + \sqrt{a}\ \mathrm{e}^{i\chi}}{\sqrt{b} + \sqrt{a}\ \mathrm{e}^{i\chi}} = \text{const.} = 1 \end{aligned} \tag{3.120}$$

and

$$\begin{aligned}\langle\hat{\Pi}_y\rangle_w &= \frac{\langle P_f|\hat{\Pi}_y|P_i\rangle}{\langle P_f|P_i\rangle} = \frac{\left[\langle I| + \langle II|\right]\left[i\mathrm{e}^{-i\chi/2}\sqrt{b}|II\rangle - i\mathrm{e}^{i\chi/2}\sqrt{a}|I\rangle\right]}{\left[\langle I| + \langle II|\right]\left[\mathrm{e}^{-i\chi/2}\sqrt{b}|I\rangle + \mathrm{e}^{i\chi/2}\sqrt{a}|II\rangle\right]} \\ &= \frac{i\sqrt{b} - i\sqrt{a}\ \mathrm{e}^{i\chi}}{\sqrt{b} + \sqrt{a}\ \mathrm{e}^{i\chi}} \end{aligned} \tag{3.121}$$

As previously with the spin operator we find that

$$\mathrm{Im}\left(\langle\hat{\Pi}_z\rangle_w\right) = -\,\mathrm{Re}\left(\langle\hat{\Pi}_y\rangle_w\right) \tag{3.122}$$

and

$$\mathrm{Re}\left(\langle\hat{\Pi}_z\rangle_w\right) = \mathrm{Im}\left(\langle\hat{\Pi}_y\rangle_w\right), \tag{3.123}$$

as well as

$$\mathrm{Abs}\left(\langle\hat{\Pi}_z\rangle_w\right) = \mathrm{Abs}\left(\langle\hat{\Pi}_y\rangle_w\right). \tag{3.124}$$

Naturally the question arises if $\langle\hat{\Pi}_x\rangle_w$ and $\langle\hat{\Pi}_y\rangle_w$ can be measured in a similar fashion as $\langle\hat{\Pi}_z\rangle_w$. Unfortunately the answer is not straight forward. $|I\rangle$ and $|II\rangle$ are not eigenstates of the x- and y-operator any more. Therefore the interaction Hamiltonian cannot be constructed simply as above. In other words: There is no spin rotation that can be performed in path I or II, so that its influence on the system can be described by a Hamiltonian of the form

$$\hat{H}_{int} \propto \hat{\Pi}_{x/y}\hat{\sigma}_i^s, \tag{3.125}$$

with $i = x, y, z$. One cannot simply use path conditioned spin rotations any more.
However, it is possible to perform a weak spin rotation in only one of the paths, which enables one to measure the weak value of $\hat{\Pi}_I$ and $\hat{\Pi}_{II}$. The interaction Hamiltonian for such a measurement is given by

$$\hat{H}_j = -\vec{\mu}\vec{B}\hat{\Pi}_j = -\gamma\hat{S}\vec{B}\hat{\Pi}_j \equiv \frac{-\alpha\hat{\sigma}_z^s\hat{\Pi}_j}{2}. \tag{3.126}$$

where the index j can become either I or II depending on the path the rotation is performed in. If only one path is marked by a weak rotation Eq. (3.61) changes into[g]

$$\langle \hat{\sigma}_x^s \rangle = \cos\left(\alpha \langle \hat{\Pi}_j \rangle\right) \tag{3.127}$$

which leads to the weak value

$$\langle \hat{\Pi}_j \rangle = \frac{1}{\alpha} \arccos\left(\frac{I_+^j - I_-^j}{I_+^j + I_-^j}\right) \tag{3.128}$$

where I_+^j and I_-^j stand for the measured intensities of the $|S_x;+\rangle$ and $|S_x;-\rangle$ state, if the rotation is performed in path j. To determine if we are really able to measure the weak value of $\hat{\Pi}_I$ and $\hat{\Pi}_{II}$, we now have to calculate those intensities:
If the rotation is performed along path I the system's wave function changes into

$$\begin{aligned}
|\psi'\rangle_I &= \mathrm{e}^{i\alpha\hat{\Pi}_I\hat{\sigma}_z^s/2}|\psi\rangle = \sqrt{\frac{1}{2\,(a+b)}}\ \mathrm{e}^{i\alpha\hat{\Pi}_I\hat{\sigma}_z^s/2}\left(\mathrm{e}^{-i\chi/2}\sqrt{b}|I\rangle + \mathrm{e}^{i\chi/2}\sqrt{a}|II\rangle\right)\left(|S_z;+\rangle + |S_z;-\rangle\right) \\
&= \sqrt{\frac{1}{2\,(a+b)}}\ \mathrm{e}^{i\alpha\hat{\Pi}_I\hat{\sigma}_z^s/2}\left(\mathrm{e}^{-i\chi/2}\sqrt{b}|I\rangle|S_z;+\rangle + \mathrm{e}^{-i\chi/2}\sqrt{b}|I\rangle|S_z;-\rangle + \right. \\
&\quad \left. + \mathrm{e}^{i\chi/2}\sqrt{a}|II\rangle|S_z;+\rangle + \mathrm{e}^{i\chi/2}\sqrt{a}|II\rangle|S_z;-\rangle\right) \\
&= \sqrt{\frac{1}{2\,(a+b)}}\ \left(\mathrm{e}^{-i\chi/2}\sqrt{b}\mathrm{e}^{i\alpha/2}|I\rangle|S_z;+\rangle + \mathrm{e}^{-i\chi/2}\sqrt{b}\mathrm{e}^{-i\alpha/2}|I\rangle|S_z;-\rangle + \right. \\
&\quad \left. + \mathrm{e}^{i\chi/2}\sqrt{a}|II\rangle|S_z;+\rangle + \mathrm{e}^{i\chi/2}\sqrt{a}|II\rangle|S_z;-\rangle\right),
\end{aligned} \tag{3.129}$$

which becomes

$$|\Phi\rangle_I = \sqrt{\frac{1}{4\,(a+b)}}\ \left\{\left[\mathrm{e}^{-i(\chi-\alpha)/2}\sqrt{b} + \mathrm{e}^{i\chi/2}\sqrt{a}\right]|S_z;+\rangle + \left[\mathrm{e}^{-i(\chi+\alpha)/2}\sqrt{b} + \mathrm{e}^{i\chi/2}\sqrt{a}\right]|S_z;-\rangle\right\}|P_f\rangle \tag{3.130}$$

after post selection on the final state $|P_f\rangle = \sqrt{\frac{1}{2}}\left(|I\rangle + |II\rangle\right)$. To evaluate Eq. (3.128) we have to calculate the matrix elements $\langle S_x;+|\Phi\rangle_I$ and $\langle S_x;-|\Phi\rangle_I$.

$$\langle S_x;+|\Phi\rangle_I = \sqrt{\frac{1}{8\,(a+b)}}\ \left\{\left[\mathrm{e}^{-i(\chi-\alpha)/2}\sqrt{b} + \mathrm{e}^{i\chi/2}\sqrt{a}\right] + \left[\mathrm{e}^{-i(\chi+\alpha)/2}\sqrt{b} + \mathrm{e}^{i\chi/2}\sqrt{a}\right]\right\}|P_f\rangle \tag{3.131}$$

and

$$\langle S_x;-|\Phi\rangle_I = \sqrt{\frac{1}{8\,(a+b)}}\ \left\{\left[\mathrm{e}^{-i(\chi-\alpha)/2}\sqrt{b} + \mathrm{e}^{i\chi/2}\sqrt{a}\right] - \left[\mathrm{e}^{-i(\chi+\alpha)/2}\sqrt{b} + \mathrm{e}^{i\chi/2}\sqrt{a}\right]\right\}|P_f\rangle. \tag{3.132}$$

[g]The calculation is exactly the same as before, except that $\hat{\Pi}_z$ has to be replaced by $\hat{\Pi}_j$ everywhere. Since this is rather trivial, it is not repeated in detail here.

This leads to the intensities

$$\begin{aligned} I_+^I &= |\langle S_x;+|\Phi\rangle_I|^2 = \frac{1}{8\,(a+b)}\ \left\{\left[\mathrm{e}^{-i(\chi-\alpha)/2}\sqrt{b}+\mathrm{e}^{i\chi/2}\sqrt{a}\right]+\left[\mathrm{e}^{-i(\chi+\alpha)/2}\sqrt{b}+\mathrm{e}^{i\chi/2}\sqrt{a}\right]\right\}\times \\ &\quad\times\left\{\left[\mathrm{e}^{i(\chi-\alpha)/2}\sqrt{b}+\mathrm{e}^{-i\chi/2}\sqrt{a}\right]+\left[\mathrm{e}^{i(\chi+\alpha)/2}\sqrt{b}+\mathrm{e}^{-i\chi/2}\sqrt{a}\right]\right\} \\ &= \frac{1}{4\,(a+b)}\ \left[2a+b+b\cos(\alpha)+4\sqrt{ab}\cos\left(\frac{\alpha}{2}\right)\cos(\chi)\right] \end{aligned} \tag{3.133}$$

and

$$\begin{aligned} I_-^I &= |\langle S_x;-|\Phi\rangle_I|^2 = \frac{1}{8\,(a+b)}\ \left\{\left[\mathrm{e}^{-i(\chi-\alpha)/2}\sqrt{b}+\mathrm{e}^{i\chi/2}\sqrt{a}\right]-\left[\mathrm{e}^{-i(\chi+\alpha)/2}\sqrt{b}+\mathrm{e}^{i\chi/2}\sqrt{a}\right]\right\}\times \\ &\quad\times\left\{\left[\mathrm{e}^{i(\chi-\alpha)/2}\sqrt{b}+\mathrm{e}^{-i\chi/2}\sqrt{a}\right]-\left[\mathrm{e}^{i(\chi+\alpha)/2}\sqrt{b}+\mathrm{e}^{-i\chi/2}\sqrt{a}\right]\right\} \\ &= \frac{b}{4\,(a+b)}\ [1-\cos(\alpha)]\,. \end{aligned} \tag{3.134}$$

With Eq. (3.128) we get the weak value of $\langle\hat{\Pi}_I\rangle_w$

$$\left|\langle\hat{\Pi}_I\rangle_w\right| = \frac{1}{\alpha}\arccos\left\{1+\frac{b\,[\cos(\alpha)-1]}{a+b+2\sqrt{ab}\cos\left(\frac{\alpha}{2}\right)\cos(\chi)}\right\}. \tag{3.135}$$

If the weak rotation is performed in path II, the same calculation can be performed to obtain the weak value of $\langle\hat{\Pi}\rangle_{II}$. Now the system's wave function becomes

$$\begin{aligned} |\psi'\rangle_{II} &= \mathrm{e}^{i\alpha\hat{\Pi}_{II}\hat{\sigma}_z^s/2}|\psi\rangle = \sqrt{\frac{1}{2\,(a+b)}}\ \mathrm{e}^{i\alpha\hat{\Pi}_{II}\hat{\sigma}_z^s/2}\left(\mathrm{e}^{-i\chi/2}\sqrt{b}|I\rangle+\mathrm{e}^{i\chi/2}\sqrt{a}|II\rangle\right)(|S_z;+\rangle+|S_z;-\rangle) \\ &= \sqrt{\frac{1}{2\,(a+b)}}\ \mathrm{e}^{i\alpha\hat{\Pi}_{II}\hat{\sigma}_z^s/2}\left(\mathrm{e}^{-i\chi/2}\sqrt{b}|I\rangle|S_z;+\rangle+\mathrm{e}^{-i\chi/2}\sqrt{b}|I\rangle|S_z;-\rangle+\right. \\ &\quad\left.+\,\mathrm{e}^{i\chi/2}\sqrt{a}|II\rangle|S_z;+\rangle+\mathrm{e}^{i\chi/2}\sqrt{a}|II\rangle|S_z;-\rangle\right) \\ &= \sqrt{\frac{1}{2\,(a+b)}}\ \left(\mathrm{e}^{-i\chi/2}\sqrt{b}|I\rangle|S_z;+\rangle+\mathrm{e}^{-i\chi/2}\sqrt{b}|I\rangle|S_z;-\rangle+\right. \\ &\quad\left.+\,\mathrm{e}^{i\chi/2}\sqrt{a}\mathrm{e}^{i\alpha/2}|II\rangle|S_z;+\rangle+\mathrm{e}^{i\chi/2}\sqrt{a}\mathrm{e}^{-i\alpha/2}|II\rangle|S_z;-\rangle\right) \end{aligned} \tag{3.136}$$

and

$$|\Phi\rangle_{II} = \sqrt{\frac{1}{4\,(a+b)}}\ \left\{\left[\mathrm{e}^{-i\chi/2}\sqrt{b}+\mathrm{e}^{i(\chi+\alpha)/2}\sqrt{a}\right]|S_z;+\rangle+\left[\mathrm{e}^{-i\chi/2}\sqrt{b}+\mathrm{e}^{i(\chi-\alpha)/2}\sqrt{a}\right]|S_z;-\rangle\right\}|P_f\rangle \tag{3.137}$$

after post selection. The matrix elements $\langle S_x;+|\Phi\rangle_{II}$ and $\langle S_x;-|\Phi\rangle_{II}$ are

$$\langle S_x;+|\Phi\rangle_{II} = \sqrt{\frac{1}{8\,(a+b)}}\ \left\{\left[\mathrm{e}^{-i\chi/2}\sqrt{b}+\mathrm{e}^{i(\chi+\alpha)/2}\sqrt{a}\right]+\left[\mathrm{e}^{-i\chi/2}\sqrt{b}+\mathrm{e}^{i(\chi-\alpha)/2}\sqrt{a}\right]\right\}|P_f\rangle \tag{3.138}$$

and

$$\langle S_x;-|\Phi\rangle_{II}=\sqrt{\frac{1}{8\,(a+b)}}\;\left\{\left[\mathrm{e}^{-i\chi/2}\sqrt{b}+\mathrm{e}^{i(\chi+\alpha)/2}\sqrt{a}\right]-\left[\mathrm{e}^{-i\chi/2}\sqrt{b}+\mathrm{e}^{i(\chi-\alpha)/2}\sqrt{a}\right]\right\}|P_f\rangle \tag{3.139}$$

leading to the intensities

$$\begin{aligned}I_{+}^{II}&=|\langle\, S_x;+|\Phi\rangle_{II}|^2=\frac{1}{8\,(a+b)}\;\left\{\left[\mathrm{e}^{-i\chi/2}\sqrt{b}+\mathrm{e}^{i(\chi+\alpha)/2}\sqrt{a}\right]+\left[\mathrm{e}^{-i\chi/2}\sqrt{b}+\mathrm{e}^{i(\chi-\alpha)/2}\sqrt{a}\right]\right\}\times\\&\quad\times\left\{\left[\mathrm{e}^{i\chi/2}\sqrt{b}+\mathrm{e}^{-i(\chi+\alpha)/2}\sqrt{a}\right]+\left[\mathrm{e}^{i\chi/2}\sqrt{b}+\mathrm{e}^{-i(\chi-\alpha)/2}\sqrt{a}\right]\right\}\\&=\frac{1}{4\,(a+b)}\;\left[a+2b+a\cos\left(\alpha\right)+4\sqrt{ab}\cos\left(\frac{\alpha}{2}\right)\cos\left(\chi\right)\right]\end{aligned} \tag{3.140}$$

and

$$\begin{aligned}I_{-}^{II}&=|\langle\, S_x;-|\Phi\rangle_{II}|^2=\frac{1}{8\,(a+b)}\;\left\{\left[\mathrm{e}^{-i\chi/2}\sqrt{b}+\mathrm{e}^{i(\chi+\alpha)/2}\sqrt{a}\right]-\left[\mathrm{e}^{-i\chi/2}\sqrt{b}+\mathrm{e}^{i(\chi-\alpha)/2}\sqrt{a}\right]\right\}\times\\&\quad\times\left\{\left[\mathrm{e}^{i\chi/2}\sqrt{b}+\mathrm{e}^{-i(\chi+\alpha)/2}\sqrt{a}\right]-\left[\mathrm{e}^{i\chi/2}\sqrt{b}+\mathrm{e}^{-i(\chi-\alpha)/2}\sqrt{a}\right]\right\}\\&=\frac{a}{4\,(a+b)}\;\left[1-\cos\left(\alpha\right)\right].\end{aligned} \tag{3.141}$$

So the weak value of $\hat{\Pi}_{II}$ is given by

$$\left|\langle\hat{\Pi}_{II}\rangle_w\right|=\frac{1}{\alpha}\arccos\left\{1+\frac{a\left[\cos\left(\alpha\right)-1\right]}{a+b+2\sqrt{ab}\cos\left(\frac{\alpha}{2}\right)\cos\left(\chi\right)}\right\}. \tag{3.142}$$

Again it is possible to simply calculate the analytic solution of $\langle\hat{\Pi}_I\rangle_w$ and $\langle\hat{\Pi}_{II}\rangle_w$ for given $|P_i\rangle$ and $|P_f\rangle$.

$$\begin{aligned}\langle\hat{\Pi}_I\rangle_w&\equiv\frac{\langle P_f|\hat{\Pi}_I|P_i\rangle}{\langle P_f|P_i\rangle}=\frac{\left[\langle I|+\langle II|\right]\left[\mathrm{e}^{-i\chi/2}\sqrt{b}|I\rangle\right]}{\left[\langle I|+\langle II|\right]\left[\mathrm{e}^{-i\chi/2}\sqrt{b}|I\rangle+\mathrm{e}^{i\chi/2}\sqrt{a}|II\rangle\right]}\\&=\frac{\sqrt{b}\;\mathrm{e}^{-i\chi/2}}{\sqrt{b}\;\mathrm{e}^{-i\chi/2}+\sqrt{a}\;\mathrm{e}^{i\chi/2}}=\frac{\sqrt{b}}{\sqrt{b}+\sqrt{a}\;\mathrm{e}^{i\chi}}\end{aligned} \tag{3.143}$$

and

$$\begin{aligned}\langle\hat{\Pi}_{II}\rangle_w&\equiv\frac{\langle P_f|\hat{\Pi}_{II}|P_i\rangle}{\langle P_f|P_i\rangle}=\frac{\left[\langle I|+\langle II|\right]\left[\mathrm{e}^{i\chi/2}\sqrt{a}|II\rangle\right]}{\left[\langle I|+\langle II|\right]\left[\mathrm{e}^{-i\chi/2}\sqrt{b}|I\rangle+\mathrm{e}^{i\chi/2}\sqrt{a}|II\rangle\right]}\\&=\frac{\sqrt{a}\;\mathrm{e}^{i\chi/2}}{\sqrt{b}\;\mathrm{e}^{-i\chi/2}+\sqrt{a}\;\mathrm{e}^{i\chi/2}}=\frac{\sqrt{a}}{\sqrt{b}\;\mathrm{e}^{-i\chi}+\sqrt{a}}\end{aligned} \tag{3.144}$$

As is shown shortly, the relations derived above will give the individual weak values of $\hat{\Pi}_I$ and $\hat{\Pi}_{II}$.

3.2.4. Expected results for the individual weak values of $\hat{\Pi}_I$ and $\hat{\Pi}_{II}$

The first question that comes into mind is the following: Do Eqs. (3.135) and (3.142) match Eqs. (3.143) and (3.144) for a certain value of α? If the absolute of $\langle\hat{\Pi}_I\rangle_w$ and $\langle\hat{\Pi}_{II}\rangle_w$ are plotted, the answer becomes quite obvious. For small values of α, i.e for $\alpha \leq 10°$, Eq. (3.135) and Eq. (3.142) represent the absolute of the operators' $\hat{\Pi}_I$ and $\hat{\Pi}_{II}$ weak value. As Figs. 3.19 to 3.22 show, the analytic solution of $\langle\hat{\Pi}_j\rangle_w$ and its simulations match up perfectly for small values of α. Figure 3.19 shows the weak value of $\hat{\Pi}_I$ for a fixed absorber value of $a = 0.5$. Figure

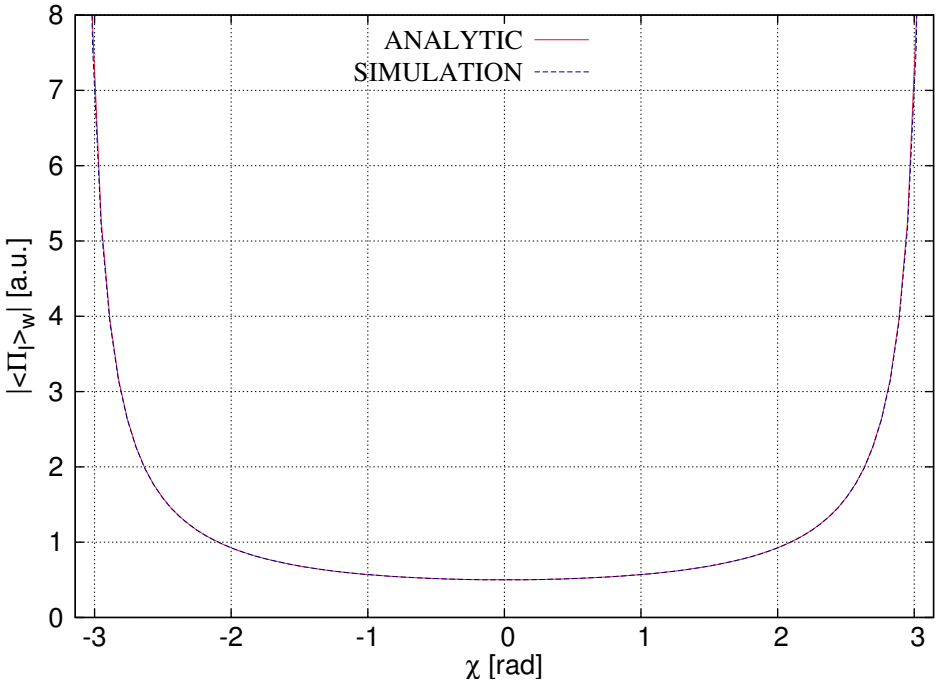

Figure 3.19.: Simulation [Eq. (3.135)] and the absolute of the weak value's analytic solution [absolute of Eq. (3.143)]. The absorber is modeled as $|P_i\rangle = \mathrm{e}^{-i\chi/2}\sqrt{b}|I\rangle + \mathrm{e}^{i\chi/2}\sqrt{a}|II\rangle$ with $a = b = 0.5$ and $\alpha = \pi/36$. χ represents the phase shifter value.

3.20 shows the weak value of $\hat{\Pi}_I$ once more, but now the phase shifter is held fixed at $\chi = 0$ and the absorber is varied. To compare $\langle\hat{\Pi}_I\rangle_w$ and $\langle\hat{\Pi}_{II}\rangle_w$ the same plots are made for $\hat{\Pi}_{II}$. Figure 3.21 shows the weak value of $\hat{\Pi}_{II}$ for a fixed absorber value of $a = 0.5$. Note that $\langle\hat{\Pi}_I\rangle_w$ and $\langle\hat{\Pi}_{II}\rangle_w$ are equal if the absorber is set to $a = 0.5$ and only the phase shifter χ is varied. Finally, Fig. 3.22 shows the weak value of $\hat{\Pi}_{II}$ for a fixed phase shifter value of $\chi = 0$. Now the weak value is mirror inverted to $\langle\hat{\Pi}_I\rangle_w$.

So we have found a way to measure not only the absolute of $\langle\hat{\Pi}_z\rangle_w$, but also Abs $\left(\langle\hat{\Pi}_I\rangle_w\right)$ and Abs $\left(\langle\hat{\Pi}_{II}\rangle_w\right)$!

The weak measurement of $\hat{\Pi}_I$ and $\hat{\Pi}_{II}$ has two big advantages . Firstly Eq. (3.135) and (3.142) are not as angle sensitive as Eq. (3.84), i.e. the equation used to calculate $\langle\hat{\Pi}_z\rangle_w$. This seems surprising, since all of the mentioned equations were practically derived in the same way. Why should the same approximation work better for one operator than for another? The answer to this question is simple. To measure $\hat{\Pi}_z$ weakly it is necessary to perform a spin rotation along both paths of the interferometer. Therefore a relative phase between path I and II is introduced,

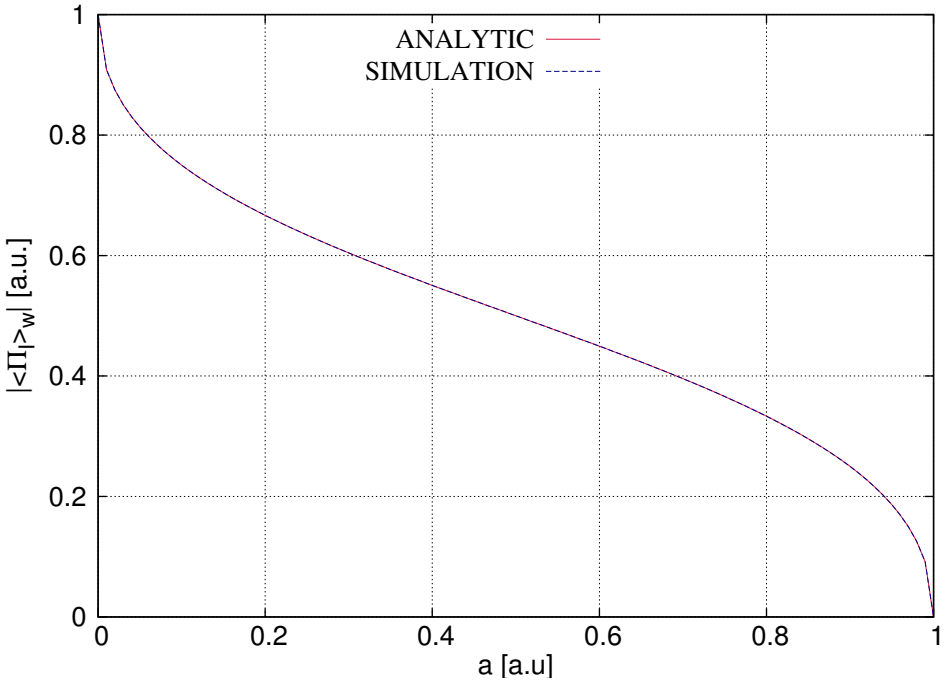

Figure 3.20.: Simulation [Eq. (3.135)] and the absolute of the weak value's analytic solution [absolute of Eq. (3.143)]. The absorber is modeled as $|P_i\rangle = \mathrm{e}^{-i\chi/2}\sqrt{b}|I\rangle + \mathrm{e}^{i\chi/2}\sqrt{a}|II\rangle$ and the phase shifter is set to $\chi = 0$. The interaction strength is given by $\alpha = \pi/36$. a represents the absorber value.

which is $2 \times \alpha$. In comparison to that, the relative phase between the paths is only α, if either $\hat{\Pi}_I$ or $\hat{\Pi}_{II}$ are measured weakly. Hence the disturbance on the system is smaller if the spin is only turned in one path and the condition of a weak measurement is fulfilled better.
There is another even bigger advantage when $\hat{\Pi}_I$ and $\hat{\Pi}_{II}$ are measured weakly instead of $\hat{\Pi}_z$. Previously it was stated, that no pure 'which-way-information' can be extracted from the system, since the experiment only permits to measure the absolute of the operator's weak value. However, the weak measurement of $\hat{\Pi}_I$ and $\hat{\Pi}_{II}$ offers a workaround:
If the first path is blocked completely Abs $\left(\langle\hat{\Pi}_I\rangle_w\right)$ becomes 0, which means that the whole ensemble went through the second path. In comparison to that it becomes 1, if the second path is blocked. More than that we can measure Abs $\left(\langle\hat{\Pi}_I\rangle_w\right)$ and Abs $\left(\langle\hat{\Pi}_{II}\rangle_w\right)$ for any combination of a, b and χ, which allows us to determine the path the ensemble took in the interferometer. Thanks to the nature of weak measurements we still observe the interference pattern, which would not be possible if a strong measurement is performed.
By turning the spin in one path, measure $\left|\langle\hat{\Pi}_I\rangle_w\right|$, then turn the spin in the other path to obtain $\left|\langle\hat{\Pi}_{II}\rangle_w\right|$, we can extract pure which way information from the measurement!

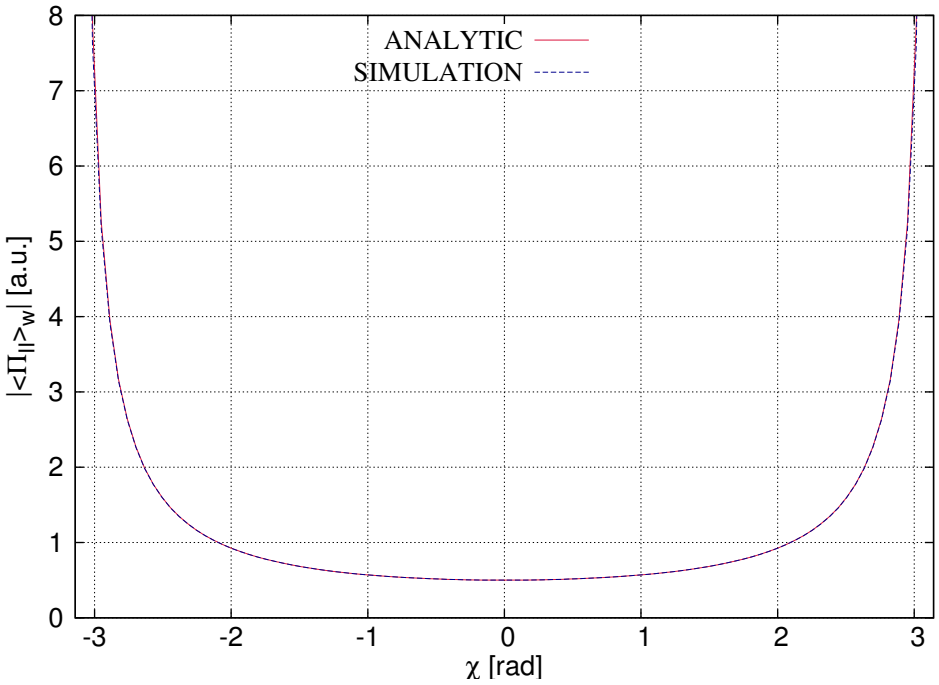

Figure 3.21.: Simulation [Eq. (3.142)] and the absolute of the weak value's analytic solution [absolute of Eq. (3.144)]. The absorber is modeled as $|P_i\rangle = \mathrm{e}^{-i\chi/2}\sqrt{b}|I\rangle + \mathrm{e}^{i\chi/2}\sqrt{a}|II\rangle$ with $a = b = 0.5$ and $\alpha = \pi/36$. χ represents the phase shifter value.

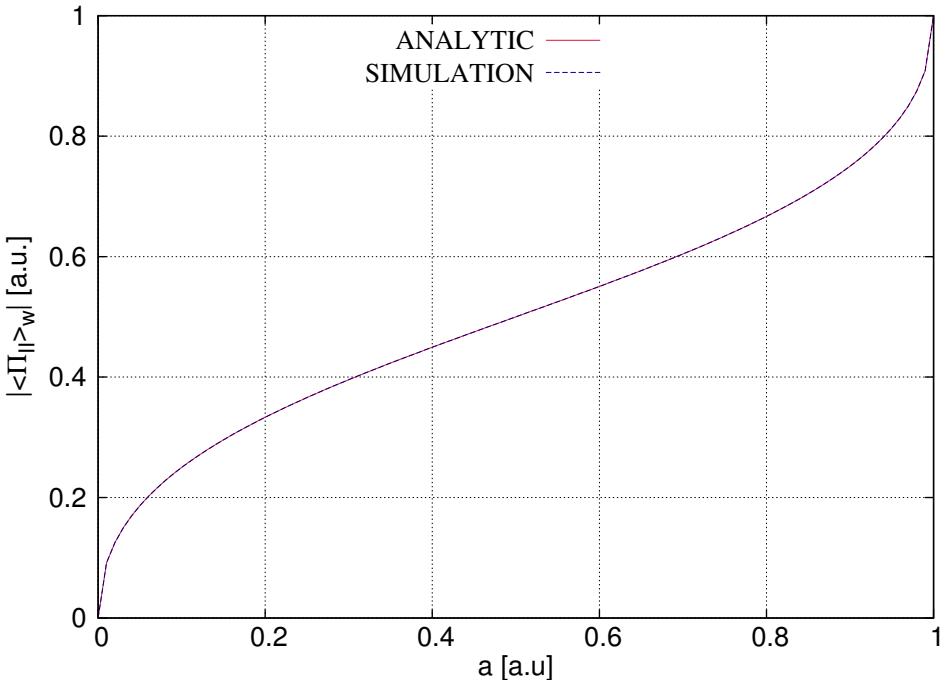

Figure 3.22.: Simulation [Eq. (3.142)] and the absolute of the weak value's analytic solution [absolute of Eq. (3.144)]. The absorber is modeled as $|P_i\rangle = \mathrm{e}^{-i\chi/2}\sqrt{b}|I\rangle + \mathrm{e}^{i\chi/2}\sqrt{a}|II\rangle$ and the phase shifter is set to $\chi = 0$. The interaction strength is given by $\alpha = \pi/36$. a represents the absorber value.

3.2.5. Evaluation of $\hat{\sigma}_y^s$ and $\hat{\sigma}_z^s$

The present experimental setup allows, to evaluate $\hat{\sigma}_x^s$ in order to extract the weak value, since hardly any loss in the count rate is introduced, by the path weak measurement. But what happens if $\hat{\sigma}_y^s$ is evaluated instead? For this we have to take the system's wave function after the weak measurement, which is given by Eq. (3.57) and calculate $\langle\hat{\sigma}_y^s\rangle$.

$$\begin{aligned}\langle\hat{\sigma}_y^s\rangle &= \frac{\langle\Phi|\hat{\sigma}_y^s|\Phi\rangle}{\langle\Phi|\Phi\rangle} = \frac{1}{2}\frac{\epsilon\epsilon^*}{\langle\Phi|\Phi\rangle}\left(\mathrm{e}^{-i\alpha\langle\hat{\Pi}_z\rangle_w/2}\langle S_z;+| + \mathrm{e}^{i\alpha\langle\hat{\Pi}_z\rangle_w/2}\langle S_z;-|\right)\times \\ &\quad\times i\left(|S_z;-\rangle\langle S_z;+| - |S_z;+\rangle\langle S_z;-|\right)\left(\mathrm{e}^{i\alpha\langle\hat{\Pi}_z\rangle_w/2}|S_z;+\rangle + \mathrm{e}^{-i\alpha\langle\hat{\Pi}_z\rangle_w/2}|S_z;-\rangle\right)\langle P_f|P_f\rangle \\ &= \frac{i}{2}\frac{|\epsilon|^2}{\langle\Phi|\Phi\rangle}\left(\mathrm{e}^{-i\alpha\langle\hat{\Pi}_z\rangle_w/2}\langle S_z;+| + \mathrm{e}^{i\alpha\langle\hat{\Pi}_z\rangle_w/2}\langle S_z;-|\right)\left(\mathrm{e}^{i\alpha\langle\hat{\Pi}_z\rangle_w/2}|S_z;-\rangle - \mathrm{e}^{-i\alpha\langle\hat{\Pi}_z\rangle_w/2}|S_z;+\rangle\right) \\ &= \frac{i}{2}\frac{|\epsilon|^2}{\langle\Phi|\Phi\rangle}\left(\mathrm{e}^{i\alpha\langle\hat{\Pi}_z\rangle_w} - \mathrm{e}^{-i\alpha\langle\hat{\Pi}_z\rangle_w}\right) = -\sin\left(\alpha\langle\hat{\Pi}_z\rangle_w\right) \end{aligned} \tag{3.145}$$

For this case the weak value becomes

$$\langle\hat{\Pi}_z\rangle_w = \frac{1}{\alpha}\arcsin\left(\frac{I_-^y - I_+^y}{I_-^y + I_+^y}\right) \tag{3.146}$$

To see if Eq. (3.146) yields the same results as previously, we have to calculate the intensities I_+^y and I_-^y. Taking the results from Eq. (3.74) and Eq. (3.75) we get the matrix elements

$$\langle S_y;+|\Phi\rangle = \sqrt{\frac{1}{8\,(a+b)}}\left\{\left[\mathrm{e}^{-i(\chi-\alpha)/2}\sqrt{b} + \mathrm{e}^{i(\chi-\alpha)/2}\sqrt{a}\right] - i\left[\mathrm{e}^{-i(\chi+\alpha)/2}\sqrt{b} + \mathrm{e}^{i(\chi+\alpha)/2}\sqrt{a}\right]\right\}|P_f\rangle \tag{3.147}$$

and

$$\langle S_y;-|\Phi\rangle = \sqrt{\frac{1}{8\,(a+b)}}\left\{\left[\mathrm{e}^{-i(\chi-\alpha)/2}\sqrt{b} + \mathrm{e}^{i(\chi-\alpha)/2}\sqrt{a}\right] + i\left[\mathrm{e}^{-i(\chi+\alpha)/2}\sqrt{b} + \mathrm{e}^{i(\chi+\alpha)/2}\sqrt{a}\right]\right\}|P_f\rangle \tag{3.148}$$

which lead us to the intensities

$$I_+^y = |\langle S_y;+|\Phi\rangle|^2 = \frac{1}{4\,(a+b)}\left[a+b+2\sqrt{ab}\cos(\chi)\cos(\alpha) + (a-b)\sin(\alpha)\right] \tag{3.149}$$

and

$$I_-^y = |\langle S_y;-|\Phi\rangle|^2 = \frac{1}{4\,(a+b)}\left[a+b+2\sqrt{ab}\cos(\chi)\cos(\alpha) + (b-a)\sin(\alpha)\right] \tag{3.150}$$

Hence, the weak value of $\hat{\Pi}_z$ is given by

$$\langle\hat{\Pi}_z\rangle_w = \frac{1}{\alpha}\arcsin\left(\frac{(b-a)\sin(\alpha)}{a+b+2\sqrt{ab}\cos(\chi)\cos(\alpha)}\right) \tag{3.151}$$

Equation (3.151) is now plotted for fixed values of α and χ and by assuming, that $b = 1 - a$. Figure 3.23 shows a plot of $\langle\hat{\Pi}_z\rangle_w$'s analytic solution compared to its simulation.one sees immediately that analyzing $\langle\hat{\sigma}_y^s\rangle$ yields the real part of $\langle\hat{\Pi}_z\rangle_w$!

Let us check if we are able to measure the real part of $\langle\hat{\Pi}_I\rangle_w$ and $\langle\hat{\Pi}_{II}\rangle_w$ in the same way. If

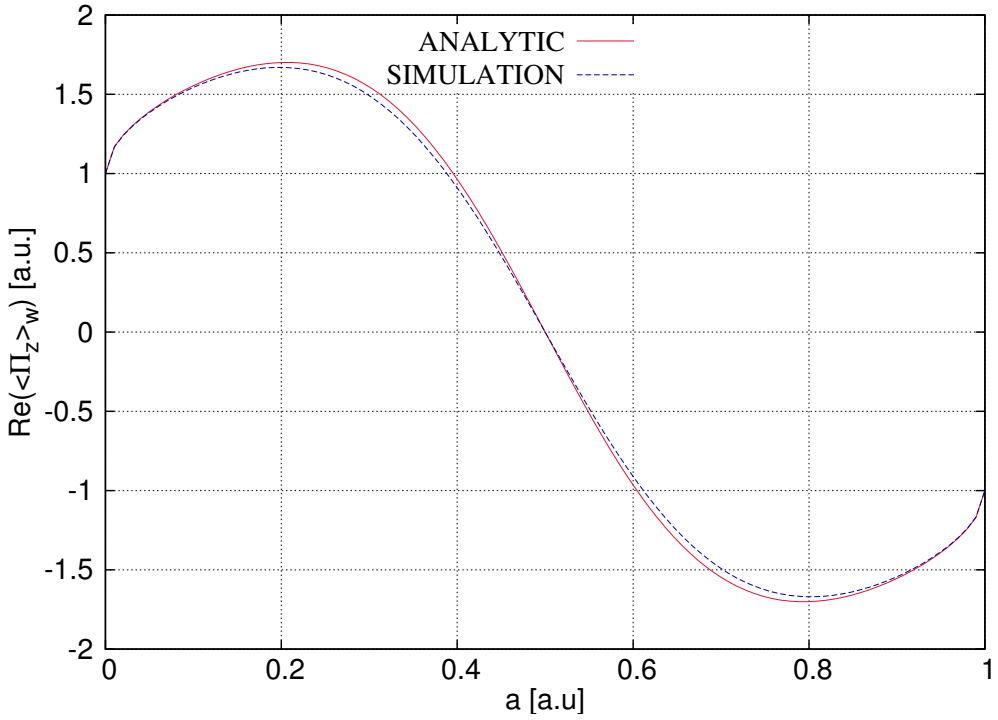

Figure 3.23.: Simulation [Eq. (3.151)] and the real part of the weak value's analytic solution [real part of Eq. (3.69)] for a fixed phase shifter value of $\chi = \frac{4\pi}{5}$ and an angle of rotation of $\alpha = \pi/18$, if $\langle\hat{\sigma}_y^s\rangle$ is analyzed. a represents the absorber value.

$\langle\hat{\sigma}_y^s\rangle$ is evaluated, Eq. (3.128) changes into

$$\langle\hat{\Pi}_j\rangle = \frac{1}{\alpha}\arcsin\left(\frac{I_-^{y_j} - I_+^{y_j}}{I_-^{y_j} + I_+^{y_j}}\right) \tag{3.152}$$

If the spin is turned along path I, evaluating the matrix elements

$$\langle S_y;+|\Phi\rangle_I = \sqrt{\frac{1}{8\,(a+b)}}\,\left\{\left[\mathrm{e}^{-i(\chi-\alpha)/2}\sqrt{b} + \mathrm{e}^{i\chi/2}\sqrt{a}\right] - i\left[\mathrm{e}^{-i(\chi+\alpha)/2}\sqrt{b} + \mathrm{e}^{i\chi/2}\sqrt{a}\right]\right\}|P_f\rangle \tag{3.153}$$

and

$$\langle S_y;-|\Phi\rangle_I = \sqrt{\frac{1}{8\,(a+b)}}\,\left\{\left[\mathrm{e}^{-i(\chi-\alpha)/2}\sqrt{b} + \mathrm{e}^{i\chi/2}\sqrt{a}\right] + i\left[\mathrm{e}^{-i(\chi+\alpha)/2}\sqrt{b} + \mathrm{e}^{i\chi/2}\sqrt{a}\right]\right\}|P_f\rangle \tag{3.154}$$

lead to the intensities

$$I_{+}^{y_I} = \frac{a+b+2\sqrt{ab}\cos(\chi)\left[\cos\left(\frac{\alpha}{2}\right)-\sin\left(\frac{\alpha}{2}\right)\right]-b\sin(\alpha)}{4(a+b)} \tag{3.155}$$

and

$$I_{-}^{y_I} = \frac{a+b+2\sqrt{ab}\cos(\chi)\left[\cos\left(\frac{\alpha}{2}\right)+\sin\left(\frac{\alpha}{2}\right)\right]+b\sin(\alpha)}{4(a+b)}, \tag{3.156}$$

which tell us the expectation value of $\hat{\sigma}_y^s$

$$\langle\hat{\sigma}_y^s\rangle_I = \frac{I_{-}^{y_I}-I_{+}^{y_I}}{I_{-}^{y_I}-I_{+}^{y_I}} = \frac{2\sqrt{ab}\ \cos(\chi)\sin\left(\frac{\alpha}{2}\right)+b\sin(\alpha)}{a+b+2\sqrt{ab}\cos\left(\frac{\alpha}{2}\right)\cos(\chi)} \tag{3.157}$$

Therefore we are expecting our measurements to yield the following result for the weak value

$$\langle\hat{\Pi}_I\rangle_w = \frac{1}{\alpha}\arcsin\left[\frac{2\sqrt{ab}\ \cos(\chi)\sin\left(\frac{\alpha}{2}\right)+b\sin(\alpha)}{a+b+2\sqrt{ab}\cos\left(\frac{\alpha}{2}\right)\cos(\chi)}\right] \tag{3.158}$$

Equation (3.158) is now plotted for fixed values of α and χ and it is assumed that $b = 1-a$ (as it was done in Fig. 3.24). It is not surprising to find, that we can measure the real part of $\langle\hat{\Pi}_I\rangle_w$ in the same way as $\mathrm{Re}\left(\langle\hat{\Pi}_z\rangle_w\right)$. For completeness sake, we finally want to show that we

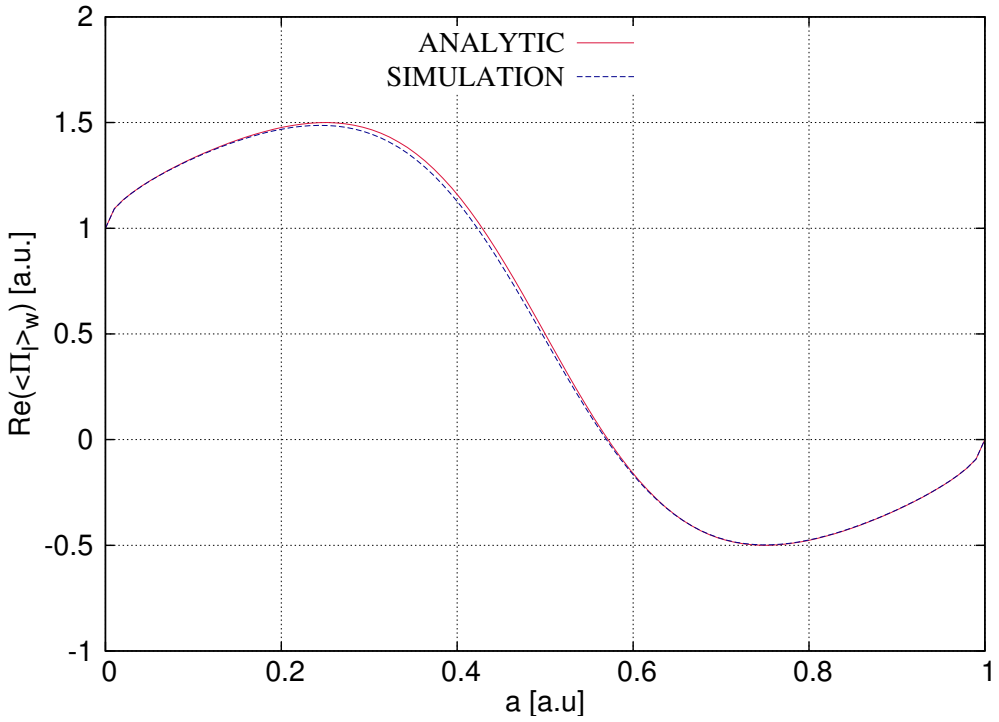

Figure 3.24.: Simulation [Eq. (3.158)] and the real part of the weak value's analytic solution [real part of Eq. (3.143)] for a fixed phase shifter value of $\chi = \frac{5\pi}{6}$ and an angle of rotation of $\alpha = \pi/18$, as well as for $b = 1-a$, if $\langle\hat{\sigma}_y^s\rangle$ is analyzed. a represents the absorber value.

can also measure the real part of $\langle\hat{\Pi}_{II}\rangle$. The matrix elements

$$\langle S_y;+|\Phi\rangle_{II} = \sqrt{\frac{1}{8\,(a+b)}}\ \left\{\left[\mathrm{e}^{-i\chi/2}\sqrt{b}+\mathrm{e}^{i(\chi+\alpha)/2}\sqrt{a}\right]-i\left[\mathrm{e}^{-i\chi/2}\sqrt{b}+\mathrm{e}^{i(\chi-\alpha)/2}\sqrt{a}\right]\right\}|P_f\rangle \tag{3.159}$$

and

$$\langle S_y;-|\Phi\rangle_{II} = \sqrt{\frac{1}{8\,(a+b)}}\ \left\{\left[\mathrm{e}^{-i\chi/2}\sqrt{b}+\mathrm{e}^{i(\chi+\alpha)/2}\sqrt{a}\right]+i\left[\mathrm{e}^{-i\chi/2}\sqrt{b}+\mathrm{e}^{i(\chi-\alpha)/2}\sqrt{a}\right]\right\}|P_f\rangle \tag{3.160}$$

yield the intensities

$$I_{+}^{y_{II}} = \frac{a+b+2\sqrt{ab}\cos(\chi)\left[\cos\left(\frac{\alpha}{2}\right)-\sin\left(\frac{\alpha}{2}\right)\right]-a\sin(\alpha)}{4\,(a+b)} \tag{3.161}$$

and

$$I_{-}^{y_{II}} = \frac{a+b+2\sqrt{ab}\cos(\chi)\left[\cos\left(\frac{\alpha}{2}\right)+\sin\left(\frac{\alpha}{2}\right)\right]+a\sin(\alpha)}{4\,(a+b)} \tag{3.162}$$

which lead to the weak value

$$\langle\hat{\Pi}_{II}\rangle_w = \frac{1}{\alpha}\arcsin\left[\frac{2\sqrt{ab}\ \cos(\chi)\sin\left(\frac{\alpha}{2}\right)+a\sin(\alpha)}{a+b+2\sqrt{ab}\cos\left(\frac{\alpha}{2}\right)\cos(\chi)}\right] \tag{3.163}$$

Again we find that we can measure $\mathrm{Re}\left(\langle\hat{\Pi}_{II}\rangle\right)$, as can be seen by looking at Fig. 3.25, which shows a plot of Eq. (3.163) for fixed values of α and χ (is assumed that $b = 1-a$).

Obviously we found a way to measure $\mathrm{Re}\left(\langle\hat{\Pi}_z\rangle_w\right)$ directly by evaluating $\langle\hat{\sigma}_y^s\rangle$. If the analysis of $\langle\hat{\sigma}_x^s\rangle$ yields $\mathrm{Abs}\left(\langle\hat{\Pi}_z\rangle_w\right)$ and the one of $\langle\hat{\sigma}_y^s\rangle$, $\mathrm{Re}\left(\langle\hat{\Pi}_z\rangle_w\right)$, it immediately suggests itself that the evaluation of $\langle\hat{\sigma}_z^s\rangle$ will give us $\mathrm{Im}\left(\langle\hat{\Pi}_z\rangle_w\right)$. However, we are going to show that this is not the case: If the spin state lies within the xy-plane and is rotated only around the z-axis, $\langle\hat{\sigma}_z^s\rangle$ will always equal zero. Therefore the axis of rotation has to be changed and our new interaction Hamiltonian is

$$\hat{H}_i \equiv -\frac{\alpha\hat{\sigma}_y^s\hat{\Pi}_z}{2}. \tag{3.164}$$

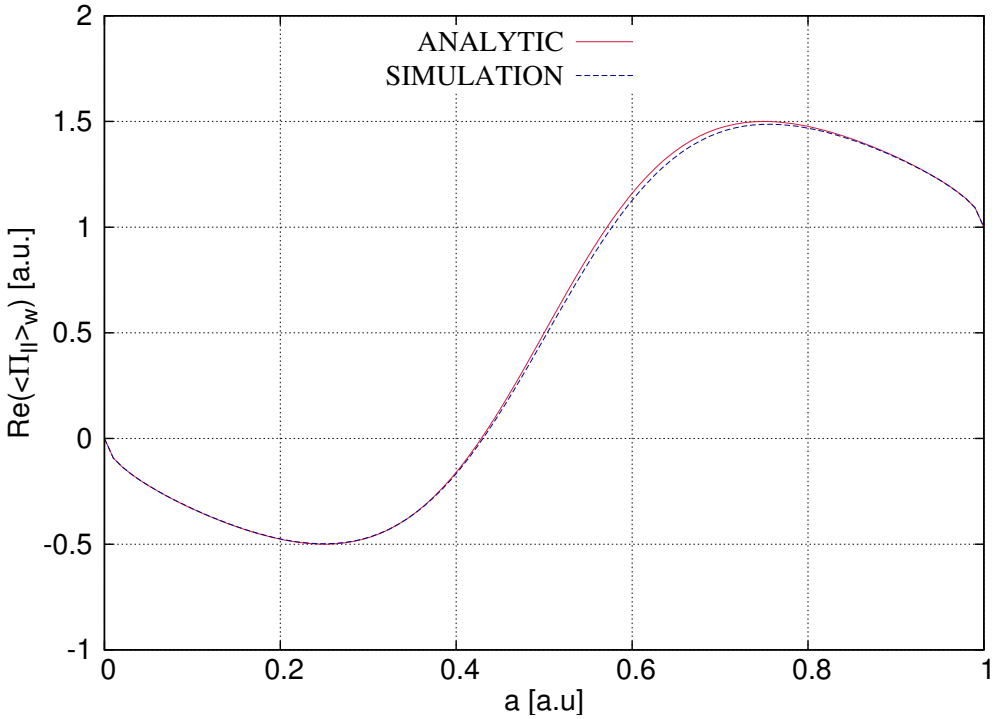

Figure 3.25.: Simulation [Eq. (3.163)] and the real part of the weak value's analytic solution [real part of Eq. (3.144)] for a fixed phase shifter value of $\chi = \frac{5\pi}{6}$ and an angle of rotation of $\alpha = \pi/18$, as well as for $b = 1 - a$, if $\langle \hat{\sigma}_y^s \rangle$ is analyzed. a represents the absorber value.

If we now let this Hamiltonian act on the system its wave function, given by Eq. (3.54), becomes

$$\begin{aligned}
|\psi'\rangle = \mathrm{e}^{i\alpha\hat{\sigma}_y^s\hat{\Pi}_z/2}|\psi\rangle \approx \left(1 + \frac{i\alpha\hat{\sigma}_y^s\hat{\Pi}_z}{2}\right)|\psi\rangle &= |P_i\rangle|S_x;+\rangle + \frac{i\alpha\hat{\Pi}_z}{2}|P_i\rangle\hat{\sigma}_y^s|S_x;+\rangle \\
&= |P_i\rangle\sqrt{\frac{1}{2}}\left(|S_z;+\rangle + |S_z;-\rangle\right) + \frac{i\alpha\hat{\Pi}_z}{2}|P_i\rangle i\sqrt{\frac{1}{2}}\left(|S_z;-\rangle - |S_z;+\rangle\right) \\
&= |P_i\rangle\sqrt{\frac{1}{2}}\left(|S_z;+\rangle + |S_z;-\rangle\right) - \frac{\alpha\hat{\Pi}_z}{2}|P_i\rangle\sqrt{\frac{1}{2}}\left(|S_z;-\rangle - |S_z;+\rangle\right). \qquad (3.165)
\end{aligned}$$

Once post selection onto the final path state $|P_f\rangle\langle P_f|$ is performed, this simplifies to

$$\begin{aligned}
|\Phi\rangle = |P_f\rangle\langle P_f|\psi'\rangle &= \left[\underbrace{\langle P_f|P_i\rangle}_{\equiv\epsilon}\sqrt{\frac{1}{2}}\left(|S_z;+\rangle + |S_z;-\rangle\right) - \frac{\alpha}{2}\langle P_f|\hat{\Pi}_z|P_i\rangle\sqrt{\frac{1}{2}}\left(|S_z;-\rangle - |S_z;+\rangle\right)\right]|P_f\rangle \\
&= \frac{\epsilon}{\sqrt{2}}\left[|S_z;+\rangle + |S_z;-\rangle + \frac{\alpha}{2}\langle\hat{\Pi}_z\rangle_w|S_z;+\rangle - \frac{\alpha}{2}\langle\hat{\Pi}_z\rangle_w|S_z;-\rangle\right]|P_f\rangle \\
&= \frac{\epsilon}{\sqrt{2}}\left[\left(1 + \frac{\alpha\langle\hat{\Pi}_z\rangle_w}{2}\right)|S_z;+\rangle + \left(1 - \frac{\alpha\langle\hat{\Pi}_z\rangle_w}{2}\right)|S_z;-\rangle\right]|P_f\rangle \\
&= \frac{\epsilon}{\sqrt{2}}\left(\mathrm{e}^{\alpha\langle\hat{\Pi}_z\rangle_w/2}|S_z;+\rangle + \mathrm{e}^{-\alpha\langle\hat{\Pi}_z\rangle_w/2}|S_z;-\rangle\right)|P_f\rangle \qquad (3.166)
\end{aligned}$$

Instead of an additional phase, the weak value now manifests itself change in the amplitude. Equation (3.166) can now be used to evaluate $\langle\hat{\sigma}_z^s\rangle$.

$$\begin{aligned}\langle\hat{\sigma}_z^s\rangle &= \frac{|\epsilon|^2}{2}\frac{\langle P_f|P_f\rangle}{\langle\Phi|\Phi\rangle}\left(\mathrm{e}^{\alpha\langle\hat{\Pi}_z\rangle_w/2}\langle S_z;+| + \mathrm{e}^{-\alpha\langle\hat{\Pi}_z\rangle_w/2}\langle S_z;-|\right)\left(\mathrm{e}^{\alpha\langle\hat{\Pi}_z\rangle_w/2}|S_z;+\rangle - \mathrm{e}^{-\alpha\langle\hat{\Pi}_z\rangle_w/2}|S_z;-\rangle\right)\\ &= \frac{1}{2}\frac{|\epsilon|^2}{\langle\Phi|\Phi\rangle}\left(\mathrm{e}^{\alpha\langle\hat{\Pi}_z\rangle_w} - \mathrm{e}^{-\alpha\langle\hat{\Pi}_z\rangle_w}\right) = \frac{|\epsilon|^2}{\langle\Phi|\Phi\rangle}\sinh\left(\alpha\langle\hat{\Pi}_z\rangle_w\right)\end{aligned} \tag{3.167}$$

With

$$\begin{aligned}\langle\Phi|\Phi\rangle &= \frac{|\epsilon|^2}{2}\left(\mathrm{e}^{\alpha\langle\hat{\Pi}_z\rangle_w}\langle S_z;+| + \mathrm{e}^{-\alpha\langle\hat{\Pi}_z\rangle_w}\langle S_z;-|\right)\left(\mathrm{e}^{\alpha\langle\hat{\Pi}_z\rangle_w}|S_z;+\rangle + \mathrm{e}^{-\alpha\langle\hat{\Pi}_z\rangle_w}|S_z;-\rangle\right)\langle P_f|P_f\rangle\\ &= |\epsilon|^2\cosh\left(\alpha\langle\hat{\Pi}_z\rangle_w\right)\end{aligned} \tag{3.168}$$

we get

$$\langle\hat{\Pi}_z\rangle_w = \frac{1}{\alpha}\operatorname{arctanh}\left(\frac{I_+^z - I_-^z}{I_+^z + I_-^z}\right) \tag{3.169}$$

To gain useful information from this equation we have to calculate the intensities I_+^z and I_-^z, for which we let $\hat{U} = \exp\left(\frac{i\alpha\hat{\Pi}_z\hat{\sigma}_y^s}{2}\right)$ act upon the system.

$$\begin{aligned}|\psi'\rangle &= \mathrm{e}^{i\alpha\hat{\Pi}_z\hat{\sigma}_y^s/2}|\psi\rangle = \sqrt{\frac{1}{2\,(a+b)}}\,\mathrm{e}^{i\alpha\hat{\Pi}_z\hat{\sigma}_y^s/2}\left(\mathrm{e}^{-i\chi/2}\sqrt{b}|I\rangle + \mathrm{e}^{i\chi/2}\sqrt{a}|II\rangle\right)(|S_z;+\rangle + |S_z;-\rangle)\\
&= \sqrt{\frac{1}{2\,(a+b)}}\,\left(\mathrm{e}^{-i\chi/2}\sqrt{b}\,\mathrm{e}^{i\alpha\hat{\sigma}_y^s/2}|I\rangle + \mathrm{e}^{i\chi/2}\sqrt{a}\,\mathrm{e}^{-i\alpha\hat{\sigma}_y^s/2}|II\rangle\right)(|S_z;+\rangle + |S_z;-\rangle)\\
&= \sqrt{\frac{1}{2\,(a+b)}}\,\left(\mathrm{e}^{-i\chi/2}\sqrt{b}\,\mathrm{e}^{i\alpha\hat{\sigma}_y^s/2}|I\rangle|S_z;+\rangle + \mathrm{e}^{-i\chi/2}\sqrt{b}\,\mathrm{e}^{i\alpha\hat{\sigma}_y^s/2}|I\rangle|S_z;-\rangle +\right.\\
&\quad \left. + \mathrm{e}^{i\chi/2}\sqrt{a}\,\mathrm{e}^{-i\alpha\hat{\sigma}_y^s/2}|II\rangle|S_z;+\rangle + \mathrm{e}^{i\chi/2}\sqrt{a}\,\mathrm{e}^{-i\alpha\hat{\sigma}_y^s/2}|II\rangle|S_z;-\rangle\right)\\
&= \sqrt{\frac{1}{2\,(a+b)}}\,\left\{\mathrm{e}^{-i\chi/2}\sqrt{b}\left[\cos\left(\frac{\alpha}{2}\right) + i\hat{\sigma}_y^s\sin\left(\frac{\alpha}{2}\right)\right]|I\rangle|S_z;+\rangle +\right.\\
&\quad + \mathrm{e}^{-i\chi/2}\sqrt{b}\left[\cos\left(\frac{\alpha}{2}\right) + i\hat{\sigma}_y^s\sin\left(\frac{\alpha}{2}\right)\right]|I\rangle|S_z;-\rangle +\\
&\quad + \mathrm{e}^{i\chi/2}\sqrt{a}\left[\cos\left(\frac{\alpha}{2}\right) - i\hat{\sigma}_y^s\sin\left(\frac{\alpha}{2}\right)\right]|II\rangle|S_z;+\rangle +\\
&\quad \left. + \mathrm{e}^{i\chi/2}\sqrt{a}\left[\cos\left(\frac{\alpha}{2}\right) - i\hat{\sigma}_y^s\sin\left(\frac{\alpha}{2}\right)\right]|II\rangle|S_z;-\rangle\right)\\
&= \sqrt{\frac{1}{2\,(a+b)}}\,\left[\mathrm{e}^{-i\chi/2}\sqrt{b}\cos\left(\frac{\alpha}{2}\right)|I\rangle|S_z;+\rangle - \mathrm{e}^{-i\chi/2}\sqrt{b}\sin\left(\frac{\alpha}{2}\right)|I\rangle|S_z;-\rangle +\right.\\
&\quad + \mathrm{e}^{-i\chi/2}\sqrt{b}\cos\left(\frac{\alpha}{2}\right)|I\rangle|S_z;-\rangle + \mathrm{e}^{-i\chi/2}\sqrt{b}\sin\left(\frac{\alpha}{2}\right)|I\rangle|S_z;+\rangle +\\
&\quad + \mathrm{e}^{i\chi/2}\sqrt{a}\cos\left(\frac{\alpha}{2}\right)|II\rangle|S_z;+\rangle + \mathrm{e}^{i\chi/2}\sqrt{a}\sin\left(\frac{\alpha}{2}\right)|II\rangle|S_z;-\rangle +\\
&\quad \left. + \mathrm{e}^{i\chi/2}\sqrt{a}\cos\left(\frac{\alpha}{2}\right)|II\rangle|S_z;-\rangle - \mathrm{e}^{i\chi/2}\sqrt{a}\sin\left(\frac{\alpha}{2}\right)|II\rangle|S_z;+\rangle\right]\end{aligned} \tag{3.170}$$

Now post selection onto $|P_f\rangle$ is performed:

$$\begin{aligned}|\Phi\rangle = |P_f\rangle\langle P_f|\psi'\rangle = \sqrt{\frac{1}{4\,(a+b)}}\ \Big\{\Big[&\mathrm{e}^{-i\chi/2}\sqrt{b}\cos\left(\frac{\alpha}{2}\right) + \mathrm{e}^{-i\chi/2}\sqrt{b}\sin\left(\frac{\alpha}{2}\right) + \mathrm{e}^{i\chi/2}\sqrt{a}\cos\left(\frac{\alpha}{2}\right) - \\ &- \mathrm{e}^{i\chi/2}\sqrt{a}\sin\left(\frac{\alpha}{2}\right)\Big]|S_z;+\rangle + \Big[\mathrm{e}^{-i\chi/2}\sqrt{b}\cos\left(\frac{\alpha}{2}\right) - \mathrm{e}^{-i\chi/2}\sqrt{b}\sin\left(\frac{\alpha}{2}\right) + \\ &+\mathrm{e}^{i\chi/2}\sqrt{a}\sin\left(\frac{\alpha}{2}\right) + \mathrm{e}^{i\chi/2}\sqrt{a}\cos\left(\frac{\alpha}{2}\right)\Big]|S_z;-\rangle\Big\}|P_f\rangle \\ = \sqrt{\frac{1}{4\,(a+b)}}\ \Big\{\Big[&\mathrm{e}^{-i\chi/2}\sqrt{2b}\sin\left(\frac{\pi}{4}+\frac{\alpha}{2}\right) + \mathrm{e}^{i\chi/2}\sqrt{2a}\sin\left(\frac{\pi}{4}-\frac{\alpha}{2}\right)\Big]|S_z;+\rangle + \\ &+ \Big[\mathrm{e}^{-i\chi/2}\sqrt{2b}\sin\left(\frac{\pi}{4}-\frac{\alpha}{2}\right) + \mathrm{e}^{i\chi/2}\sqrt{2a}\sin\left(\frac{\pi}{4}+\frac{\alpha}{2}\right)\Big]|S_z;-\rangle\Big\}|P_f\rangle \end{aligned} \tag{3.171}$$

Now we are able to calculate the matrix elements $\langle S_z;+|\Phi\rangle$ and $\langle S_z;-|\Phi\rangle$.

$$\langle S_z;+|\Phi\rangle = \sqrt{\frac{1}{4\,(a+b)}}\ \Big[\mathrm{e}^{-i\chi/2}\sqrt{2b}\sin\left(\frac{\pi}{4}+\frac{\alpha}{2}\right) + \mathrm{e}^{i\chi/2}\sqrt{2a}\sin\left(\frac{\pi}{4}-\frac{\alpha}{2}\right)\Big]|P_f\rangle \tag{3.172}$$

and

$$\langle S_z;-|\Phi\rangle = \sqrt{\frac{1}{4\,(a+b)}}\ \Big[\mathrm{e}^{-i\chi/2}\sqrt{2b}\sin\left(\frac{\pi}{4}-\frac{\alpha}{2}\right) + \mathrm{e}^{i\chi/2}\sqrt{2a}\sin\left(\frac{\pi}{4}+\frac{\alpha}{2}\right)\Big]|P_f\rangle \tag{3.173}$$

which leads to the intensities

$$I_+^z = |\langle S_z;+|\Phi\rangle|^2 = \frac{1}{4\,(a+b)}\Big[a+b+2\sqrt{ab}\cos(\alpha)\cos(\chi) + (b-a)\sin(\alpha)\Big] \tag{3.174}$$

and

$$I_-^z = |\langle S_z;+|\Phi\rangle|^2 = \frac{1}{4\,(a+b)}\Big[a+b+2\sqrt{ab}\cos(\alpha)\cos(\chi) + (a-b)\sin(\alpha)\Big] \tag{3.175}$$

Therefore the weak value is now given by

$$\langle\hat{\Pi}_z\rangle_w = \frac{1}{\alpha}\operatorname{arctanh}\left(\frac{(b-a)\sin(\alpha)}{a+b+2\sqrt{ab}\cos(\chi)\cos(\alpha)}\right) \tag{3.176}$$

Performing the same analysis as previously shows, that Eq. (3.176) fails to give us the imaginary part of $\langle\hat{\Pi}_z\rangle_w$, but instead it yields the real part again!
Why our educated guess is wrong, is not clear at the moment. Let us summarize what we know so far:
There are twelve different ways to conduct the experiment described above. For every initial spin state there are three different possibilities. Once $|S_i\rangle$ is prepared, it is possible to perform rotations around two different axes and finally there are two different directions of analysis. The results of the calculations performed so far are presented in Table 3.2.[h] It seems that, the measurements are fundamentally restricted by the choice of axis of rotation and direction of analysis and that it is possible to only measure the real part as well as the absolute values of

[h] All of the results presented in Table 3.2 were minutely calculated, however not all of them are presented in detail above.

Initial Spin State	Axis of Rotation	Direction of Analysis	Weak Value
$\|S_x;+\rangle$	z	x	$\mathrm{Abs}\left(\langle\hat{\Pi}_z\rangle_w\right)$
$\|S_x;+\rangle$	z	y	$\mathrm{Re}\left(\langle\hat{\Pi}_z\rangle_w\right)$
$\|S_x;+\rangle$	y	x	$\mathrm{Abs}\left(\langle\hat{\Pi}_z\rangle_w\right)$
$\|S_x;+\rangle$	y	z	$\mathrm{Re}\left(\langle\hat{\Pi}_z\rangle_w\right)$
$\|S_z;+\rangle$	x	x	$\mathrm{Abs}\left(\langle\hat{\Pi}_z\rangle_w\right)$

Table 3.2.: Summary of what the measurement will yield for certain initial spin state, axis of rotation and direction of analysis.

$\langle\hat{\Pi}\rangle_w$, but not its imaginary part. To be certain one would have to calculate all twelve possible ways to perform the experiment.
Nevertheless, since

$$\mathrm{Abs}\left(\langle\hat{\Pi}\rangle_w\right) = \left|\mathrm{Re}\left(\langle\hat{\Pi}\rangle_w\right)\right| + \left|\mathrm{Im}\left(\langle\hat{\Pi}\rangle_w\right)\right| \tag{3.177}$$

the experiment yields the imaginary part's absolute, which can be extracted by measuring $\mathrm{Abs}\left(\langle\hat{\Pi}\rangle_w\right)$ and then subtract the real part's absolute from that.

3.3. The 'Cheshire Cat' - a quantum paradox

In this section a neutron interferometer experiment is proposed, in which weak spin rotations are used to measure a so called 'Cheshire Cat'.
The 'Cheshire Cat' is an experiment conceived by Y. Aharonov et al. [26] and aims to detangle a physical property from the object it belongs to. For the case of a neutron interferometer experiment this would mean to detangle neutron's location from its spin. How this can be done, is explained here:
Fig. 3.26 shows an experimental setup, that allows to measure such a 'Cheshire Cat'. The neutron beam is prepared so that its polarization is parallel to the z-axis, i.e. the neutrons' spin is in the $|S_z;+\rangle$ state. After the $\frac{\pi}{2}$-turn the spin state is given by $|S_x;+\rangle$. As soon as the neutrons enter the interferometer their wave function has to be extended by a path dependent part $|P\rangle$ so that it is given by $|\Psi\rangle = |S\rangle|P\rangle$. To complete the pre selection of the ensemble a π-rotator is put into path II. The pre selected wave function then becomes

$$|i\rangle = |S\rangle|P_i\rangle = \sqrt{\frac{1}{2}}|S_x;+\rangle|I\rangle + \sqrt{\frac{1}{2}}|S_x;-\rangle|II\rangle \tag{3.178}$$

After the pre selection a weak measurement takes place. How this is done and how the interaction Hamiltonian for such a system looks like, is described below. Finally the ensemble is post selected onto the state

$$|f\rangle = |S_x;-\rangle|P_f\rangle = \frac{1}{2}\left(|S_z;+\rangle - |S_z;-\rangle\right)\left(|I\rangle + |II\rangle\right), \tag{3.179}$$

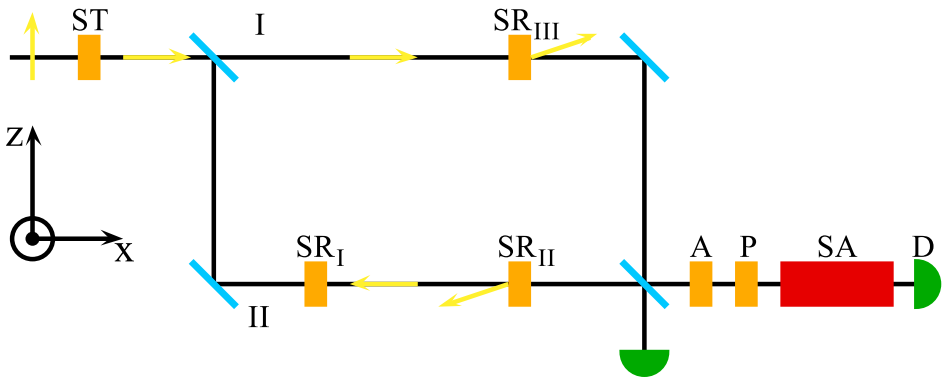

Figure 3.26.: Experimental setup for measuring a Cheshire Cat: It consists of a $\frac{\pi}{2}$-turner (ST) and a π-rotator (SR_I) to pre select the states, the neutron interferometer itself, two spin rotators to perform the weak measurement (SR_{II} & SR_{III}) and a post selector [two coils to select the azimuth and polar angle (A & P), the red spin analyzer (SA) and a detector (D)].

where $|P_f\rangle$ is given by $|P_f\rangle = \sqrt{\frac{1}{2}}\,(|I\rangle + |II\rangle)$. To understand the nature of the 'Cheshire Cat' paradox we have to look at weak values of the products of the operators $\hat{\Pi}_I$, $\hat{\Pi}_{II}$, $\hat{\sigma}^s_+$ and $\hat{\sigma}^s_-$. Those operators are the projectors onto the path I and II and the $|S_z;+\rangle$ and $|S_z;-\rangle$ spin states respectively. They are given by

$$\langle\hat{\Pi}_I\hat{\sigma}^s_+\rangle_w = \frac{\langle f|\hat{\Pi}_I\hat{\sigma}^s_+|i\rangle}{\langle f|i\rangle} = \frac{(\langle S_x;-|\langle P_f|)\,(|I\rangle\langle I|)\,(|S_z;+\rangle\langle S_z;+|)\,(|S_x;+\rangle|I\rangle + |S_x;-\rangle|II\rangle)}{(\langle S_x;-|\langle P_f|)\,(|S_x;+\rangle|I\rangle + |S_x;-\rangle|II\rangle)} = \frac{1}{2}$$

$$\langle\hat{\Pi}_I\hat{\sigma}^s_-\rangle_w = \frac{\langle f|\hat{\Pi}_I\hat{\sigma}^s_-|i\rangle}{\langle f|i\rangle} = \frac{(\langle S_x;-|\langle P_f|)\,(|I\rangle\langle I|)\,(|S_z;-\rangle\langle S_z;-|)\,(|S_x;+\rangle|I\rangle + |S_x;-\rangle|II\rangle)}{(\langle S_x;-|\langle P_f|)\,(|S_x;+\rangle|I\rangle + |S_x;-\rangle|II\rangle)} = -\frac{1}{2}$$

$$\langle\hat{\Pi}_{II}\hat{\sigma}^s_+\rangle_w = \frac{\langle f|\hat{\Pi}_{II}\hat{\sigma}^s_+|i\rangle}{\langle f|i\rangle} = \frac{(\langle S_x;-|\langle P_f|)\,(|II\rangle\langle II|)\,(|S_z;+\rangle\langle S_z;+|)\,(|S_x;+\rangle|I\rangle + |S_x;-\rangle|II\rangle)}{(\langle S_x;-|\langle P_f|)\,(|S_x;+\rangle|I\rangle + |S_x;-\rangle|II\rangle)} = \frac{1}{2}$$

$$\langle\hat{\Pi}_{II}\hat{\sigma}^s_-\rangle_w = \frac{\langle f|\hat{\Pi}_{II}\hat{\sigma}^s_-|i\rangle}{\langle f|i\rangle} = \frac{(\langle S_x;-|\langle P_f|)\,(|II\rangle\langle II|)\,(|S_z;-\rangle\langle S_z;-|)\,(|S_x;+\rangle|I\rangle + |S_x;-\rangle|II\rangle)}{(\langle S_x;-|\langle P_f|)\,(|S_x;+\rangle|I\rangle + |S_x;-\rangle|II\rangle)} = \frac{1}{2}$$

What do those operators mean? They represent occupations of a certain path and a certain spin state, e.g. $\langle\hat{\Pi}_I\hat{\sigma}^s_+\rangle_w$ represents the occupation of path one by the spin state $|S_z;+\rangle$.
The weak values of the operators above show a very interesting picture. The neutron has to be in path II, since $\langle\hat{\Pi}_{II}\rangle_w$ is the sum of $\langle\hat{\Pi}_{II}\hat{\sigma}^s_+\rangle_w$ and $\langle\hat{\Pi}_{II}\hat{\sigma}^s_-\rangle_w$ and both equal $\frac{1}{2}$. At the same time the sum of $\langle\hat{\Pi}_I\hat{\sigma}^s_+\rangle_w$ and $\langle\hat{\Pi}_I\hat{\sigma}^s_-\rangle_w$ vanishes, which means, that the neutron is not in path I. Now $\langle\hat{\Pi}_{II}\hat{\sigma}^s_+\rangle_w$ represents a $|S_z;+\rangle$ state in path II, while $\langle\hat{\Pi}_{II}\hat{\sigma}^s_-\rangle_w$ represents a $|S_z;-\rangle$ state in the same path. Therefore there is no net weak spin in path II. $\langle\hat{\Pi}_I\hat{\sigma}^s_+\rangle_w$ and $\langle\hat{\Pi}_I\hat{\sigma}^s_-\rangle_w$ both represent the $|S_z;+\rangle$ state in path I. Therefore the net weak spin is in path I while the neutron's weak location is in path II! For this pre and post selected system the neutron's spin and location are detangled and any interaction in the weak regime will show, that the particle and its property are at two different locations [27].
To demonstrate this apparent paradox it would be necessary to measure the weak values of $\hat{\sigma}^s_z\hat{\Pi}_I$ and $\hat{\sigma}^s_z\hat{\Pi}_{II}$. While the first one equals 1 the latter one vanishes.
In principle the weak measurement can be performed using weak spin rotations. To measure

$\langle\hat{\sigma}_z^s\hat{\Pi}_I\rangle_w$, a weak and positive spin rotation is performed only along path I. The interaction Hamiltonian for this measurement is

$$\hat{H}_1 = -\vec{\mu}\vec{B}\hat{\Pi}_I = -\gamma\hat{S}\vec{B}\hat{\Pi}_I \equiv -\frac{\alpha\hat{\sigma}_z^s\hat{\Pi}_I}{2} \tag{3.180}$$

By making the angle of rotation α small the condition for a weak measurement is fulfilled. The evolution of the initial state caused by the weak measurement is given by

$$|i'\rangle = \mathrm{e}^{i\alpha\hat{\sigma}_z^s\hat{\Pi}_I/2}|i\rangle \approx \left(1 + \frac{i\alpha}{2}\hat{\sigma}_z^s\hat{\Pi}_I - \frac{\alpha^2}{8}\left[\hat{\sigma}_z^s\hat{\Pi}_I\right]^2\right)|i\rangle = |i\rangle + \frac{i\alpha}{2}\hat{\sigma}_z^s\hat{\Pi}_I|i\rangle - \frac{\alpha^2}{8}\hat{\Pi}_I|i\rangle \tag{3.181}$$

It is interesting to note that the formula $\exp(i\hat{\sigma}\cdot\hat{n}\alpha) = \mathbb{1}\cos(\alpha) + i\hat{\sigma}\cdot\hat{n}\sin(\alpha)$ is not valid for this calculation, since $\left(\hat{\Pi}_I\right)^2 \neq \mathbb{1}$. Because $\hat{\Pi}_I$ is a projector, one gets $\left(\hat{\Pi}_I\right)^2 = \hat{\Pi}_I$.
Now the system is post selected onto the state $\langle f|$

$$\langle f|i'\rangle = \langle f|i\rangle + \frac{i\alpha}{2}\langle f|\hat{\sigma}_z^s\hat{\Pi}_I|i\rangle - \frac{\alpha^2}{8}\langle f|\hat{\Pi}_I|i\rangle \tag{3.182}$$

which leads to the intensity at the O-detector[i]

$$\begin{aligned}
I_1^{\mathrm{on}} = |\langle f|i'\rangle|^2 &= \left(\langle f|i\rangle + \frac{i\alpha}{2}\langle f|\hat{\sigma}_z^s\hat{\Pi}_I|i\rangle - \frac{\alpha^2}{8}\langle f|\hat{\Pi}_I|i\rangle\right)\left(\langle i|f\rangle - \frac{i\alpha}{2}\langle i|\hat{\sigma}_z^s\hat{\Pi}_I|f\rangle - \frac{\alpha^2}{8}\langle i|\hat{\Pi}_I|f\rangle\right) \\
&= |\langle f|i\rangle|^2 + \frac{i\alpha}{2}\langle i|f\rangle\langle f|\hat{\sigma}_z^s\hat{\Pi}_I|i\rangle - \frac{\alpha^2}{8}\langle f|\hat{\Pi}_I|i\rangle\langle i|f\rangle - \frac{i\alpha}{2}\langle f|i\rangle\langle i|\hat{\sigma}_z^s\hat{\Pi}_I|f\rangle + \frac{\alpha^2}{4}|\langle f|\hat{\sigma}_z^s\hat{\Pi}_I|i\rangle|^2 + \\
&\quad + \frac{\alpha^2}{8}\frac{i\alpha}{2}\langle f|\hat{\Pi}_I|i\rangle\langle i|\hat{\sigma}_z^s\hat{\Pi}_I|i\rangle - \frac{\alpha^2}{8}\langle f|i\rangle\langle i|\hat{\Pi}_I|f\rangle - \frac{\alpha^2}{8}\frac{i\alpha}{2}\langle f|\hat{\Pi}_I|i\rangle\langle i|\hat{\sigma}_z^s\hat{\Pi}_I|i\rangle + \frac{\alpha^4}{64}|\langle f|\hat{\Pi}_I|i\rangle|^2 \\
&= |\langle f|i\rangle|^2 - \frac{\alpha^2}{4}\langle f|\hat{\Pi}_I|i\rangle\langle i|f\rangle + \frac{\alpha^2}{4}|\langle f|\hat{\sigma}_z^s\hat{\Pi}_I|i\rangle|^2 + \mathcal{O}\left(\alpha^3\right)
\end{aligned} \tag{3.183}$$

Eq. (3.183) can be further simplified, if its second term is evaluated using the definitions of $|i\rangle$ and $|f\rangle$

$$\frac{\alpha^2}{4}\langle f|\hat{\Pi}_I|i\rangle\langle i|f\rangle = \frac{1}{2}\langle f|\hat{\Pi}_I|i\rangle\frac{\alpha^2}{4} = 0 \tag{3.184}$$

Experimentally it can be verified easily that the matrix element $\langle f|\hat{\Pi}_I|i\rangle$ is zero. An absorber has to be inserted into the interferometer, to check if the detected intensity changes or not.
So the intensity at the O-detector is really given by

$$I_1^{\mathrm{on}} = |\langle f|i\rangle|^2 + \frac{\alpha^2}{4}|\langle f|\hat{\sigma}_z^s\hat{\Pi}_I|i\rangle|^2 \tag{3.185}$$

If the weak spin rotation is turned off, the intensity at the O-detector becomes

$$I_1^{\mathrm{off}} = |\langle f|i\rangle|^2 \tag{3.186}$$

[i] The following equation is valid, since all matrix elements are real and terms of the order $\mathcal{O}\left(\alpha^3\right)$ can be neglected, because $\alpha \ll 1$.

By making a consecutive on and off measurement it is possible to extract the absolute square of $\langle\hat{\sigma}_z^s\hat{\Pi}_I\rangle_w$ which is then given by

$$\left|\langle\hat{\sigma}_z^s\hat{\Pi}_I\rangle_w\right|^2 \equiv \frac{\left|\langle f|\hat{\sigma}_z^s\hat{\Pi}_I|i\rangle\right|^2}{|\langle f|i\rangle|^2} = \frac{4}{\alpha^2}\left(\frac{I_1^{\text{on}}}{I_1^{\text{off}}} - 1\right) \tag{3.187}$$

To measure $\langle\hat{\sigma}_z^s\hat{\Pi}_{II}\rangle_w$ a weak rotation only along path II is performed. The interaction Hamiltonian for this procedure is

$$\hat{H}_2 = -\vec{\mu}\vec{B}\hat{\Pi}_{II} = -\gamma\hat{S}\vec{B}\hat{\Pi}_{II} \equiv -\frac{\alpha\hat{\sigma}_z^s\hat{\Pi}_{II}}{2} \tag{3.188}$$

The same calculation as previously leads to the intensities for on and off-measurement

$$I_2^{\text{on}} = |\langle f|i\rangle|^2 - \frac{\alpha^2}{4}\langle f|\hat{\Pi}_{II}|i\rangle\langle i|f\rangle + \frac{\alpha^2}{4}|\langle f|\hat{\sigma}_z^s\hat{\Pi}_{II}|i\rangle|^2 + \mathcal{O}\left(\alpha^3\right) \tag{3.189}$$

and

$$I_2^{\text{off}} = |\langle f|i\rangle|^2. \tag{3.190}$$

Just as previously, Eq. (3.189) can be simplified by evaluating its second term

$$\frac{\alpha^2}{4}\langle f|\hat{\Pi}_{II}|i\rangle\langle i|f\rangle = \frac{\alpha^2}{4}\langle f|\hat{\Pi}_{II}|i\rangle\frac{1}{2} = \frac{\alpha^2}{16}, \tag{3.191}$$

which leads to the intensity.

$$I_1^{\text{on}} = |\langle f|i\rangle|^2 - \frac{\alpha^2}{16} + \frac{\alpha^2}{4}|\langle f|\hat{\sigma}_z^s\hat{\Pi}_I|i\rangle|^2 \tag{3.192}$$

The weak value of $\hat{\sigma}_z^s\hat{\Pi}_{II}$ becomes

$$\left|\langle\hat{\sigma}_z^s\hat{\Pi}_{II}\rangle_w\right|^2 \equiv \frac{\left|\langle f|\hat{\sigma}_z^s\hat{\Pi}_{II}|i\rangle\right|^2}{|\langle f|i\rangle|^2} = \frac{4}{\alpha^2}\left(\frac{I_2^{\text{on}}}{I_2^{\text{off}}} - 1 + \frac{\alpha^2}{4}\right) \tag{3.193}$$

Thus it should be possible to extract absolute values of $\langle\hat{\sigma}_z^s\hat{\Pi}_I\rangle_w$ and $\langle\hat{\sigma}_z^s\hat{\Pi}_{II}\rangle_w$ by making four consecutive measurements using weak spin rotations in each arm of the interferometer. In addition to that absorber measurements in path I and II have to be performed, in order to check the contributions of $\langle f|\hat{\Pi}_I|i\rangle$ and $\langle f|\hat{\Pi}_{II}|i\rangle$.
For the 'Cheshire Car' paradox it does not matter that only the absolute of the weak value is measured, since one has at most to distinguish where the cat, i.e. the physical object, and where the grin, i.e. its property, are.
One might also object that the measurements are performed one after another and that not all the relevant information is extracted at once. However, the very nature of weak measurement guarantees that the system is not altered and it does not matter if the information is extracted piece by piece in several measurements or all at once. The system stays the same and its properties do not change.
As with previous experiments it is possible to analytically calculate the intensities that are expected for small rotations of the spin. Instead of expanding the system's evolution operator

we let it act on $|i\rangle$ and get

$$\begin{aligned}|i'\rangle_I &= \mathrm{e}^{i\alpha\hat{\sigma}_z^s\hat{\Pi}_I/2}|i\rangle = \frac{1}{2}\mathrm{e}^{i\alpha\hat{\sigma}_z^s\hat{\Pi}_I/2}\left[|I\rangle\left(|S_z;+\rangle+|S_z;-\rangle\right)+|II\rangle\left(|S_z;+\rangle-|S_z;-\rangle\right)\right]\\ &= \frac{1}{2}\left[\mathrm{e}^{i\alpha\hat{\sigma}_z^s/2}|I\rangle\left(|S_z;+\rangle+|S_z;-\rangle\right)+|II\rangle\left(|S_z;+\rangle-|S_z;-\rangle\right)\right]\\ &= \frac{1}{2}\left[|I\rangle\left(\mathrm{e}^{i\alpha/2}|S_z;+\rangle+\mathrm{e}^{-i\alpha/2}|S_z;-\rangle\right)+|II\rangle\left(|S_z;+\rangle-|S_z;-\rangle\right)\right]\end{aligned} \tag{3.194}$$

when the weak rotation is performed along path I and

$$\begin{aligned}|i'\rangle_{II} &= \mathrm{e}^{i\alpha\hat{\sigma}_z^s\hat{\Pi}_{II}/2}|i\rangle = \frac{1}{2}\mathrm{e}^{i\alpha\hat{\sigma}_z^s\hat{\Pi}_{II}/2}\left[|I\rangle\left(|S_z;+\rangle+|S_z;-\rangle\right)+|II\rangle\left(|S_z;+\rangle-|S_z;-\rangle\right)\right]\\ &= \frac{1}{2}\left[|I\rangle\left(|S_z;+\rangle+|S_z;-\rangle\right)+\mathrm{e}^{i\alpha\hat{\sigma}_z^s/2}|II\rangle\left(|S_z;+\rangle-|S_z;-\rangle\right)\right]\\ &= \frac{1}{2}\left[|I\rangle\left(|S_z;+\rangle+|S_z;-\rangle\right)+|II\rangle\left(\mathrm{e}^{i\alpha/2}|S_z;+\rangle-\mathrm{e}^{-i\alpha/2}|S_z;-\rangle\right)\right]\end{aligned} \tag{3.195}$$

when it is performed along path II. To get the intensities, we first have to calculate the matrix elements $\langle f|i'\rangle_I$, $\langle f|i'\rangle_{II}$ and $\langle f|i\rangle$.

$$\begin{aligned}\langle f|i'\rangle_I &= \frac{1}{2}\left(\langle S_z;+|\langle I|-\langle S_z;-|\langle I|+\langle S_z;+|\langle II|-\langle S_z;-|\langle II|\right)\times\\ &\quad\times\frac{1}{2}\left(\mathrm{e}^{i\alpha/2}|S_z;+\rangle|I\rangle+\mathrm{e}^{-i\alpha/2}|S_z;-\rangle|I\rangle+|S_z;+\rangle|II\rangle-|S_z;-\rangle|II\rangle\right)\\ &= \frac{1}{4}\left(\mathrm{e}^{i\alpha/2}-\mathrm{e}^{-i\alpha/2}+1+1\right)=\frac{1}{4}\left(2i\sin\left(\frac{\alpha}{2}\right)+2\right)=\frac{1}{2}\left[i\sin\left(\frac{\alpha}{2}\right)+1\right]\end{aligned} \tag{3.196}$$

$$\begin{aligned}\langle f|i'\rangle_{II} &= \frac{1}{2}\left(\langle S_z;+|\langle I|-\langle S_z;-|\langle I|+\langle S_z;+|\langle II|-\langle S_z;-|\langle II|\right)\times\\ &\quad\times\frac{1}{2}\left(|S_z;+\rangle|I\rangle+|S_z;-\rangle|I\rangle+\mathrm{e}^{i\alpha/2}|S_z;+\rangle|II\rangle-\mathrm{e}^{-i\alpha/2}|S_z;-\rangle|II\rangle\right)\\ &= \frac{1}{4}\left(\mathrm{e}^{i\alpha/2}+\mathrm{e}^{-i\alpha/2}+1-1\right)=\frac{1}{4}\left(\mathrm{e}^{i\alpha/2}+\mathrm{e}^{-i\alpha/2}\right)=\frac{1}{2}\cos\left(\frac{\alpha}{2}\right)\end{aligned} \tag{3.197}$$

$$\begin{aligned}\langle f|i\rangle &= \frac{1}{2}\left(\langle S_z;+|\langle I|-\langle S_z;-|\langle I|+\langle S_z;+|\langle II|-\langle S_z;-|\langle II|\right)\times\\ &\quad\times\frac{1}{2}\left(|S_z;+\rangle|I\rangle+|S_z;-\rangle|I\rangle+|S_z;+\rangle|II\rangle-|S_z;-\rangle|II\rangle\right)\\ &= \frac{1}{4}\left(1-1+1+1\right)=\frac{1}{2}\end{aligned} \tag{3.198}$$

From Eqs. (3.196), (3.197) and (3.198) we get the intensities

$$I_1^{\mathrm{on}} = |\langle f|i'\rangle_I|^2 = \frac{1}{4}\left[1+i\sin\left(\frac{\alpha}{2}\right)\right]\left[1-i\sin\left(\frac{\alpha}{2}\right)\right]=\frac{1}{4}\left[1+\sin^2\left(\frac{\alpha}{2}\right)\right] \tag{3.199}$$

$$I_2^{\mathrm{on}} = |\langle f|i'\rangle_{II}|^2 = \frac{1}{4}\cos^2\left(\frac{\alpha}{2}\right) \tag{3.200}$$

$$I_1^{\mathrm{off}} = I_2^{\mathrm{off}} = \frac{1}{4} \tag{3.201}$$

Equations (3.187) and (3.193) now become

$$\left|\langle\hat{\sigma}_z^s\hat{\Pi}_I\rangle_w\right|^2 = \frac{4}{\alpha^2}\left(\frac{I_1^{\text{on}}}{I_1^{\text{off}}}-1\right) = \frac{4}{\alpha^2}\left(\frac{\frac{1}{4}\left[1+\sin^2\left(\frac{\alpha}{2}\right)\right]}{\frac{1}{4}}-1\right) \approx \frac{4}{\alpha^2}\left(1+\frac{\alpha^2}{4}-1\right) = 1 \quad (3.202)$$

and

$$\left|\langle\hat{\sigma}_z^s\hat{\Pi}_{II}\rangle_w\right|^2 = \frac{4}{\alpha^2}\left(\frac{I_2^{\text{on}}}{I_2^{\text{off}}}-1+\frac{\alpha^2}{4}\right) = \frac{4}{\alpha^2}\left(\frac{\frac{1}{4}\cos^2\left(\frac{\alpha}{2}\right)}{\frac{1}{4}}-1+\frac{\alpha^2}{4}\right) \approx \frac{4}{\alpha^2}\left(1-\frac{\alpha^2}{4}-1+\frac{\alpha^2}{4}\right) = 0 \quad (3.203)$$

which is exactly what we would expect from the theory of weak measurements. Note that the approximations made in Eqs. (3.202) and (3.203) are only valid for small values of α! If (3.202) and (3.203) are not approximated and put into a computational program like Mathematica it is possible to obtain actual values. For $\alpha = \frac{\pi}{36}$ the results are $\left|\langle\hat{\sigma}_z^s\hat{\Pi}_I\rangle_w\right| = 0.999683$ and $\left|\langle\hat{\sigma}_z^s\hat{\Pi}_{II}\rangle_w\right|^2 = 0.0251885$.
All calculations presented so far are for a perfect circumstances. For a more realistic description of an experiment the parameter p, which describes the degree of polarization, has to be introduced. For a neutron beam, which is not completely polarized, the pre selected state is

$$\begin{aligned}|i\rangle &= \sqrt{\frac{n}{2}}\left[(1-p)\,|S_x;+\rangle + p|S_x;-\rangle\right]|I\rangle + \sqrt{\frac{n}{2}}\left[p|S_x;+\rangle + (1-p)\,|S_x;-\rangle\right]|II\rangle \\ &= \frac{\sqrt{n}}{2}\left[|S_z;+\rangle + (1-2p)\,|S_z;-\rangle\right]|I\rangle + \frac{\sqrt{n}}{2}\left[|S_z;+\rangle - (1-2p)\,|S_z;-\rangle\right]|II\rangle \end{aligned} \quad (3.204)$$

with $0 \le p \le 1$ and $n = \frac{1}{1-2p+2p^2}$. The post selected state $|f\rangle$ does not change. The products of the operators $\hat{\Pi}_I$, $\hat{\Pi}_{II}$, $\hat{\sigma}_+^s$ and $\hat{\sigma}_-^s$ then become

$$\begin{aligned}\langle\hat{\Pi}_I\hat{\sigma}_+^s\rangle_w &= \frac{\langle f|\hat{\Pi}_I\hat{\sigma}_+^s|i\rangle}{\langle f|i\rangle} = \frac{1}{2} \\ \langle\hat{\Pi}_I\hat{\sigma}_-^s\rangle_w &= \frac{\langle f|\hat{\Pi}_I\hat{\sigma}_-^s|i\rangle}{\langle f|i\rangle} = -\frac{(1-2p)}{2} \\ \langle\hat{\Pi}_{II}\hat{\sigma}_+^s\rangle_w &= \frac{\langle f|\hat{\Pi}_{II}\hat{\sigma}_+^s|i\rangle}{\langle f|i\rangle} = \frac{1}{2} \\ \langle\hat{\Pi}_{II}\hat{\sigma}_-^s\rangle_w &= \frac{\langle f|\hat{\Pi}_{II}\hat{\sigma}_-^s|i\rangle}{\langle f|i\rangle} = \frac{(1-2p)}{2}\end{aligned}$$

Of course $\langle\hat{\Pi}_I\hat{\sigma}_z^s\rangle_w$ and $\langle\hat{\Pi}_{II}\hat{\sigma}_z^s\rangle_w$ change accordingly

$$\langle\hat{\Pi}_I\hat{\sigma}_z^s\rangle_w = 1-p \quad (3.205)$$

$$\langle\hat{\Pi}_{II}\hat{\sigma}_z^s\rangle_w = p \quad (3.206)$$

This shows that an imperfect degree of polarization prevents a complete detanglement of the particle and its spin. Nevertheless a paradoxical situation remains. While most of the neutrons pass through path II most of their spin passes through path I.

The matrix elements in Eqs. (3.184) and (3.191) change into

$$\frac{\alpha^2}{4}\langle f|\hat{\Pi}_I|i\rangle\langle i|f\rangle = \frac{1}{2}\langle f|\hat{\Pi}_I|i\rangle\frac{\alpha^2}{4} = \frac{\alpha^2 p}{16\left(1-2p+2p^2\right)} \tag{3.207}$$

and

$$\frac{\alpha^2}{4}\langle f|\hat{\Pi}_{II}|i\rangle\langle i|f\rangle = \frac{\alpha^2}{4}\langle f|\hat{\Pi}_{II}|i\rangle\frac{1}{2} = \frac{\alpha^2\left(1-p\right)}{16\left(1-2p+2p^2\right)} \tag{3.208}$$

Therefore the weak values of $\hat{\sigma}_z^s\hat{\Pi}_I$ and $\hat{\sigma}_z^s\hat{\Pi}_{II}$ are now given by

$$\left|\langle\hat{\sigma}_z^s\hat{\Pi}_I\rangle_w\right|^2 \equiv \frac{\left|\langle f|\hat{\sigma}_z^s\hat{\Pi}_I|i\rangle\right|^2}{\left|\langle f|i\rangle\right|^2} = \frac{4}{\alpha^2}\left(\frac{I_1^{\text{on}}}{I_1^{\text{off}}} - 1 + \frac{\alpha^2 p}{4}\right) \tag{3.209}$$

and

$$\left|\langle\hat{\sigma}_z^s\hat{\Pi}_{II}\rangle_w\right|^2 \equiv \frac{\left|\langle f|\hat{\sigma}_z^s\hat{\Pi}_{II}|i\rangle\right|^2}{\left|\langle f|i\rangle\right|^2} = \frac{4}{\alpha^2}\left(\frac{I_2^{\text{on}}}{I_2^{\text{off}}} - 1 + \frac{\alpha^2\left(1-p\right)}{4}\right). \tag{3.210}$$

For an imperfect degree of polarization we expect the intensities to change as well. Since Eqs. (3.194) and (3.195) change into

$$|i'\rangle_I = \frac{\sqrt{n}}{2}\left\{|I\rangle\left[\mathrm{e}^{i\alpha/2}|S_z;+\rangle + \mathrm{e}^{-i\alpha/2}\left(1-2p\right)|S_z;-\rangle\right] + |II\rangle\left[|S_z;+\rangle - \left(1-2p\right)|S_z;-\rangle\right]\right\} \tag{3.211}$$

and

$$|i'\rangle_{II} = \frac{\sqrt{n}}{2}\left\{|I\rangle\left[|S_z;+\rangle + \left(1-2p\right)|S_z;-\rangle\right] + |II\rangle\left[\mathrm{e}^{i\alpha/2}|S_z;+\rangle - \left(1-2p\right)\mathrm{e}^{-i\alpha/2}|S_z;-\rangle\right]\right\}, \tag{3.212}$$

the matrix elements $\langle f|i'\rangle_I$ and $\langle f|i'\rangle_{II}$ become

$$\langle f|i'\rangle_I = \frac{\sqrt{n}}{2}\left[i\sin\left(\frac{\alpha}{2}\right) + 1 + p\ \mathrm{e}^{-i\alpha/2} - p\right] \tag{3.213}$$

$$\langle f|i'\rangle_{II} = \frac{\sqrt{n}}{2}\left[\cos\left(\frac{\alpha}{2}\right) - p\ \mathrm{e}^{-i\alpha/2} + p\right]. \tag{3.214}$$

This leads to the intensities

$$I_1^{\text{on}} = |\langle f|i'\rangle_I|^2 = \frac{\sin^2\left(\frac{\alpha}{2}\right)\left(1-2p\right) + 2p^2\left[1-\cos\left(\frac{\alpha}{2}\right)\right] + 1 - 2p + 2p\cos\left(\frac{\alpha}{2}\right)}{4\left(1-2p+p^2\right)} \tag{3.215}$$

$$I_2^{\text{on}} = |\langle f|i'\rangle_{II}|^2 = \frac{\cos^2\left(\frac{\alpha}{2}\right)\left(1-2p\right) + 2p^2\left[1-\cos\left(\frac{\alpha}{2}\right)\right] + 2p\cos\left(\frac{\alpha}{2}\right)}{4\left(1-2p+p^2\right)} \tag{3.216}$$

$$I_1^{\text{off}} = I_2^{\text{off}} = \frac{1}{4\left(1-2p+p^2\right)} \tag{3.217}$$

which finally yield the weak values

$$\left|\langle\hat{\sigma}_z^s\hat{\Pi}_I\rangle_w\right|^2 = \frac{4}{\alpha^2}\left\{\sin^2\left(\frac{\alpha}{2}\right)(1-2p) + 2p^2\left[1-\cos\left(\frac{\alpha}{2}\right)\right] - 2p + 2p\cos\left(\frac{\alpha}{2}\right) + \frac{\alpha^2 p}{4}\right\} \tag{3.218}$$

$$\left|\langle\hat{\sigma}_z^s\hat{\Pi}_{II}\rangle_w\right|^2 = \frac{4}{\alpha^2}\left\{\cos^2\left(\frac{\alpha}{2}\right)(1-2p) + 2p^2\left[1-\cos\left(\frac{\alpha}{2}\right)\right] + 2p\cos\left(\frac{\alpha}{2}\right) - 1 + \frac{\alpha^2(1-p)}{4}\right\} \tag{3.219}$$

If the values $p = 0.02$ and $\alpha = \frac{\pi}{36}$ are inserted into Eq. (3.218) and (3.219) they yield $\left|\langle\hat{\sigma}_z^s\hat{\Pi}_I\rangle_w\right|^2 = 0.9598$ and $\left|\langle\hat{\sigma}_z^s\hat{\Pi}_{II}\rangle_w\right|^2 = 0.0010$, where a theoretical value of 0.9604 for the first and 0.0002 for the second one would be expected. The smaller the angle of rotation, the better the results become. If the spin is rotate by only one degree, i.e. $\alpha = \frac{\pi}{180}$ the results improve to $\left|\langle\hat{\sigma}_z^s\hat{\Pi}_I\rangle_w\right|^2 = 0.9634$ and $\left|\langle\hat{\sigma}_z^s\hat{\Pi}_{II}\rangle_w\right| = 0.0004$.
In an actual experiment it would be difficult to control the spin rotation to such a small degree. Rotation angles between $\alpha = 10°$ and $\alpha = 20°$ are more feasible. If p stays at $p = 0.02$ one would get $\left|\langle\hat{\sigma}_z^s\hat{\Pi}_I\rangle_w\right|^2 = 0.9580$ and $\left|\langle\hat{\sigma}_z^s\hat{\Pi}_{II}\rangle_w\right|^2 = 0.0028$, when the angle of rotation is given by $\alpha = 10°$ and $\left|\langle\hat{\sigma}_z^s\hat{\Pi}_I\rangle_w\right|^2 = 0.9507$ and $\left|\langle\hat{\sigma}_z^s\hat{\Pi}_{II}\rangle_w\right|^2 = 0.0102$, when the angle of rotation is given by $\alpha = 20°$.
To summarize: A quantum paradox called the 'Cheshire Cat' is considered here. The aim of the paradox is to detangle a physical property from the object it belongs to. It turned out that an experimental demonstration of this paradox is feasible: In a neutron interferometer experiment it is in theory possible to measure a 'Cheshire Cat', using small path dependent spin rotations and absorbers. Theory predicts that it is possible to demonstrate, that the particle took one path of the interferometer, while its spin went trough the other.
In an actual experiment great care has to be put into the preparation of the ensemble. As the calculations above showed, it is necessary to have a high degree of polarization to arrive at a paradoxical situation. In addition to that it is important that the spin rotation can be controlled with high precision.
Nevertheless, those difficulties are not adamant and can be overcome, if enough care is taken in the experiment.

4. Spin weak values in a neutron polarimeter

In chapter 3 several new experiments involving weak values are described. The theory of weak measurements has been used to design experiments, which allow to extract the weak value. It is of interest to perform those experiments to extract actual weak values.
The simplest of all proposed experiments in chapter 3, is the polarimeter experiment, because a higher stability compared to an interferometer experiment is expected. In addition to that a polarimeter setup is available at the Institute of Atomic and Subatomic Physics of the Vienna University of Technology (ATI), while a setup for polarized neutron interferometry is only available at the ILL in Grenoble.
Therefore a polarimeter experiment was carried out at the TRIGA Mark II at ATI. A very good agreement between theory and experiment has been found.

4.1. The experimental setup

The experimental setup consists of a polarizing supermirror, two DC-coils, a magnetic guide field, a second supermirror, which serves as analyzer and a detector. A schematic drawing of the setup is displayed in Fig. 4.1.

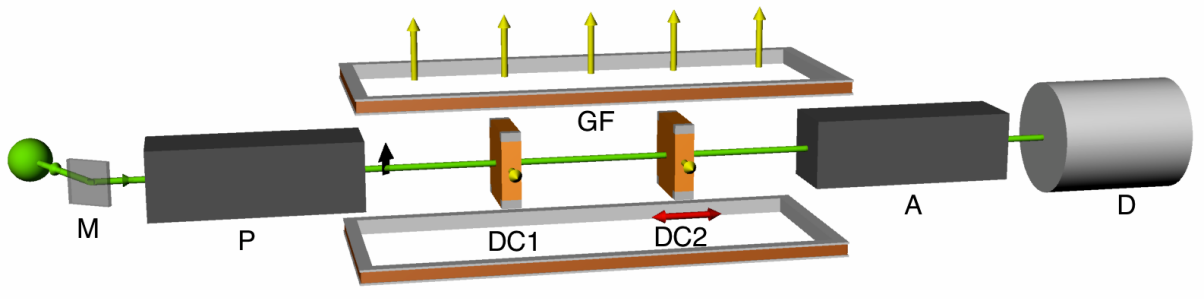

Figure 4.1.: Schematic drawing of a polarimeter beamline: A complete polarimeter beamline consist of a monochromizing crystal (M), a polarizer to prepare the neutron beam (P), at least two DC-coils (DC1 & DC2), a guide field (GF), an analyzer (A) and a detector (D).

A TRIGA Mark II research reactor is used as a neutron source. From the broad neutron energy spectrum a monochromator crystal selects neutrons with a wave length of $\lambda = 1.74$ Å. A Helium-3 counter tube served as a detector.

4.1.1. DC1 adjustment

To yield good results, it is important that the pre and post selection of the spin state is performed well. Great care was take when the DC-coils were adjusted. This happens in three steps:

(i) In order for the DC-coils to operate correctly one has to assure that the magnetic field that points in the x-direction, $\vec{B}_x$, is exactly perpendicular to the one pointing in z-direction, $\vec{B}_z$. To do this, it is possible to tilt the coil in the xz-plane. After adjusting the tilt, a varying current is applied to the coils in order to produce $\vec{B}_x$. For every current value, a measurement of the neutron count is performed. By plotting count rate versus applied current, one sees that the results can be fitted with a sine function. However, when $\vec{B}_x$ and $\vec{B}_z$ are not perpendicular to each other, the fit function will appear to be asymmetric: One minimum will be deeper than the other and maximum will not be situated in the middle. Therefore the tilt of the coil has to be readjusted and the whole measurement has to be repeated, till a minimum asymmetry is found in the fit.

(ii) Once the optimum tilt of the coil is found, one has to tune the strength of the compensation field. A current is applied to the coil producing $\vec{B}_c$, while the current producing $\vec{B}_x$ is turned on as well. Again, for every current value, the count rate is measured. It has a minimum at the current value where the external guide field is compensated. A polynomial fit through the data points is performed. By finding its minimum one can find the right current value to compensate the external field.

(iii) Since $\vec{B}_c$ changes the z-component of the total magnetic field, one hast to readjust the tilt of the DC-coil, once the compensating field is turned on. Basically, one has to redo the first step until a minimum in phase shift and asymmetry is found.

Figure 4.2 shows the final result of this adjusment.

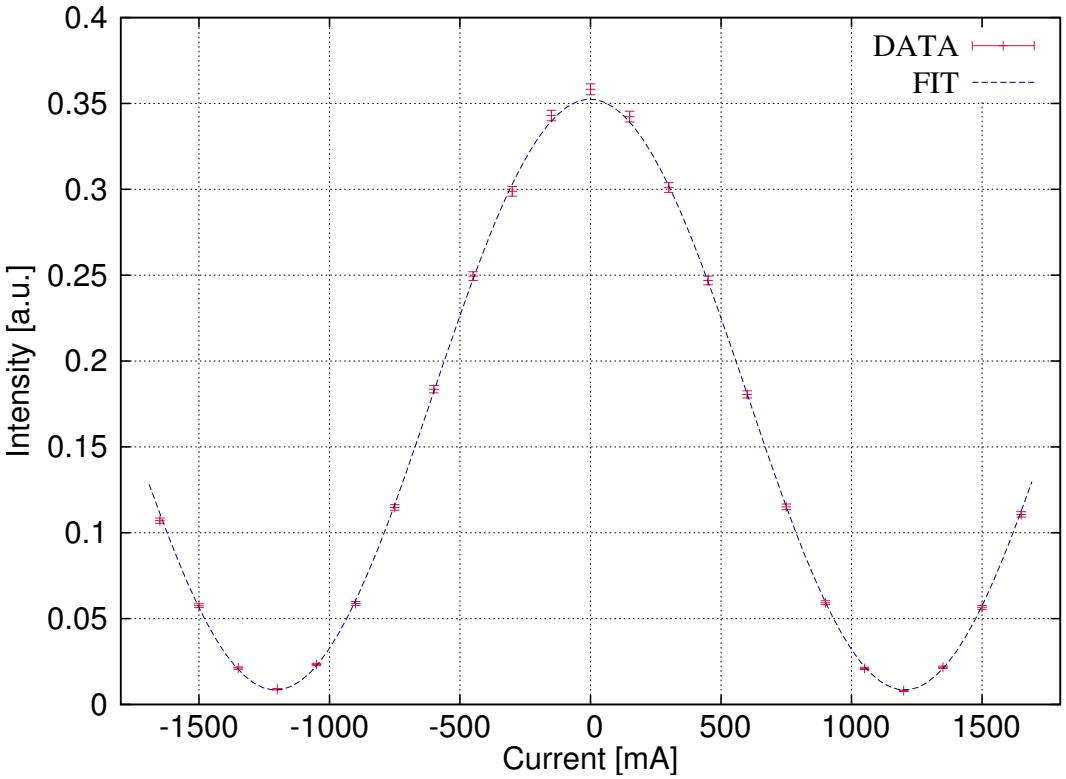

Figure 4.2.: Currentscan of the DC1-coil: To adjust the first DC-coil the current, that produces the magnetic field to flip the neutron spin, is scanned. For this scan the second coil is turned off.

Finally, we obtained the following parameters for the first coil (DC1):

- Flipping ratio: 41.9 ± 3.8
- Phase shift: $90.24° \pm 0.15°$
- Contrast: 0.95 ± 0.004

4.1.2. DC2 adjustment

For the second coil the same procedure as described above was done as well. Again the final result is presented here, which is shown in Fig. 4.3. The second coil showed the following

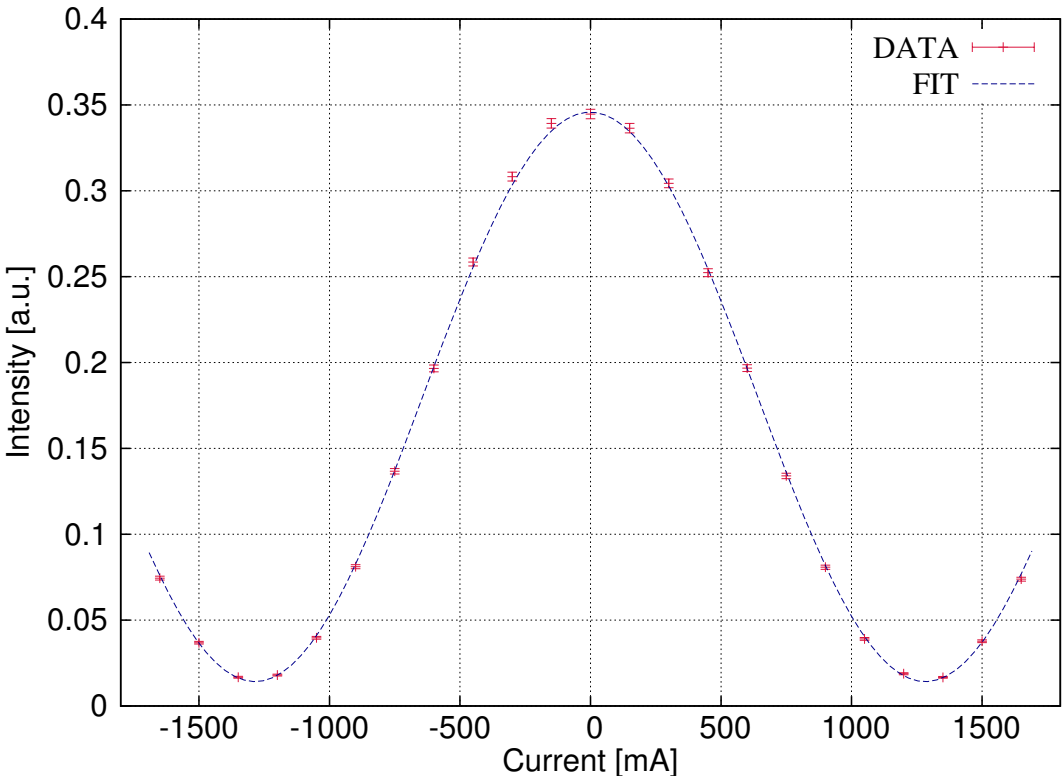

Figure 4.3.: Currentscan of the DC2-coil: To adjust the second DC-coil the current, that produces the magnetic field to flip the neutron spin, is scanned. For this scan the first coil is turned off.

properties:

- Flipping ratio: 24.3 ± 1.2
- Phase shift: $90.19° \pm 0.14°$
- Contrast: 0.92 ± 0.004

Note that the flipping ratio of the second coil is much lower then the first one. Due to the limited space of the polarimeter, the second coil always operated close to the analyzer. The supermirror produces a large magnetic stray field, which lowers the coil's efficiency and therefore also its flipping ratio.

4.1.3. Pre and post selection of the spin state

At the beginning of the polarimeter the neutrons have to pass through a polarizing supermirror, which sorts out the $|S_z;-\rangle$ spin component. To finish the preparation of the initial state a DC-coil is used to rotate the neutron spin by $\frac{\pi}{2}$, so that it lies in the xy-plain. This is done by applying the current found in adjusting the DC1. At this point the spin state is given by $|S_x;+\rangle$.
Due to the magnetic guide field that points into the $(z;+)$-direction the spin starts Larmor precessions around the z-axis. This precession is used to select the azimuth angle ϕ, by mounting the second DC-coil on a translation stage. To scan ϕ, both DC1 and DC2 are adjusted to rotate the spin by $\frac{\pi}{2}$ and the position of the DC2 coil is scanned. Figure 4.4 shows such a position scan.
Flipping ratio and contrast of the position scan are

- Flipping ratio: 18.362 ± 0.689
- Contrast: 0.897 ± 0.0037

To complete the post selection of the final state, not only ϕ, but also θ has to be fixed. This is done by fixing current to the second DC-coil.
The extra π-rotation that is necessary to extract the weak value is also done by moving the second DC-coil along the direction of neutron propagation, using the spin's Larmor precession. After θ and ϕ are selected by the right current and position values, the neutrons have to pass through a second supermirror, the analyzer, which performs the post selection.

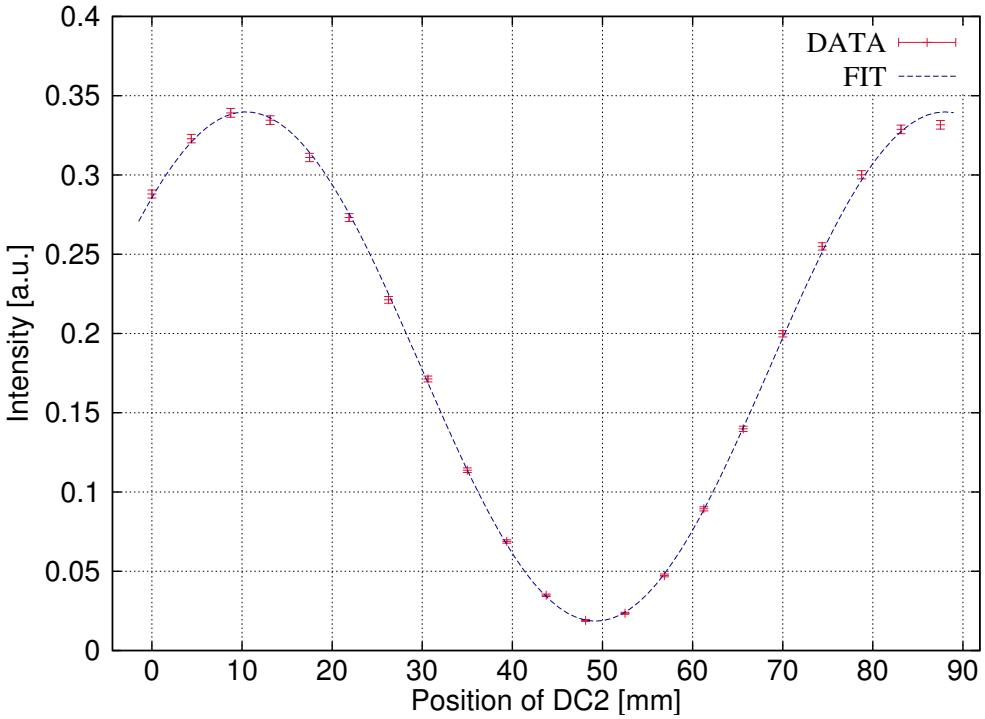

Figure 4.4.: Position scan of the DC2-coil: The position of the second DC-coil is varied, while the applied current is held constant to achieve a $\frac{\pi}{2}$-rotation. This makes it possible to select the azimuth angle ϕ. Maximum intensity corresponds to $\phi = 0°$, minimum to $\phi = 180°$.

4.2. Raw data

All measurements are performed in the following manner: A certain value of ϕ is picked, by choosing a position. Then the current value is set and the measurement is performed at the ϕ and at the $\phi + \pi$ position. This is done for all current values. In this way it was possible to record scans of the polar angle. Such scans can be seen in Figs. 4.5 to 4.7.
For every pair of angles ϕ and θ two points are recorded. They represent the π-rotator turned on and off.
Note that for plots intensities varies around a common offset of ~ 0.17. The only exception are the measurements for the azimuthal angle $\phi = 0°$ and $\phi = 60°$. The explanation for this is simple. For the azimuthal angle $\phi = 0°$ and $\phi = 60°$ two additional (unused) copper coils were present in the beam. Since copper absorbs neutrons this lead to a loss in intensity.

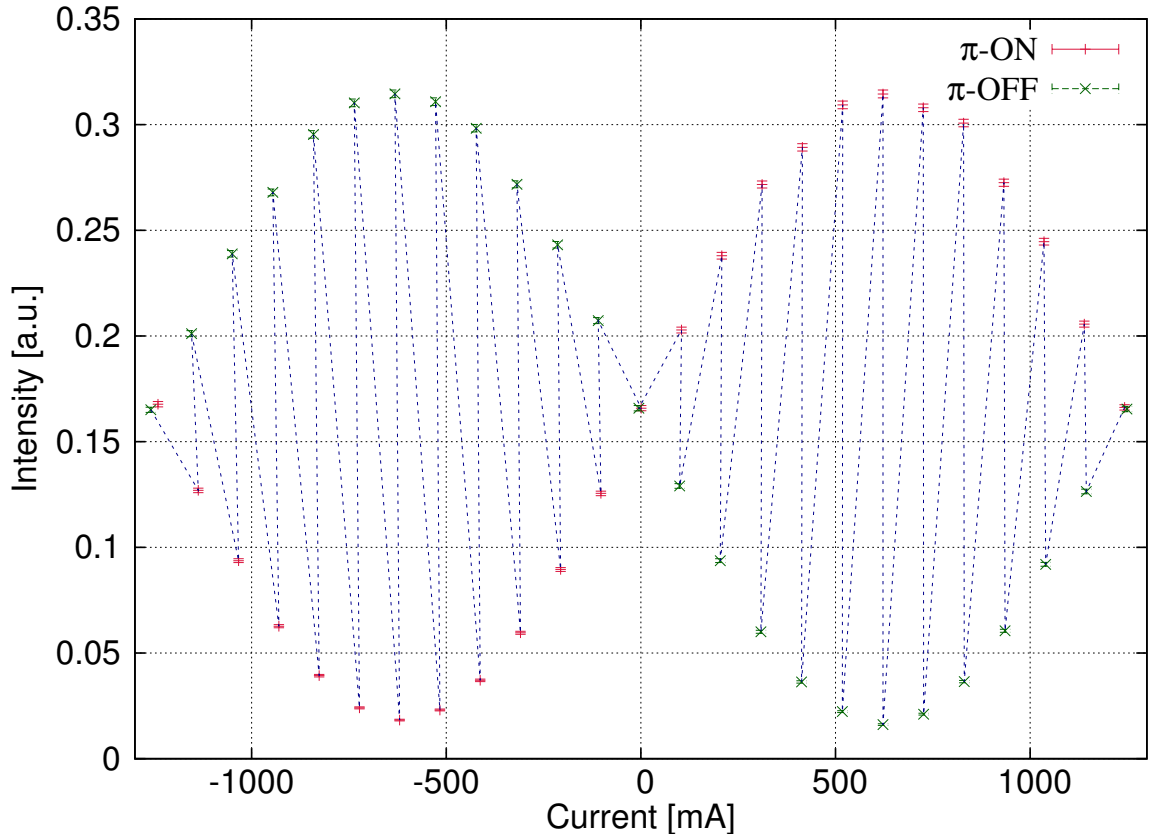

Figure 4.5.: Measurement data for fixed azimuth angle $\phi = 180°$. The variation of the current scans the polar angel θ.

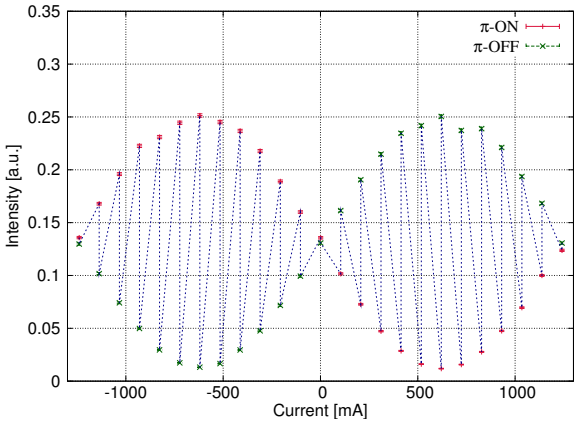

(a) Thetascan for $\phi = 0°$.

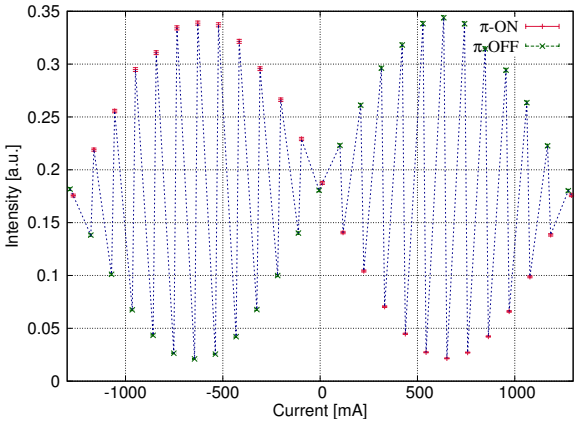

(b) Thetascan for $\phi = 15°$.

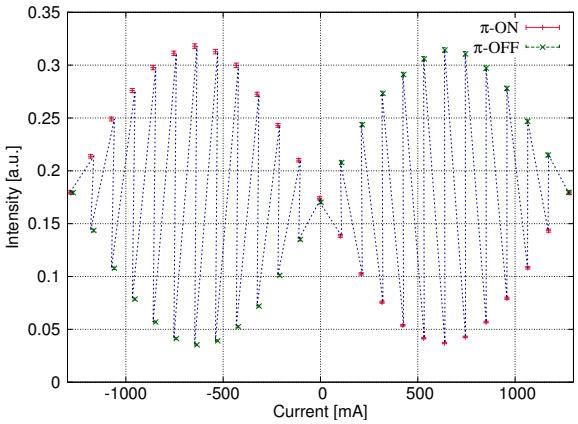

(c) Thetascan for $\phi = 30°$.

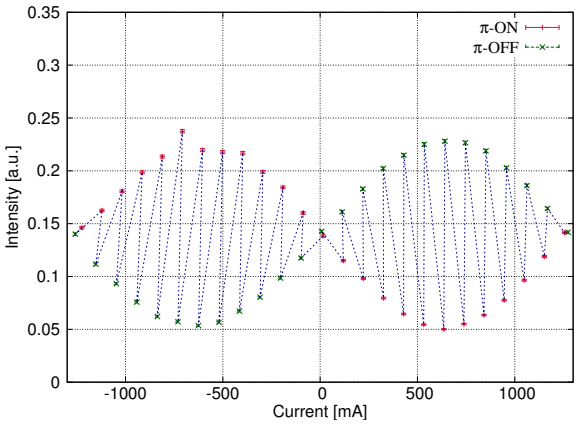

(d) Thetascan for $\phi = 45°$.

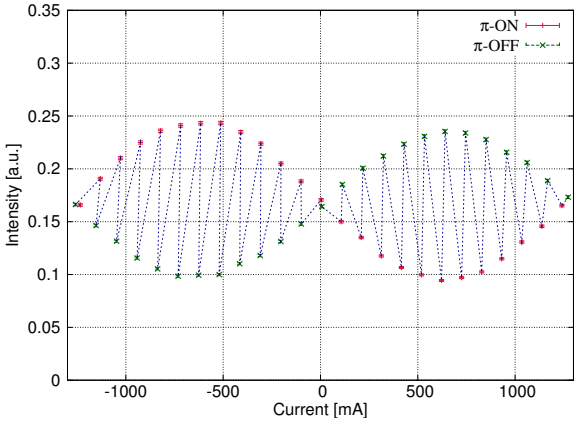

(e) Thetascan for $\phi = 60°$.

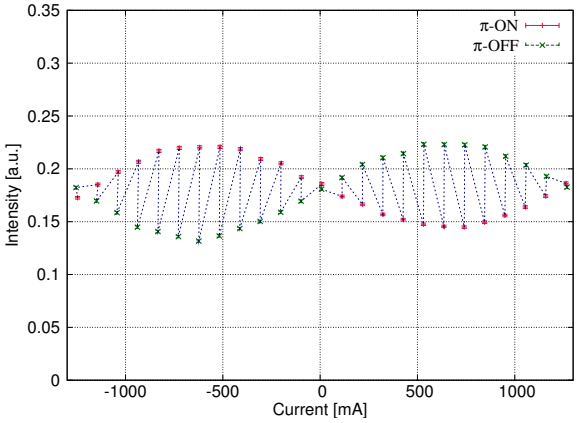

(f) Thetascan for $\phi = 75°$.

Figure 4.6.: Measurement data for fixed azimuth angle $\phi = 0°, 15°, 30°, 45°, 60°, 75°$. The variation of the current scans the polar angel θ.

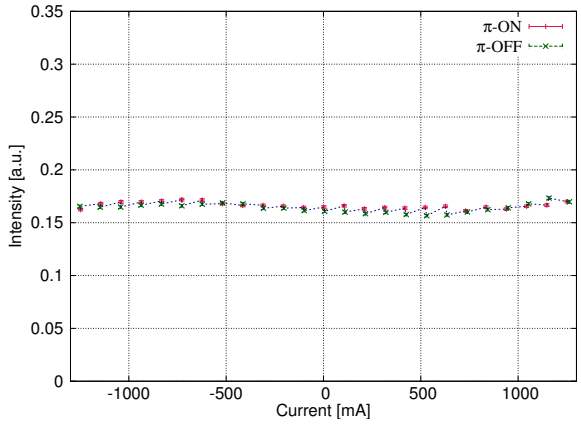

(a) Thetascan for $\phi = 90°$.

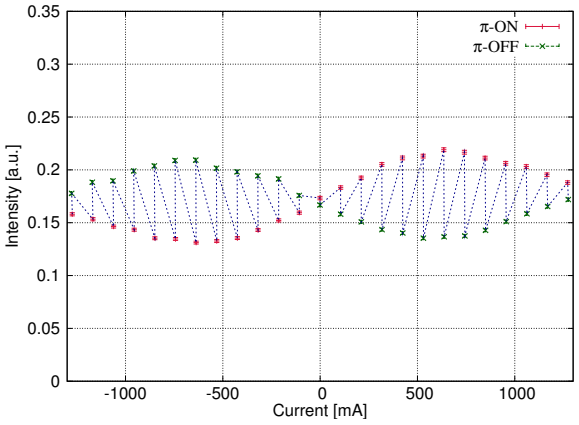

(b) Thetascan for $\phi = 105°$.

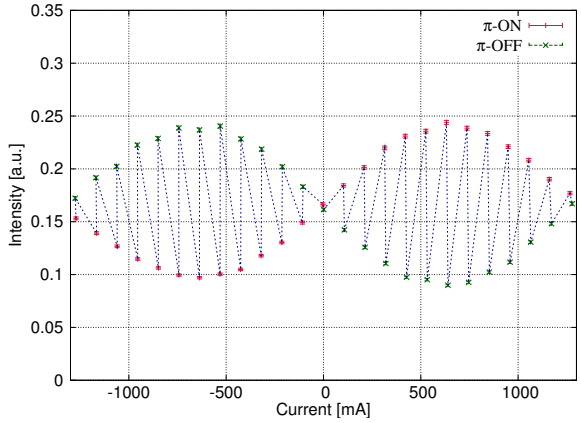

(c) Thetascan for $\phi = 120°$.

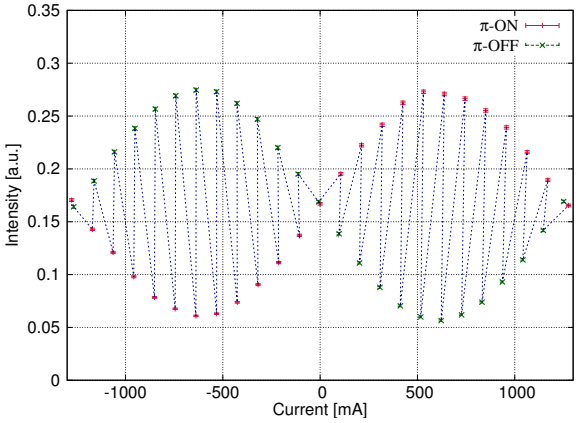

(d) Thetascan for $\phi = 135°$.

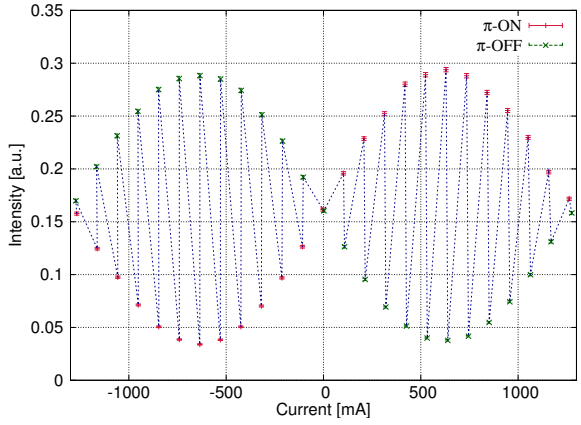

(e) Thetascan for $\phi = 150°$.

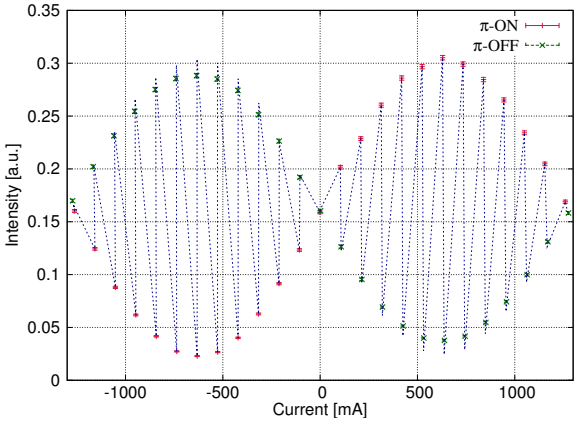

(f) Thetascan for $\phi = 165°$.

Figure 4.7.: Measurement data for fixed azimuth angle $\phi = 90°, 105°, 120°, 135°, 150°, 165°$. The variation of the current scans the polar angel θ.

4.3. Measurement results

For all measurements we set the initial spin state to $|S_x;+\rangle$, the final one by $|\hat{S}\cdot\hat{n};+\rangle = \cos\left(\frac{\theta}{2}\right)\mathrm{e}^{-i\phi/2}|S_z;+\rangle + \sin\left(\frac{\theta}{2}\right)\mathrm{e}^{i\phi/2}|S_z;-\rangle$. The π-rotation is performed around the z-axis, which means that the weak value of $\hat{\sigma}_z^s$ is determined. From Eq. (3.16) one can easily find that the absolute of the spin operators weak value is given by

$$|\langle\hat{\sigma}_z^s\rangle_w| = \sqrt{\frac{1-\cos(\phi)\sin(\theta)}{1+\cos(\phi)\sin(\theta)}} \tag{4.1}$$

There are several experimental imperfections:

(i) The neutron beam's degree of polarization is practically about 96% which is lower than the ideal of 100%.

(ii) The flipping ratio[a] of the DC-coils is limited to ~ 35. This is of course mainly a consequence of the low degree of polarization.

(iii) The efficiency of a spin manipulation by the coils, despite being quite high, is limited to roughly 99%.

All those effects add up and decrease the polarimeter's contrast, which is finally obtained by $\sim 90\%$. To take all imperfections into account, the measurement results have been fitted by the function

$$f(\theta,\phi,\mathfrak{C}) = \sqrt{\frac{1-\mathfrak{C}\cos(\phi)\sin(\theta)}{1+\mathfrak{C}\cos(\phi)\sin(\theta)}}. \tag{4.3}$$

This is simply the weak value given by Eq. (4.1), with its angle dependent part weighted by a contrast factor $\mathfrak{C}$.
The measurement results for a set of $\phi = 0°,\ 15°,\ 30°, \cdots,\ 180°$ and $\theta = 0°$ are plotted in Figs. 4.8 to 4.10:

[a] The flipping ratio R of a coil is defined by

$$R = \frac{I}{I_f}, \tag{4.2}$$

where I and I_f are intensities with the spin flipper turned off and on.

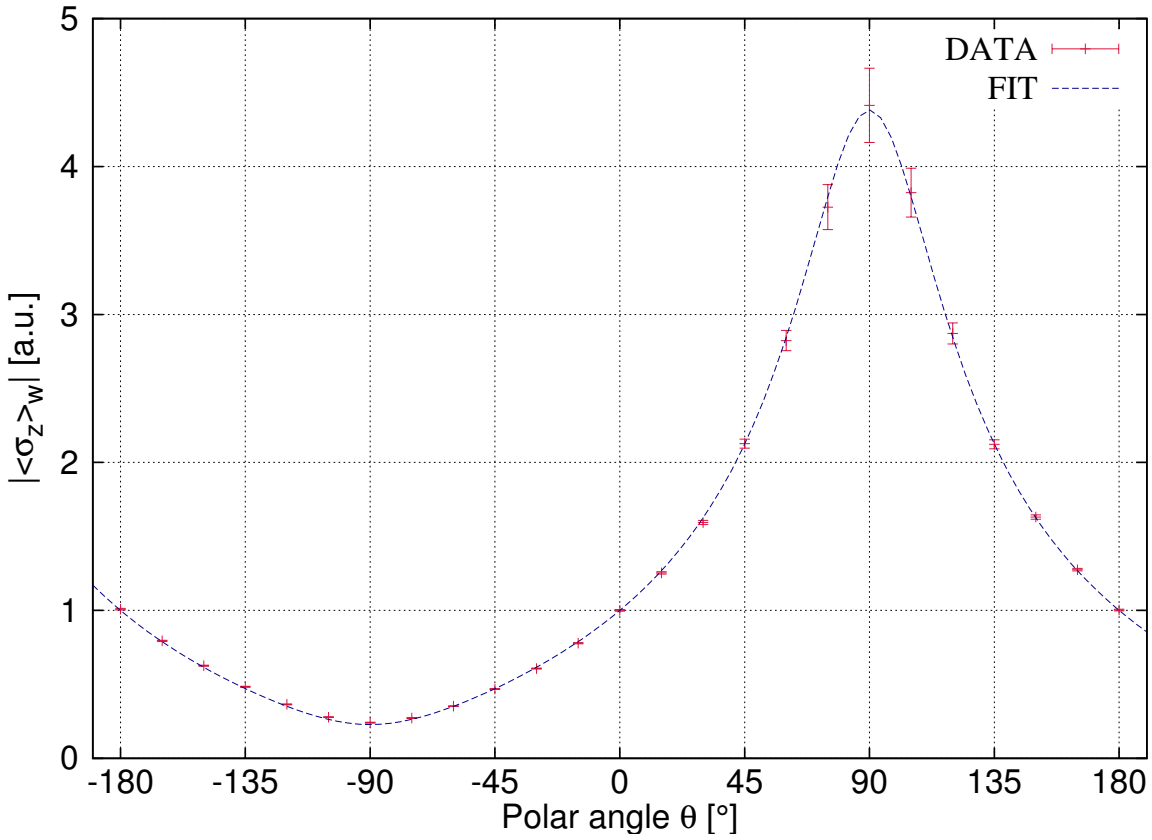

Figure 4.8.: Typical polarimeter measurement results of $|\langle\hat{\sigma}_z\rangle_w|$ for a fixed azimuthal angle of $\phi = 180°$. The fit has been performed with one parameter: the contrast. It was set to $c = 0.90 \pm 0.006$.

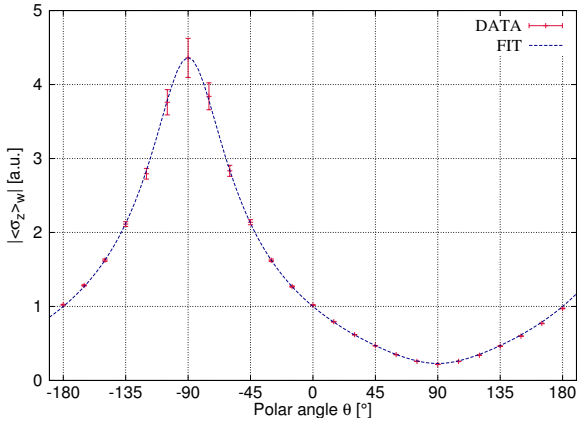

(a) $\phi = 0°$; $c = 0.90 \pm 0.001$.

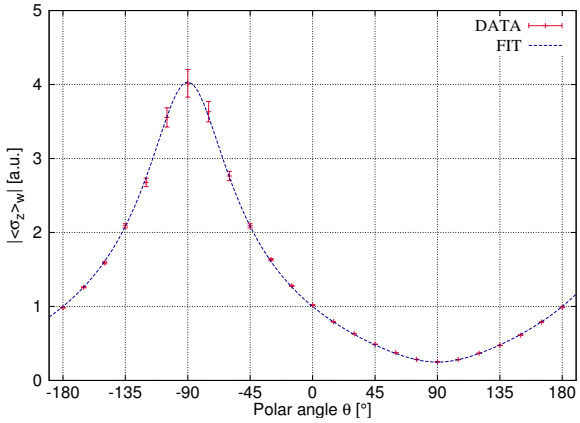

(b) $\phi = 15°$; $c = 0.92 \pm 0.001$.

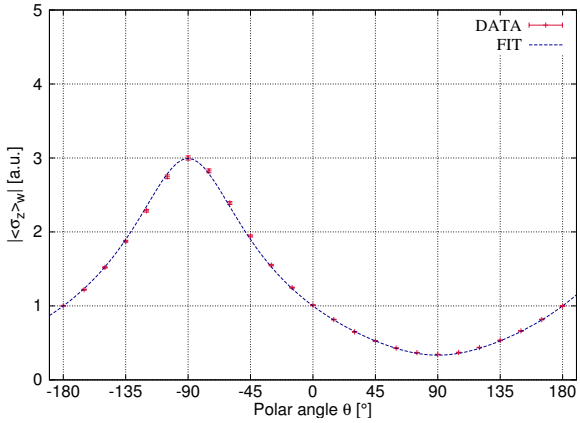

(c) $\phi = 30°$; $c = 0.92 \pm 0.002$.

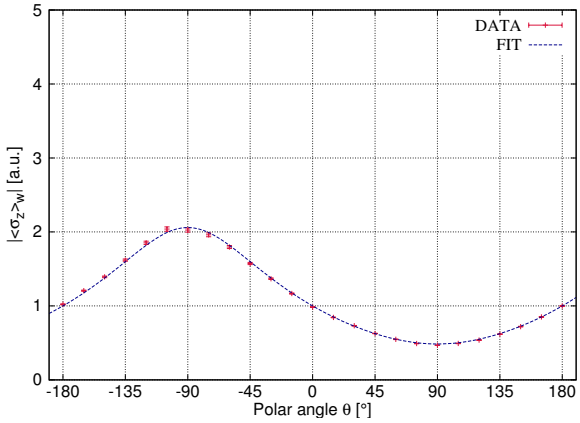

(d) $\phi = 45°$; $c = 0.88 \pm 0.004$.

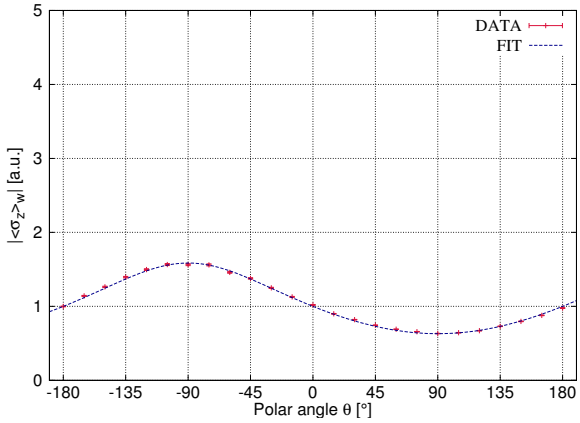

(e) $\phi = 60°$; $c = 0.86 \pm 0.006$.

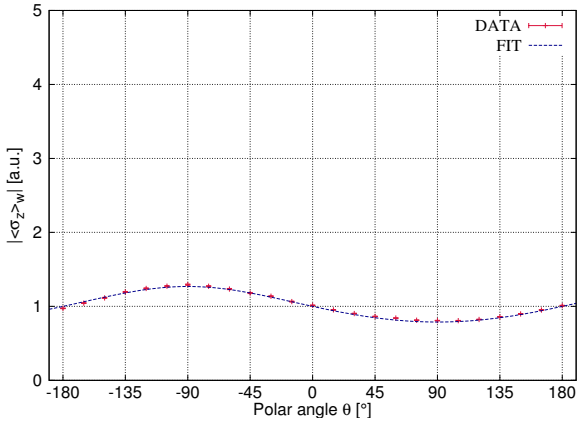

(f) $\phi = 75°$; $c = 0.90 \pm 0.016$.

Figure 4.9.: Polarimeter measurement results of $|\langle\hat{\sigma}_z\rangle_w|$ for a fixed azimuthal angle $\phi = 0°, 15°, 30°, 45°, 60°, 75°$. For all measurements the a fit with one parameter, the contrast c, is performed.

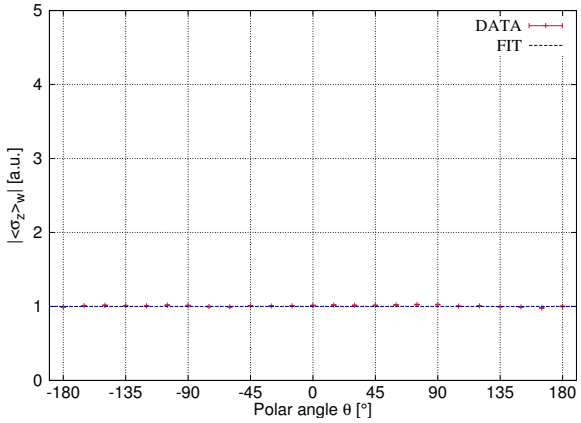

(a) $\phi = 90°$; $c \equiv 1$.

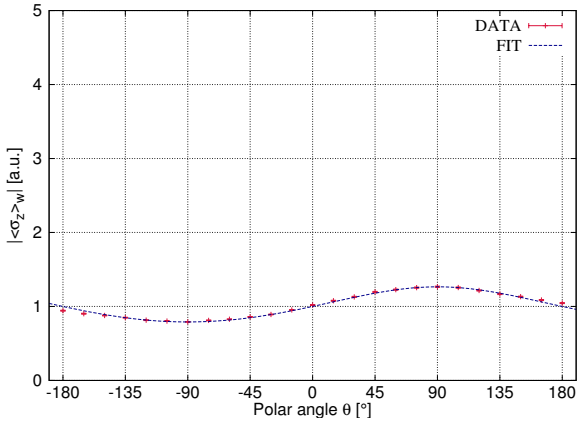

(b) $\phi = 105°$; $c = 0.89 \pm 0.020$.

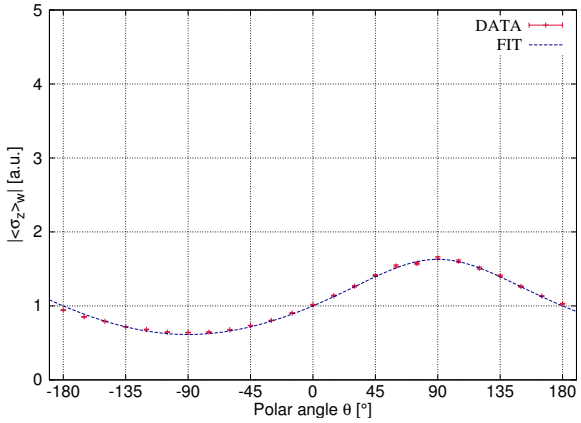

(c) $\phi = 120°$; $c = 0.91 \pm 0.009$.

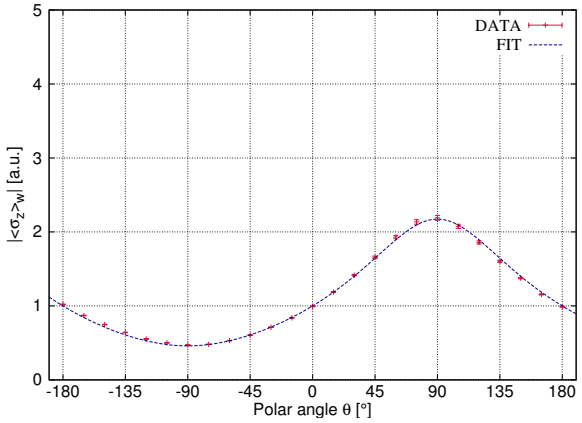

(d) $\phi = 135°$; $c = 0.92 \pm 0.004$.

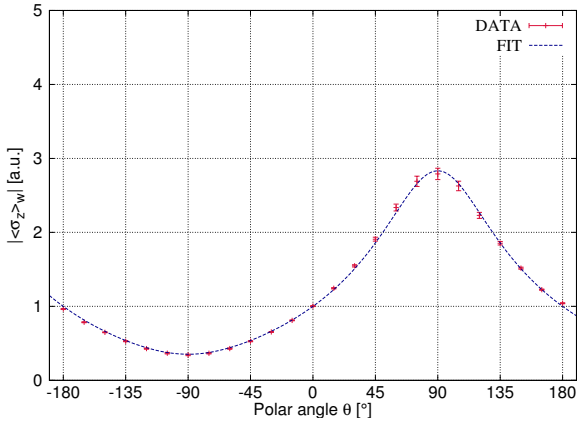

(e) $\phi = 150°$; $c = 0.90 \pm 0.003$.

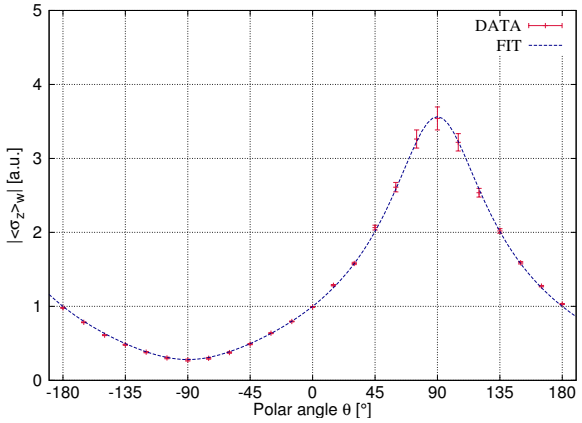

(f) $\phi = 165°$; $c = 0.88 \pm 0.001$.

Figure 4.10.: Polarimeter measurement results of $|\langle\hat{\sigma}_z\rangle_w|$ for a fixed azimuthal angle $\phi = 90°, 105°, 120°, 135°, 150°, 165°$. For all measurements the a fit with one parameter, the contrast c, is performed.

To sum the results up, Fig. 4.11 shows all results together with the expected behaviour (fit) in a 3D view:

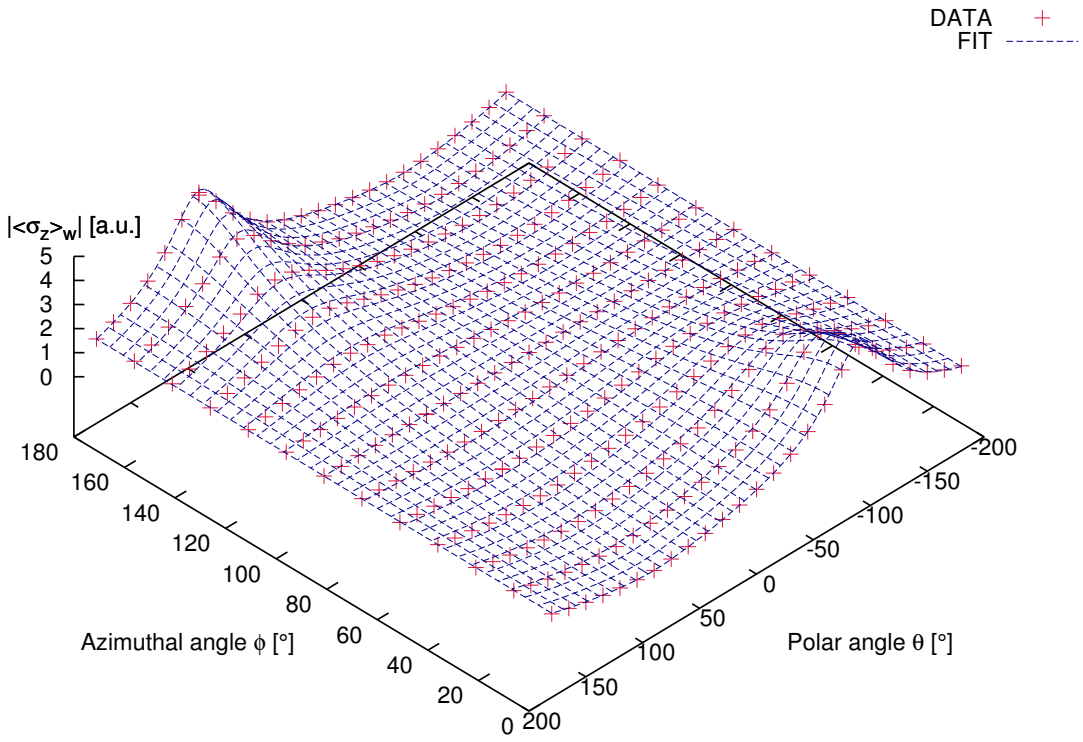

Figure 4.11.: 3D Plot of all measurements: The data of all measurements has been put together. The fitted curve uses a mean contrast of c=0.9. It is clearly visible that the experiment is in excellent agreement with the theory[b].

4.4. Discussion of the measurement results and concluding remarks

The measurement results of the previous section show an excellent agreement with the theory. The contrast of the polarimeter is a very good fitting parameter. However, some curves are fitted with a contrast lower than 90%. This is a systematic error: For larger values of ϕ the second DC-coil moves closer to the supermirror. Now the supermirror produces an additional field in the z-direction, which causes the spin to precess faster. It is difficult to select the azimuth angle ϕ correctly. If ϕ is bigger then expected for one scan of the polar angle θ, then this will manifest itself in a smaller $\mathfrak{C}$ in the fit.
By introducing a contrast parameter the theoretical curve is matched with the measurement results. However, a slightly different approach can be taken by normalizing the count rates and therefore matching the measured weak values to the (unaltered) theoretical curve. For this the

[b]The measurement error was not taken into account for this plot!

contrast of the whole polarimter has to be determined. This can be done in any measurement that involves the same pre and post selection as the extraction of the weak value requires. To take all systematic errors into account it would be best to use the contrast $\mathfrak{C}$ measured with a position scan of the second DC-coil. The normalized count rates are then given by

$$I_{\text{off}}^{\text{N}} = \frac{I_{\text{off}} + I_{\text{on}}}{2} + \frac{I_{\text{off}} - I_{\text{on}}}{2\mathfrak{C}} \tag{4.4}$$

and

$$I_{\text{on}}^{\text{N}} = \frac{I_{\text{off}} + I_{\text{on}}}{2} + \frac{I_{\text{on}} - I_{\text{off}}}{2\mathfrak{C}} \tag{4.5}$$

The weak value's absolute can then be determined from the experimental data by

$$|\langle\hat{\sigma}_z^s\rangle_w| = \sqrt{\frac{I_{\text{on}}^{\text{N}}}{I_{\text{off}}^{\text{N}}}} \tag{4.6}$$

The advantage of this method is that the contrast parameter $\mathfrak{C}$ is independent from the post selection angle ϕ.
Nevertheless, no matter how the systematic errors are dealt with, it does not change the fact that the system behaves exactly as predicted in chapter 2. For nearly orthogonal initial and final spin states the weak value becomes very large, and we report a maximum weak value of the spin operator of $|\langle\hat{\sigma}_z^s\rangle_w| = 4.41 \pm 0.25$.
One of the aims of this work, is to confirm the validity of the weak value formulation for the absolute of the spin weak value. A polarimter experiment was carried out at the ATI.
It contained some systematic imperfections that manifested themselfes in a limited contrast of $\sim 90\%$ at the polarimeter beamline. This was taken into account in the analysis of the experiment.
The results agree perfectly with the theory which is described in chapter 3. This experiment confirms once more, that neutron matter waves are useful to investigate the foundations of quantum mechanics in general and in particular the weak value formalism.
The experimental success sparks hope that the other experiments described in the previous chapter can be performed as well. Further developement of the topic of weak values and weak measurements with neutrons can be expected.

5. Conclusion

In this thesis, quantum theory has been used to analyse and develop experiments to extract weak values, in particular those of the spin and the path operator. All those experiments allow the use of neutron matter waves, which can only be understood by a purely quantum mechanical treatment.
Three different experiments are proposed and analyzed:

(i) The first kind of experiment allows to extract the absolute of the spin operator's weak value. It can be performed using a polarimeter or an interferometer setup. In addition to that it has been conclusively shown that the spin operator's weak value itself is accessible without a weak measurement. This is something that has not been considered in the literature yet and raises the question about the meaning of the weak value outside of the weak regime.

(ii) In the second experiment small spin rotations allow to extract the path operator's weak value in an interferometer experiment. The use of the neutron spin allows to measure not only the absolute of the path operator's weak value, but also its real part. In addition to that pure 'which-way-information' can be extracted by pre and post selecting the path state using variable absorbers.

(iii) A clever combination of weak path and spin operator measurements makes it possible to demonstrate a 'Cheshire Cat' in a neutron interferometer experiment. The way how such a measurement has to be performed has been shown in this thesis. This allows to accomplish the first experimental realization of this quantum paradox ever.

In addition a polarimeter experiment was carried out at the TRIGA Mark II research reactor at the Institute of Atomic and Subatomic Physics of the Vienna University of Technology. In this experiment certain pre and post selected spin states are prepared. By performing consecutive measurements of I_{on} and I_{off}, it is possible to measure the absolute of the spin operator's weak value[a]. The experimental results agree very well with the theory and spin weak values far outside the eigenvalue range of the spin operator were measured. This is an impressive demonstration, showing that neutron optics are a powerful tool to investigate weak values.
The success of this experiment sparks hope, that the other theoretically treated ones can be performed equally well. It is of importance that the experiments concerning weak measurements of the spin and the path operator are actually performed. Once this is accomplished and potential experimental obstacles are overcome, a 'Cheshire Cat' is within reach. A measurement of this paradox would once more prove the strange nature of quantum mechanics.

[a] I_{on} and I_{off} are the intensities when an extra π-spin rotator is turned on and off.

A. Acknowledgement

Writing this thesis would not have been possible without the help of many people:
First of all I want to thank my parents Manfred and Helga Denkmayr for their support throughout the time of my studies. They made it possible for me to study at a University and gave me their full support from the very first moment.
I would also like to thank all my fellow students, who were a great source of discussion. They made my whole studies so much more interesting and helped me whenever needed. Specifically I want to thank (in no particular order) Lorenz Hruby, Martin Fölser, Michael Scheucher, Bernhard Mistelberger, Lukas Schrangel, Daniel Föger, Alexander Reismann, Andreas Eder, Lukas Sölkner and Wolfgang Schlichtner.
Particular thanks goes to my colleagues Stephan Sponar and Hermann Geppert. They shared their vast experience in theory and experiment with me, which came in handy more than once. Moreover, they supported me with the measurements presented in chapter 4.
Very helpful discussions by letter with Alexandre Matzkin and Dibankar Home are acknowledged was well.
I also want to express my deep gratitude towards my supervisor Yuji Hasegawa. He guided me very well throughout the work on this thesis and helped me to gain a deeper and more fundamental understanding of physics. He showed me the right directions and made sure I stayed focused, but he also gave me the freedom to follow my own ideas.
Finally I want to thank Anna Frauscher for being there for me.
To all that I might have mistakenly omitted: thank you!

Bibliography

[1] T. Folger, Is Quantum Mechanics Tried, True, Wildly Successful, and Wrong?, *Science* **324**, 1512 (2009).

[2] M. Kaku, *Hyperspace: A Scientific Odyssey Through Parallel Universes, Time Warps, and the 10th Dimension*, p. 263 (Oxford University Press, 1994).

[3] J. von Neumann, *Mathematical Foundations of Quantum Mechanics* (Princeton University Press, 1955).

[4] J. Erhart, S. Sponar, G. Sulyok, G. Badurek, M. Ozawa and Y. Hasegawa, Experimental demonstration of a universally valid error-disturbance uncertainty relation in spin measurements, *Nat. Phys.* **8**, 185 (2012).

[5] Y. Aharonov, D. Z. Albert and L. Vaidman, How the result of a measurement of a component of the spin of a spin- *1/2* particle can turn out to be 100, *Phys. Rev. Lett.* **60**, 1351 (1988).

[6] N. W. M. Ritchie, J. G. Story and R. G. Hulet, Realization of a measurement of a "weak value", *Phys. Rev. Lett.* **66**, 1107 (1991).

[7] P. B. Dixon, D. J. Starling, A. N. Jordan and J. C. Howell, Ultrasensitive Beam Deflection Measurement via Interferometric Weak Value Amplification, *Phys. Rev. Lett.* **102**, 173601 (2009).

[8] S. Kocsis, B. Braverman, S. Ravets, M. J. Stevens, R. P. Mirin, L. K. Shalm and A. M. Steinberg, Observing the Average Trajectories of Single Photons in a Two-Slit Interferometer, *Science* **332**, 1170 (2011).

[9] F. Hasselbach, Progress in electron- and ion-interferometry, *Rep. Prog. Phys.* **73**, 016101 (2010).

[10] H. Rauch and S. A. Werner, *Neutron Interferometry - Lessons in Experimental Quantum Mechanics* (Oxford at the Clarendon Press, 2000).

[11] A. D. Cronin, J. Schmiedmayer and D. E. Pritchard, Optics and interferometry with atoms and molecules, *Rev. Mod. Phys.* **81**, 1051 (2009).

[12] B. J. Hiley, Weak Values: Approach through the Clifford and Moyal Algebras, *J. Phys.: Conf. Ser.* **361**, 012014 (2012).

[13] J. J. Sakurai, *Modern Quantum Mechanics*, pp. 1–66 (Addison-Wesley, 2010).

[14] I.-O. Stamatescu, *Compendium of Quantum Physics*, pp. 813–822 (Springer Berlin / Heidelberg, 2009).

[15] I. M. Duck, P. M. Stevenson and E. C. G. Sudarshan, The sense in which a "weak measurement" of a spin-$\frac{1}{2}$ particle's spin component yields a value 100, *Phys. Rev. D* **40**, 2112 (1989).

[16] R. Jozsa, Complex weak values in quantum measurement, *Phys. Rev. A* **76**, 044103 (2007).

[17] A. J. Leggett, Comment on "How the result of a measurement of a component of the spin of a spin-(1/2) particle can turn out to be 100", *Phys. Rev. Lett.* **62**, 2325 (1989).

[18] A. Peres, Quantum measurements with postselection, *Phys. Rev. Lett.* **62**, 2326 (1989).

[19] Y. Aharonov and L. Vaidman, Aharonov and Vaidman reply, *Phys. Rev. Lett.* **62**, 2327 (1989).

[20] Y. Aharonov, S. Popescu and J. Tollaksen, A time-symmetric formulation of quantum mechanics, *Physics Today* **63**, 27 (2010).

[21] W. H. Kraan, *Instrumentation to handle thermal polarized neutron beams.* Ph.D. thesis, Delft University of Technology, Mekelweg 15, 2629 JB Delft, The Netherlands (2004).

[22] F. Mezei, The principles of neutron spin echo. In F. Mezei, editor, *Neutron Spin Echo*, volume 128 of *Lecture Notes in Physics*, pp. 1–26 (Springer Berlin / Heidelberg, 1980).

[23] V. K. I. Masahiko Utsuro, *Handbook Of Neutron Optics* (Wiley-VCH, 2010).

[24] D. J. Hughes and M. T. Burgy, Reflection of Neutrons from Magnetized Mirrors, *Phys. Rev.* **81**, 498 (1951).

[25] F. Mezei, Neutron spin echo: A new concept in polarized thermal neutron techniques, *Z. Phys. A* **255**, 146 (1972). 10.1007/BF01394523.

[26] Y. Aharonov, S. Popescu and P. Skrzypczyk, Quantum Cheshire Cats, arXiv:1202.0631 (2012).

[27] Y. Aharonov and D. Rohrlich, *Quantum Paradoxes*, pp. 251–253 (Wiley-VCH, 2005).